TIME-RESOLVED TUNNELING IN
GaAs QUANTUM WELL STRUCTURES

by

Theodore Blake Norris*

Submitted in Partial Fulfillment

of the

Requirements for the Degree

DOCTOR OF PHILOSOPHY

Supervised by

Professor Gerard A. Mourou
The Institute of Optics

Professor Robert S. Knox
*Department of Physics and Astronomy

University of Rochester

Rochester, New York

1989

CURRICULUM VITAE

Theodore B. Norris was born on December 30, 1960, in Huntingdon, Pennsylvania. From 1978 to 1982 he attended Oberlin College, receiving a Bachelor of Arts degree with Highest Honors in Physics. While at Oberlin he began research in dynamical laser interactions with atomic vapors as an NSF summer intern and as an Honors student under the direction of Prof. Robert C. Hilborn. After a summer in the Quantum Chemistry group at the Sohio research center in Cleveland, he commenced graduate study in Physics at the University of Rochester in the Fall of 1982. He earned the Master's degree in 1984. Since 1983 he has performed research in the Ultrafast Science group at the Laboratory for Laser Energetics under the direction of Professors Gerard A. Mourou and Robert S. Knox, developing new lasers and experimental techniques for optical studies in the picosecond and femtosecond regime, and applying these techniques to the study of carrier dynamics in condensed matter systems. He has been supported at Rochester as a teaching assistant, a Rush Rhees Fellow, and an LLE Fellow. He is also a member of Phi Beta Kappa, Sigma Xi, and the American Physical Society.

ACKNOWLEDGEMENT

It is with great pleasure that I acknowledge the support and guidance of Professor Gerard Mourou. His vision and enthusiasm have been invaluable for the work presented in this dissertation. I also wish to thank Professor Robert Knox for many useful and stimulating discussions.

This work would have been impossible without the contributions of many people. Xiao Song of Cornell University did much of the difficult and unglamorous sample growth and processing, as well as generating many interesting and useful ideas. Bill Schaff, also of Cornell, provided critical advice on sample design and fabrication. Gary Wicks generated many of the initial ideas and suggestions at the beginning of this work. The double-well luminescence experiments were carried out in collaboration with Nakita Vodjdani, Borge Vinter, and Claude Weisbuch of Thomson-CSF research laboratories. It is a pleasure to acknowledge their input, both material, in the form of samples, and intellectual, in the form of some of the central ideas of this work.

The Ultrafast Science, née Picosecond research group has provided a uniquely stimulating and supportive research environment at LLE. I wish to thank Tod Sizer, Irl Duling, and Steve Williamson for their help in the early part of my career at LLE. Maurice Pessot and Kevin Meyer were labmates whose

helpfulness and understanding made it possible to perform three utterly different projects simultaneously in the same lab. Thanks are due to all the other Laser Labbers, past or present, who generously lent their expertise or equipment; without them this work would have been impossible.

The work in our laboratory has been supported over the years by AFOSR, NSF, and LLE's Laser Fusion Feasibility Project.

Thanks are also due to my classmates Dan Koon, Joe Rogers, Wolfgang Scherer, Michele Migliuolo, and Warnick Kernan, whose amiable competition and friendship lightened the rigors of graduate school.

I especially wish to thank my family for their continual love and support. Finally, I thank my wife Penny for her constant encouragement, patience, and love throughout my graduate career.

To Penny

ABSTRACT

Tunneling in quantum well structures has been a subject of considerable interest in semiconductor physics in recent years. Few time-domain experiments, however, have been brought to bear on the questions of the mechanisms or time-dependence of tunneling. We have developed techniques for the measurement of picosecond and femtosecond optical spectra, and applied them for the first time to the study of tunneling in quantum well structures.

We have developed a novel dye oscillator and amplifier to generate optical pulses of 100-fs duration at the 15-μJ level with a repetition rate of 1 kHz. These pulses were used to generate a white-light continuum, which enabled us to perform optical absorption spectroscopy over the visible and near-infrared regions of the spectrum with a time resolution of about 100 fs. We have also developed an experimental setup for time-resolved photoluminescence appropriate for GaAs quantum well studies, utilizing a picosecond near-infrared dye laser in conjunction with a synchroscan streak camera.

Using time-resolved photoluminescence, we have studied the tunneling escape rate of electrons from a quantum well through a thin barrier into a continuum, and its dependence on barrier height and width, and on an applied electric field. The

;

observed rates are well-described by a straightforward semiclassical theory.

We have investigated the problem of tunneling between coupled quantum wells using both time-resolved luminescence and absorption spectroscopy. We have directly observed in luminescence the buildup of a "charge-transfer" state via electron and hole tunneling in opposite directions, and the dependence of this charge transfer on an electric field. At moderate fields (2.5 x 10^4 V/cm), the charge transfer occur faster than 20 ps, indicating an unexpectedly fast hole tunneling rate. The time-resolved absorption experiments measure the time electrons initially excited into one quantum well require to tunnel into a second well. The experiments, performed at room temperature, indicate the possibility of vary fast (<300 fs) tunneling into the second well. These experiments were the first ultrafast optical measurements of carrier dynamics in coupled quantum well systems.

TABLE OF CONTENTS

LIST OF TABLES

LIST OF FIGURES

;

CHAPTER I

INTRODUCTION

I.A.   Historical Overview and Motivation

Tunneling is an old and time-honored subject in condensed-matter physics. The first interpretation of an experimental phenomenon in terms of tunneling was given by Fowler and Nordheim in 1928 in their explanation of field-induced electron emission from cold metals.[1] Since then many physical systems, both naturally occurring and man-made, have been observed to display tunneling. A comprehensive review of the state of the understanding of tunneling in solids as of 1969 is given in Burstein and Lundqvist.[2] Of particular interest were tunneling in metal-insulator-metal junctions,[3] superconductors, and interband tunneling in semiconductors. The latter process is principally manifested in the tunnel diode, which was introduced by Esaki in 1957.[4] Tunneling is also important in studies of excitation transfer in chemical and biological systems,[5] and of hopping transport in disordered solids.[6]

In 1969 Esaki and Tsu[7] proposed that ultrathin layers of semiconductors with different bandgaps could be grown epitaxially in a repeated structure to produce a "superlattice." The motivating idea was to construct a structure that would exhibit

resonant tunneling, negative differential resistance (NDR), and ultimately, Bloch oscillations.[8] The principal requirement of such structures is that the layers must be thin enough that the potential (*i.e.* the band edge) is modulated on a length scale comparable to the de Broglie wavelength of a band electron; this allows the electrons to be confined in a "quantum well" (QW). Furthermore the "heterostructure" interface, *i.e.* the boundary between the two semiconductor layers, must be smooth on an atomic scale for the effects of confinement to be clearly seen. The proposal of Esaki and Tsu gave great impetus to the development of crystal growth techniques that could satisfy these stringent requirements. The most successful of these to date has been molecular beam epitaxy (MBE),[9] though many other techniques have been developed to grow semiconductor microstructures. MBE enables one to grow the crystal atomic layer by layer, and thus control the heterostructure parameters with high precision. The most commonly studied system has been the $GaAs/Al_xGa_{1-x}As$ lattice-matched system, though considerable progress has been made in recent years on lattice-mismatched (strained) systems[10] and on other III-V and II-VI compounds.[11] A generic GaAs/AlGaAs superlattice structure is shown in Fig. 1.1.

The first observations of NDR in heterostructures were by Esaki *et. al.*[12] in 1972 in a superlattice and by Chang, Esaki, and Tsu[13] in 1974 in a double-barrier structure. The NDR was interpreted in terms of transport of electrons through the
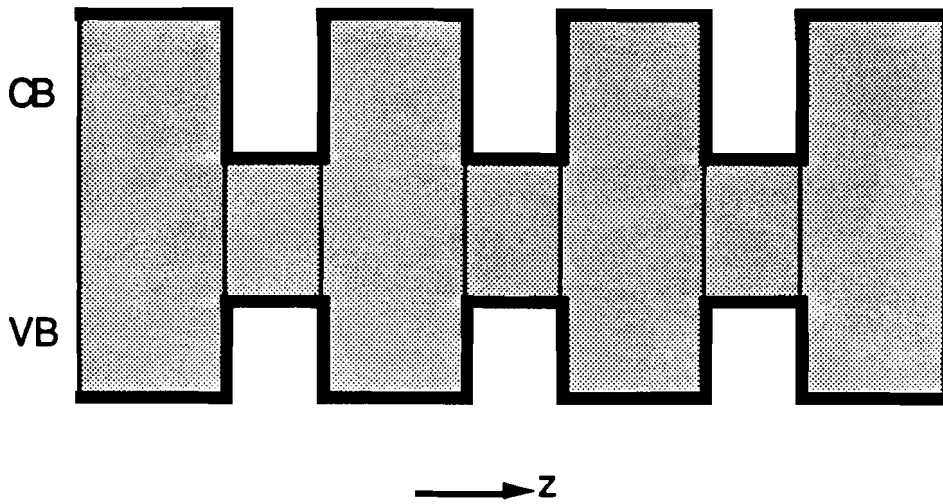
Figure 1.1.   Typical multiple-quantum well structure. Plotted are
the conduction band (CB) and valence band (VB)
edges vs. growth direction z. The shaded area
indicates the forbidden gap. Typically the well
regions are GaAs, and the barrier regions AlGaAs.

confined state between the barriers. Further evidence that electrons are confined in QW's was provided in 1974 by Dingle *et. al.*[14] in a seminal experiment that showed by optical means that the electron energies in a QW are quantized. Thus as MBE technology developed, interest in properties of low-dimensional systems in semiconductors burgeoned. The great advantages of semiconductor heterostructures are that to a very good approximation the transport of carriers in the growth direction can be described as one-dimensional, and if the carriers are strongly confined in the QW, the motion in the plane perpendicular to the growth direction is two-dimensional.

The study of systems of reduced dimensionality has been one of the most fruitful areas of research in solid state physics in recent years. The confinement of carriers in quasi-two-dimensional structures has led to discoveries of the integral[15] and fractional[16] quantum Hall effects. The optical properties of QW's are of both fundamental and practical interest.[17] The enhanced excitonic binding energy in quasi-2D systems has led to many interesting studies of the linear,[18] nonlinear,[19] and electric-field-dependent[20] optical properties of QW's. The electric-field-dependent properties are particularly interesting for applications to optical modulators[21,22] and devices for optical bistability.[23] QW lasers are of great interest because of their tunability and generally superior operating characteristics to conventional laser diodes.[24-26] The extremely high mobilities[27] obtainable with 2-D electron and hole gases have made possible the design of whole new classes of high speed electronic devices.[28]

All of the structures mentioned above derive their properties from the confinement of carriers in one dimension. Considerable effort is currently being directed at further reducing the dimensionality, as many interesting effects are expected in 1-D "quantum wires" and 0-D "quantum dots."[29-31]

For tunneling studies, superlattices have yet to live up to their promise; Bloch oscillations have never been observed in these structures, although recent experiments have observed some miniband transport.[32,33] However, the double-barrier diode

(DBD) has proved to be very successful. Since the first observation of NDR in these structures in 1974,[13] a tremendous volume of work has developed, made possible in large part by the rapid progress in the ability to grow very high quality structures by MBE. Room-temperature NDR is now routinely observed, and DBD's have demonstrated oscillations up to 56 GHz[34] and detecting and mixing up to 2.5 THz.[35] (Further discussion of previous experimental and theoretical work on DBD's is given in section III.A.)

Despite the volume of work on resonant tunneling structures to date, there are still many unanswered questions regarding the nature of the transport through multiple-barrier structures, and particularly regarding the time-dependence. Yet at the time the work presented here was begun, there were no time-domain studies of tunneling in semiconductor heterostructures. One reason such studies were not considered is that tunneling can be very fast, so the appropriate experimental probes had to be developed.

Concurrent with the development of epitaxial growth technology and the study of low-dimensional semiconductor physics has been rapid progress in the field of ultrafast optics. Reviews of the field of ultrashort optical pulse generation and measurement techniques are given in refs. 36-42. The last fifteen years have witnessed the development of many new laser oscillators and amplifiers capable of generating picosecond or

subpicosecond pulses over much of the visible and near-infrared spectrum. With the development of oscillators capable of generating pulses as short as 27 fs,[43] and of pulse compression techniques enabling generation of pulses as short as 6 fs,[44] experiments with extraordinarily high time resolution may now be performed.

The principal experimental techniques used in the work presented here were picosecond time-resolved photoluminescence using a synchroscan streak camera and subpicosecond absorption spectroscopy. The use of a synchronously pumped dye laser in conjunction with a streak camera, where the laser and streak camera deflection plate sweep voltage are phase-locked (hence the term "synchroscan"), was first reported by Adams, Sibbett, and Bradley[45] in 1978. The generation of a subpicosecond white light continuum pulse, making possible spectroscopic measurements on a 100-fs time scale, was first reported by Fork et. al.[46] in 1983. The first amplifiers capable of producing subpicosecond pulses with sufficient energy to produce a useful continuum at kHz repetition rates were developed in 1984.[47,48] Thus in the last few years, the time became ripe to apply ultrafast optical techniques to the study of tunneling in semiconductor QW structures.

The work presented in this thesis represents a first attempt to perform a time-domain study of tunneling in QW's. There have been a few studies published concurrently with this work, but on

structures significantly different from those considered here, and generally at lower time resolution.

The outline of this thesis is as follows. In the remainder of this chapter I review the electronic structure of QW's, and discuss those optical properties necessary for understanding the experiments presented here. Then I will give a brief overview of previous work on time-resolved optical studies of carrier dynamics in GaAs/AlGaAs QW's. Finally, I will briefly discuss tunneling studies in the GaAs/AlGaAs system that have been performed to date. In the second chapter I will describe the lasers and experimental apparatus developed to perform the experiments reported here. In the third chapter, I present the results of experiments which measured the rate at which electrons escape from a QW through a thin barrier in the presence of an electric field. This experiment is particularly relevant for the complete understanding of DBD structures. In the fourth chapter, I discuss the double-well problem, and the application of time-resolved photoluminescence and absorption spectroscopy to the direct observation of tunneling in coupled-well systems. Finally, in the fifth chapter, I summarize the experimental conclusions of this dissertation, and suggest directions for future work.

I.B. GaAs/AlGaAs Quantum Well Structures

I.B.1. Bandgap Engineering

As I mentioned in the previous section, if one can grow layered crystals so that the potential seen by the carriers is modulated on the scale of the de Broglie wavelength (or shorter), many new physical phenomena can be observed. In particular, the dimensionality of the system can be reduced.

In the $GaAs/Al_xGa_{1-x}As$ system, this works as follows. GaAs is a direct-gap semiconductor, with the fundamental gap at zone center (Γ symmetry point), and lattice constant 5.2 Å. The band structure of GaAs is shown in Fig. 1.2. As aluminum is added to form the ternary compound $Al_xGa_{1-x}As$, the Γ bandgap increases approximately as[20]

$$E_{AlGaAs} = E_{GaAs} + 1.425x - 0.9x^2 + 1.1x^3 . \qquad (1)$$

Since the bandgap increases with x, the desired bandgap modulation can be obtained by successively growing thin layers of AlGaAs with different aluminum composition x. In the AlGaAs system, this is possible since the lattice constant of $Al_xGa_{1-x}As$ is very close to that of GaAs for all x ($0 \leq x \leq 1$). In other semiconductor systems, where the lattices may not be so closely matched, the layered crystal may still be grown if the layers are

T-300 K

ENERGY ($\epsilon - \epsilon_V$) (Electron Volts)

3

2

1

0

-1

L_6

Γ_6

1.71 eV

1.42 eV

1.90 eV

(V I)
Heavy holes

Light holes
(V2)

Γ_8

Γ_7

0.34 eV

Split-off bond
(V3)

X_7

X_6

Δ_5

0.40 eV

ϵ_c

ϵ_v

$L(\frac{1}{2}\frac{1}{2}\frac{1}{2})$ Λ $\Gamma(000)$ Δ $X(100)$

REDUCED WAVE VECTOR q
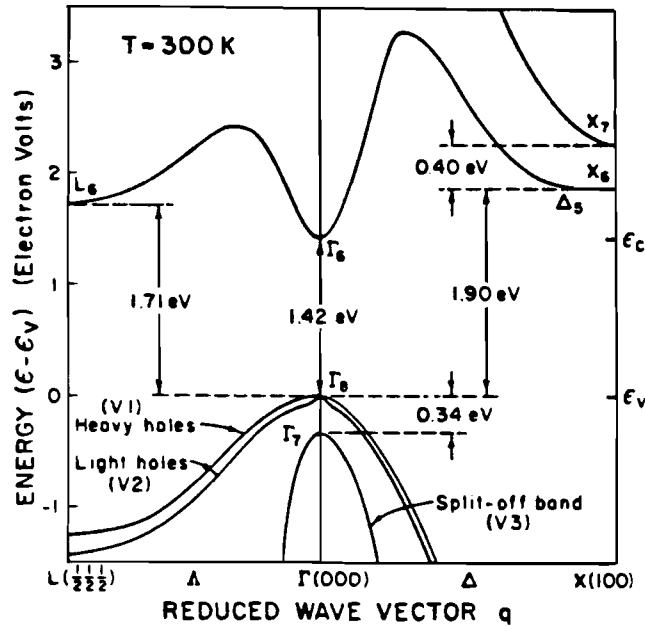
Figure 1.2.   GaAs band structure near the fundamental gap. (From ref. 89).

thin enough.   In this case, the strain due to the lattice mismatch is coherently taken up in the crystal, and high quality material with good interface quality can be grown.[10]   An example of such a system is $GaAs/GaAs_xP_{1-x}$.   A generic layered heterostructure was shown in Fig. 1.1; what is plotted is the Γ edge vs. growth direction z.

I.B.2.   Electronic Structure

In this section I describe in simple terms the structure of the electronic states of QW's.   A review of the detailed calculation of electronic states in QW's is given by Bastard and Brum.[49]   For

the lowest energy states in QW's it is a good approximation to consider only the Γ states of the host crystal.[49] In the envelope function approximation, the total electron wavefunction can be written as

$$\chi = \sum_n c_n u_{nk}(r) e^{ik\cdot\rho} \phi(z), \qquad (2)$$

where n is the band index, u is the Bloch wavefunction of the bulk crystal, k is the momentum in the plane of the layers, $\rho = xe_x + ye_y$, and ϕ is the envelope function in the growth direction. The Bloch functions (*i.e.* the rapidly varying part of the wavefunction) therefore determine the effective masses, interband p matrix elements, and the band structure in the QW plane. The band structure in the plane is very close to that of the bulk for the electrons. For the holes the situation is much more complicated, and the light and heavy-hole states are strongly mixed. (In-depth discussions of the valence-band structure in the QW plane are given in refs. 17 and 49).

In the growth direction, the band structure is determined to a good approximation by assuming bulk Γ Bloch functions in the well and barrier regions, in which case the problem reduces to the textbook square-well problem for the envelope functions $\phi(z)$, with the appropriate effective masses in the well and barrier regions. I take the effective masses to be[50]

$$m_e^* = (0.0665 + 0.0833x)\, m_e$$

$$m_{hh}^* = (0.48 + 0.31x)\, m_e \qquad\qquad (3)$$

$$m_{lh}^* = (0.088 + 0.049x)\, m_e ,$$

where m_e is the bare electron mass and x is the aluminum composition. It is important to note that the well and barrier masses are different, so the boundary conditions on ϕ are that ϕ and $(1/m^*)d\phi/dz$ be continuous at the interfaces (from the conservation of probability current density).

Application of these boundary conditions yields implicit equations for the wavevectors of the odd and even states

$$\frac{k_w}{m_w} \cot\left(\frac{k_w L}{2}\right) = -\frac{k_b}{m_b} \qquad\qquad (4)$$

and

$$\frac{k_w}{m_w} \tan\left(\frac{k_w L}{2}\right) = \frac{k_b}{m_b} \qquad\qquad (5)$$

respectively. Here m_w (m_b) is the mass in the well (barrier), and similarly for the wavevectors:

$$k_w = \sqrt{\frac{2 m_w E}{\hbar^2}} \qquad\qquad (6)$$

;

$$k_b = \sqrt{\frac{2m_b(V-E)}{\hbar^2}} \,.$$ (7)

The equations are solved numerically for the k's, which then give the energies E.

The remaining variable is the well depth V. The total band offset, which is the sum of the conduction and valence band offsets, was given in eqn. (1) above. The depths of the electron and hole wells are then determined by the ratio of the conduction to the valence band offset. The band offset ratio has been a point of controversy for some time now. The first optical measurements of Dingle[14] indicated that the conduction to valence band offset ratio is 85:15. Since then many measurements, both electrical and optical, have been made in an attempt to determine the band offset ratio. Most recent experiments indicate a ratio consistent with that of Wang *et.al.*,[51] who reported 0.62(±0.05):0.38(±0.02).

For the states where the carriers are confined to the wells (and if the wells of a multiple-QW structure are sufficiently well-separated that superlattice miniband formation can be ignored), the system is effectively two-dimensional. In this case the density of states for the electrons or holes is given by

$$\rho = \frac{m^*}{\pi\hbar^2} \quad (cm^{-2}eV^{-1})$$ (8)

where m* is the relevant effective mass. Hence at each QW

subband the density of states steps to a constant value, as shown in Fig. 1.3.
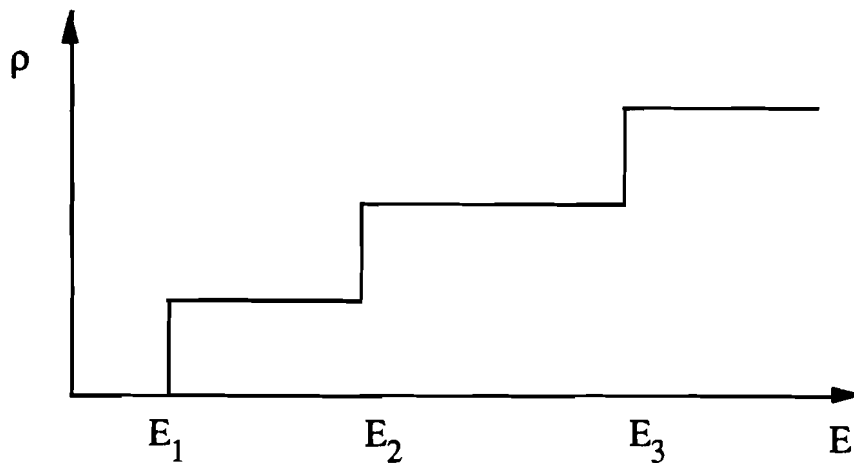
Figure 1.3. Density of states (in units of $m^*/\pi\hbar^2$) vs. energy.

In optical experiments, of course, electron-hole pairs are generated by absorption of light. The Coulomb interaction between the electrons and holes cannot be ignored. At low temperatures and carrier densities, the electrons and holes bind into excitons. At higher temperatures and densities, excitons quickly ionize (as will be discussed in chapter IV), but the electron and hole motion is still strongly correlated. The exciton problem for bulk GaAs has been treated in detail by Baldereschi and Lipari.[52] The binding energy of the 1s exciton state is 4 meV, and the Bohr radius is 150 Å. If the electrons and holes are confined to precisely two dimensions, then the exciton problem is analytically solvable; the solution has been given by Shinada and

Sugano.[53] The result is that the binding energy of the 1s state increases to 4x the 3-D binding energy, and the Bohr radius decreases by 1/4.

Of course, in real QW systems, the electrons and holes are confined in layers of nonzero thickness, with finite barrier height V. Thus the system is more properly described as quasi-two-dimensional. The exciton problem in this case cannot be solved exactly. Most solutions therefore have taken a variational approach. The Hamiltonian in cylindrical coordinates is[54,20]

$$H = -\frac{\hbar^2}{2m_e}\frac{\partial^2}{\partial z_e^2} + V_e(z_e) - \frac{\hbar^2}{2m_h}\frac{\partial^2}{\partial z_h^2} + V_h(z_h)$$

$$-\frac{\hbar^2}{2\mu_{\parallel}}\left(\frac{1}{\rho}\frac{\partial}{\partial\rho}\rho\frac{\partial}{\partial\rho} + \frac{1}{\rho^2}\frac{\partial^2}{\partial\phi^2}\right) - \frac{e^2}{\varepsilon\sqrt{\rho^2 + z^2}} \qquad (9)$$

where the transformation to the center-of-mass coordinates in the plane has been made, and the center-of-mass kinetic energy term has been dropped. In this expression m_e (m_h) is the electron (hole) effective mass in the growth direction z, and

$$\mu_{\parallel} = \frac{m_{e\parallel} m_{h\parallel}}{m_{e\parallel} + m_{h\parallel}} \qquad (10)$$

is the reduced effective mass in the QW plane. V_e and V_h are the conduction and valence band square-well potentials, respectively. Of course, there are two different excitons to be considered, the heavy and light hole excitons.

The most complete solution has probably been given by Greene, Bajaj, and Phelps.[54] They use a trial wavefunction of the form

$$U(r) = \phi_e(z_e)\, \phi_h(z_h)\, g(r), \qquad (11)$$

where the ϕ's are the electron and hole square well wavefunctions, and g is an appropriately chosen function which is used to variationally minimize the energy. Their results for the binding energy are shown in Fig. 1.4. The most important conclusions are first, that the binding energy is between the 3-D value of 4 meV and the 2-D value of 16 meV, and second, because the well depth is finite, the binding energy reaches a maximum value for a well width of about 50 Å. For much wider wells, the effect of the square well confining potential decreases, and the binding energy approaches the 3-D result. For narrower wells, the effect of the confining potential is again reduced, since in this case the single-particle wavefunctions have substantial amplitude in the barrier region; thus the exciton binding energy approaches the binding energy for bulk $Al_xGa_{1-x}As$ in the limit of very narrow wells.

The electronic structure of QW's in the presence of an electric field has also been a subject of great interest. A thorough study has been performed by Miller et. al.[20] Useful reviews may also be found in Chemla et. al.,[55] and Bastard and Brum.[20] Again, for the finite square well, the problem is not exactly solvable. Many methods have been applied to calculate the electronic states of a QW in an electric field. The most important result is that the
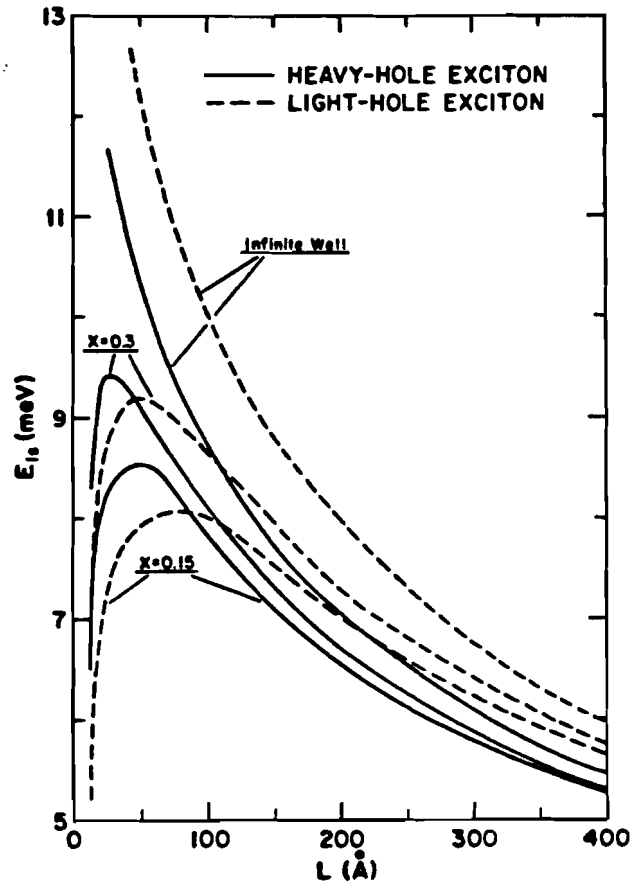
Figure 1.4. Calculated exciton ground state (1s) binding energy vs. well width L, for both infinite and finite barrier heights corresponding to Al compositions x=0.15 and 0.3. (From ref. 54).

electron and hole levels shift to lower energies, so that the optical absorption edge shifts to the red. For optical experiments, however, one must consider the exciton interaction, and this is important because in the presence of an electric field, the electrons and holes are spatially separated and hence the binding energy decreases. This tends to cancel the red shift of the continuum edge. Both effects of the field must be included in the calculation. Miller *et. al.*[20] have performed such a calculation, and found good agreement with optical absorption experiments (Fig. 1.5). Sha[56] has repeated the calculation for the very narrow wells
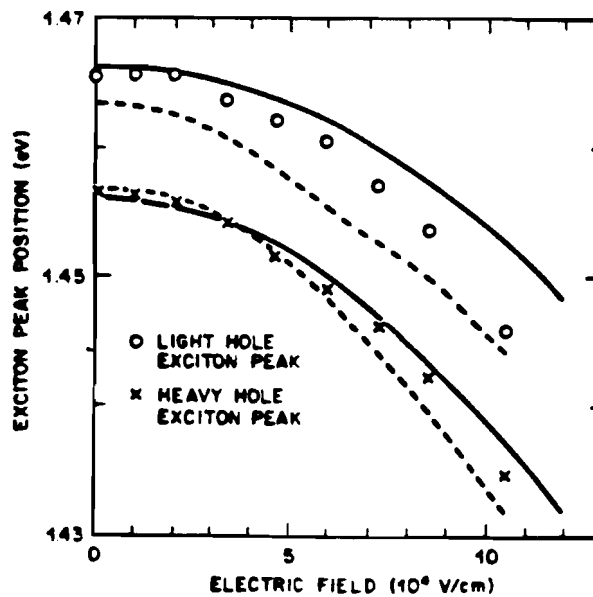
Figure 1.5. Quantum well exciton absorption peak positions vs. electric field. The solid lines are the calculated shifts assuming a conduction to valence band offset ratio of 57:43, and the dotted lines are the calculated shifts for a ratio of 85:15. (From ref. 20).

used in some of the experiments of this thesis (samples A and B described in section IV.A), and found the net shift to be quite small (a few meV, with the exciton binding energy shift essentially negligible). This is expected since for narrow wells the energy levels and binding energies cannot shift by much due to the strong spatial confinement of the wavefunctions.

I.B.3.   Optical Properties

The optical properties of QW's are of great interest both for fundamental investigations of QW physics, and for useful applications to optical and opto-electronic devices such as QW lasers and modulators. A comprehensive review of the optical properties of QW's has been given by Weisbuch.[17]

Photoluminescence (PL) is the simplest and most commonly used optical probe of QW's, mainly due to the ease of performing the experiments and the high quantum efficiency of QW luminescence. Another reason such experiments are useful is that the luminescence appears in high quality samples at cryogenic temperatures as a single strong line, which has been shown to originate from free excitons.[17] At higher temperatures free carrier recombination is also possible, and has been investigated by a number of groups,[57-59] but for the work described in this thesis, all the PL experiments are at low temperature (6K), and therefore monitor exciton luminescence.

The amount of information obtainable with just PL experiments is rather limited, however. The exciton origin (*i.e.* the QW continuum edge minus the binding' energy) can be obtained from the peak of the PL spectrum. The spectral lineshape, though, is still not well understood, although the linewidth has been used as an indication of interface quality.[60] Considerably more information can be obtained from the absorption spectrum, which directly probes the density of states of the QW structure. For interband (*i.e.* continuum) transitions, the linear absorption coefficient α is proportional to $|M_{cv}|^2 g(E)$, where M_{cv} is the interband **p** matrix element, and g is the joint density of states given by[55]

$$g = \frac{\mu_{\shortparallel}}{\pi \hbar^2} \theta (E\text{-}E_0) , \qquad (12)$$

where θ is the Heaviside step function, E_0 is the continuum edge energy, and $\mu_{\shortparallel}$ is the in-plane reduced mass defined above. Thus the basic form of the absorption spectrum is a series of steps corresponding to the confined QW energy levels.

At each continuum edge, however, the exciton effects radically alter the spectrum. The linear absorption coefficient for an exciton in state n is given by[61,62]

$$\alpha = B \sum_n |U_n(0)|^2 \delta (E_n \text{-} E_0 \text{-} \hbar \omega) , \qquad (13)$$

where B is a constant (which includes the square of the interband

dipole matrix element), and $U_n(0)$ is the amplitude of the exciton envelope wavefunction at the origin (*i.e.* the probability density for the electron and hole to be in the same unit cell). For the form of U given in eqn. (11), Miller *et. al.*[22] have shown that

$$\alpha = B \sum_{l,q,n} |<\phi_{e_l} | \phi_{h_q}>|^2 |g_n(0)|^2 \delta (E_l + E_q + E_n - E_0 - \hbar\omega),$$

where l and q are the quantum numbers for the square well electron and hole levels, respectively, and n is the exciton principal quantum number.

This results in strong absorption peaks below the continuum edge corresponding to bound exciton states, and an enhancement of the above-gap absorption due to the unbound states. The 1s exciton peak dominates, so the absorption spectrum generally shows two peaks, corresponding to the heavy and light hole 1s excitons, at each continuum step; this is clearly visible in the absorption spectrum shown in Fig. 1.6. It is also important to note that the enhanced exciton binding energy (combined with the reduced thermal broadening in 2-D[19]) allows the exciton peaks to be clearly observable even at room temperature.

A large number of studies have been performed of the linear absorption spectra (or alternatively, luminescence excitation spectra) to investigate the electronic and excitonic states of QW's. Of particular interest recently have been the states in the presence of an electric field.[20] For fields parallel to the QW plane, the results are essentially the same as for the 3-D case,
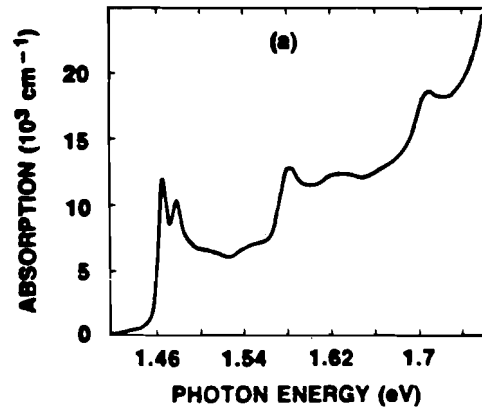
Figure 1.6. Absorption spectrum of a multiple-quantum well structure at room temperature, with well width of 100 Å. (From ref. 19)

where the exciton peak rapidly broadens and disappears due to field-induced ionization. For fields perpendicular to the plane, however, the situation is much more interesting. In this case the QW confinement prevents the exciton ionization up to very high fields ($\approx 10^5$ V/cm); hence substantial (25 meV) red shifts in the absorption edge can be observed before the exciton broadens and disappears. This is known as the quantum-confined Stark effect.[63] (The shift of the edge vs. field was shown in Fig. 1.5). Miller has taken advantage of this field-induced shift to produce optical modulators and novel bistable devices called SEED's ("self-electrooptic effect devices").[23]

In this thesis I am not so much concerned with the linear absorption, but rather with the nonlinear absorption, since the intention is to use absorption as a probe of QW populations. The basic idea is that carriers will block interband transitions as

$$\alpha = \alpha_0 (1 - f_e - f_h) \ . \tag{14}$$

Here α_0 is the absorption coefficient without carriers present, and f_e (f_h) is the distribution function of the electrons (holes). Thus absorption spectroscopy directly probes carrier distribution functions. The situation is somewhat complicated by the fact that the position of the continuum edge lowers in energy as the carrier density increases. This is a many-body effect that is referred to as bandgap renormalization.[64,65] Furthermore, the presence of carriers screens the Coulomb interaction, thus reducing the exciton oscillator strength. This bleaching of the absorption profile via screening of the exciton occurs at much lower carrier densities than the saturation of the interband absorption. The precise mechanisms of the absorption saturation are discussed by Chemla, Miller, and Schmitt-Rink.[19,66] How this nonlinear absorption may be used to probe QW carrier populations is further discussed in chapter IV, section C.1.

I.C. Time-Resolved Optical Studies of GaAs/AlGaAs Quantum Wells

In this section I give an overview of previous applications of time-resolved optical spectroscopy to the study of carrier dynamics in QW's. All of the experiments described in this section were performed to probe the dynamics of carriers within isolated QW's. I will discuss experiments that probe transport perpendicular to the QW planes in the next section.

Time-resolved PL has been used to determine the recombination time of free carriers in photoexcited QW's.[57-59] Decay times of a few ns are typically observed, depending on the temperature, carrier density, and well width. Carrier trapping and trap saturation have been shown to be important processes contributing to the density dependence of the decay rate.[67,68] Time-resolved PL has also been used to investigate recombination at low temperatures, where the luminescence is excitonic.[69,70] Recombination times of about 350-800 ps, depending on the well width, are observed. The faster recombination of QW excitons compared to that for bulk GaAs (≈ 1 ns) is attributed to the enhanced confinement of the exciton in the quasi-2-D QW. Time-resolved PL has also been used to investigate exciton transport dynamics in the QW plane.[71] I believe it is important to note that (to my knowledge), there have still been no careful experiments

performed to understand the rise time of QW. excitonic luminescence.

Thermalization and cooling of hot carriers in QW's have been a subjects of considerable interest in the last few years.[72-74] Time-resolved PL has been used to probe the time dependence of hot luminescence from photoexcited QW's.[75,76] Cooling rates of hot carriers may be directly determined this way, but the results depend strongly on the initial carrier temperature (*i.e.* on the pump laser wavelength) and injected carrier density. Time-resolved absorption spectroscopy has also been used to probe the picosecond and femtosecond dynamics of hot carriers,[77] and the use of short (100 fs) optical pulses has enabled the generation and observation of nonthermal carrier distributions.[78] The basic picture of carrier relaxation in QW's that emerges from these studies is as follows. A short optical pulse generates a nonthermal carrier distribution corresponding to the pulse spectrum, as the conduction and valence band states coupled by the optical pulse are filled. Within about 200 fs (depending on the carrier density and initial excess energy), the electron and hole distributions have thermalized, principally by carrier-carrier scattering. These distributions are described by temperatures that are (for most experiments) higher than the lattice temperature, so the carriers subsequently cool by interaction with the lattice phonons. The observed cooling rates vary widely, but are typically in the 10^{10} s^{-1} range. Carrier thermalization and cooling are complicated

physical processes, and their understanding is still a very active field of research.

The above-discussed experiments on carrier cooling all assume a single subband in the QW (*i.e.* they measure intrasubband relaxation). Seilmeir *et. al.*[79] have used time-resolved infrared spectroscopy to directly measure the intersubband relaxation rate in an n-doped QW. They found the n=2 to n=1 subband relaxation time to be about 10 ps at room temperature.

Several interesting experiments have probed the dynamics of resonantly and virtually created excitons. Knox *et. al.*[80] resonantly pumped the exciton origin of a room-temperature multiple-QW structure with 100-fs optical pulses, and found that the screening of the exciton by other excitons is about twice as efficient as the screening by free carriers. Hence the ionization of the exciton, which at room temperature occurs in about 300 fs, was directly observed as an overshoot in the differential absorption spectrum. (I will discuss this further in chapter IV.) Mysyrowicz *et. al.*[81] and Von Lehmen *et. al.*[82] pumped multiple-QW structures below the exciton absorption, and found that the excitonic absorption peak shifts to the blue with a temporal dependence following the excitation pulse envelope. The dependence of the blue shift on the detuning of the pump from the exciton resonance and on the intensity of the pump indicated that the effect was due to an ac-Stark effect on the ground state of

the exciton. The ac-Stark effect is a well-known phenomenon in atomic physics, and is due to the "dressing" of the atomic levels by the laser pump field.[83] Schmitt-Rink and Chemla[84] have shown how the ac-Stark effect in a semiconductor may be interpreted as being due to the generation of "virtual" excitons by the nonresonant pump beam. The field of coherent optical interactions with semiconductors is still quite young, and promises to be of great interest for both fundamental studies and practical applications of QW's.

I.D. Tunneling Studies of QW Structures

In this section I briefly describe previous work investigating tunneling processes in QW's. As I mentioned previously, several studies performed concurrently with the work presented in this thesis have begun to address the question of the time-dependence of tunneling and perpendicular transport using time-domain optical techniques. Tsuchiya *et. al.*[85] used time-resolved PL to observe tunneling in a DBD structure with thin AlAs barriers, and found that for sufficiently thin barriers, the observed rate was reasonably close to the value calculated with a simple theory similar to the one I present in chapter III. Whitaker *et. al.*[86] used electro-optic sampling to measure the switching time of a DBD. Tada *et. al.*[87] have investigated electron tunneling in a coupled-QW structure using time-resolved PL, however there are several

significant differences between their experiment and those reported here. The most significant differences are that the time resolution of their system was only 300 ps, so the tunneling was not clearly resolved, and that their sample was not designed to allow the application of an electric field. Furthermore, they do not display the full time-resolved spectrum.

Time-resolved PL has also been applied to the study of perpendicular transport in superlattice structures. Masumoto *et. al.*[88] have investigated the tunneling of electrons from the QW's of a multiple-QW structure (which may be thought of as a weakly-coupled superlattice). Deveaud *et. al.*[32,33] have investigated perpendicular transport in strongly and weakly coupled superlattices, and found evidence that for sufficiently strong coupling (*i.e.* for narrow barriers) the transport does take place as Bloch transport through the superlattice miniband.

As I mentioned in the introduction to this chapter, most studies of tunneling in QW structures have investigated the tunnel current. The vast majority of tunneling studies in QW's have been concerned with the DBD structure, which is interesting from both fundamental and practical points of view due to the large NDR such structures exhibit. I conclude this introductory chapter with a description of the origin of the NDR.

The conduction band of a typical DBD structure is shown in Fig. 1.7. The GaAs continuum regions on each side of the double barrier are n-doped to about 10^{18} cm^{-3} (the Fermi sea of electrons
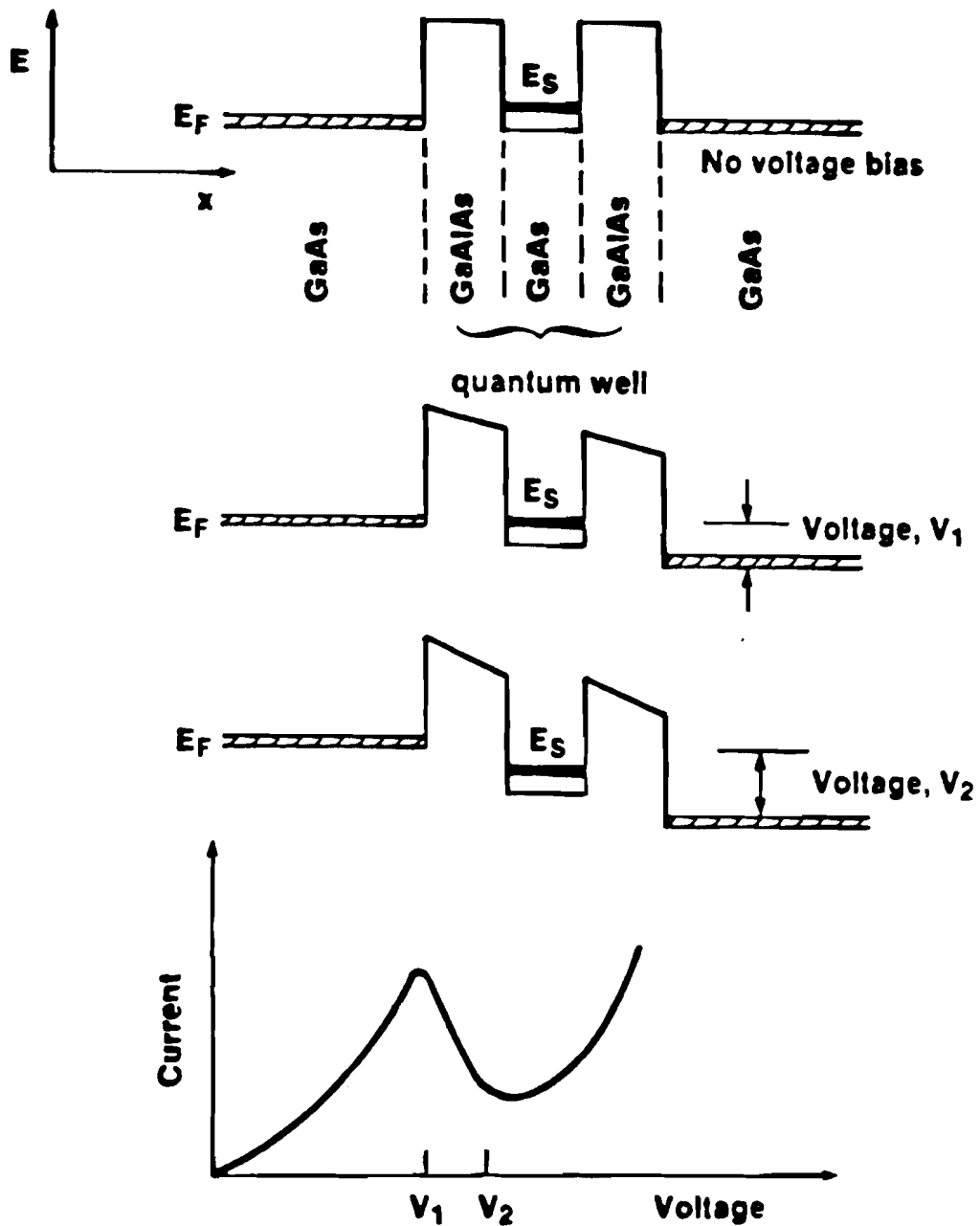
Figure 1.7. Double-barrier diode structure and operation. The peak tunneling current occurs at a bias of V_1, and the minimum at V_2. E_F denotes the Fermi level in the continuum regions. (From ref. 88).

is indicated by the hatched regions of Fig. 1.7); these serve as the emitter and collector contact electrodes. Under flat-band conditions and at low bias voltages the confined QW state is above the Fermi level of the continuum region. Hence the electron wave is evanescent in the entire barrier/QW region, and the tunneling probability is small, leading to a small current through the diode at low bias. When the applied bias V_1 is sufficient that the bottom of the emitter conduction band is aligned with the confined QW state, a resonant probability amplitude can build up inside the well (since the wavevector of the incident electron is now real inside the well). This greatly enhances the tunneling probability through the double barrier and leads to a large current at V_1. As the bias is increased further (V_2), the QW level drops below the emitter band edge, and electrons can no longer tunnel into the well while still conserving their momentum parallel to the QW plane (*i.e.* the electron wave is again evanescent). Hence the tunneling current drops, leading to the NDR. As the bias is increased further, the current slowly increases as the barrier height to the incident electrons effectively lowers.

Of course, the tunneling in real DBD's is much more complicated, particularly since the above description ignores all scattering processes that can occur. The precise dynamics of the tunneling in these structures is still an open question. I give a further discussion of this question and a complete set of references at the beginning of chapter III.

I.E. References

1. R.H. Fowler and W. Nordheim, "Electron Emission in Intense Electric Fields," Proc. Roy. Soc., A **119**, 173 (1928).

2. E. Burstein and S. Lundqvist, eds., <u>Tunneling Phenomena in Solids</u>, (Plenum, New York, 1969).

3. C.B. Duke, <u>Tunneling in Solids</u>, (Academic Press, New York, 1969).

4. L. Esaki, "New Phenomenon in Narrow Germanium p-n Junctions," Phys. Rev. **109**, 603 (1957).

5. B. Chance *et. al.*, eds., <u>Tunneling in Biological Systems</u>, (Academic, New York, 1979).

6. A qualitative discussion of hopping transport is given in O. Madelung, <u>Introduction to Solid State Theory</u>, (Springer-Verlag, Berlin, 1978), pp. 447-456.

7. L. Esaki and R. Tsu, "Superlattice and Negative Conductivity in Semiconductors," IBM Res. Note, RC-2418, 1969.

8. L. Esaki, "A Bird's-Eye View on the Evolution of Semiconductor Superlattices and Quantum Wells," IEEE J. Quant. Electron. **QE-22**, 1611 (1986).

9. A concise review and introduction to the literature on MBE is given in A.C. Gossard, "Growth of Microstructures by Molecular Beam Epitaxy," IEEE J. Quant. Electron. **QE-22**,1649 (1986).

10. G.C. Osbourn, P.L. Gourley, I.J. Fritz, R.M. Biefeld, L.R. Dawson, and T.E. Zipperian, "Principles and Applications of Semiconductor Strained-Layer Superlattices," in <u>Applications of Multiquantum Wells, Selective Doping, and Superlattices</u>, Semiconductors and Semimetals vol 24, ed. by R. Dingle (Academic, San Diego, 1987).

11. L.A. Kolodziejski, R.L. Gunshor, N. Otsuka, S. Datta, W.M. Becker, and A.V. Nurmikko, "Wide-Gap II-VI Superlattices," IEEE J. Quant. Electron. **QE-22**, 1666 (1986).

12. L. Esaki, L.L. Chang, W.E. Howard, and V.L. Rideout, "Transport Properties of a GaAs-GaAlAs Superlattice," Proc. 11th Int. Conf. Phys. Semiconductors, Warsaw, Poland, 1972, pp. 431-436.

13. L.L. Chang, L. Esaki, and R. Tsu, "Resonant Tunneling in Semiconductor Double Barriers," Appl. Phys. Lett. **24**, 593 (1974).

14. R. Dingle, W. Wiegmann, and C.H. Henry, "Quantum States of Confined Carriers in Very Thin $Al_xGa_{1-x}As$-GaAs-$Al_xGa_{1-x}As$ Heterostructures," Phys. Rev. Lett. **33**, 827 (1974).

15. K. von Klitzing, G. Dorda, and M. Pepper, "New Method for High-Accuracy Determination of the Fine-Structure Constant Based on Quantized Hall Resistance," Phys. Rev. Lett. **45**, 494 (1980).

16. D.C. Tsui, H.L. Störmer, and A.C. Gossard, "Two-Dimensional Magneto-Transport in the Extreme Quantum Limit," Phys. Rev. Lett. **48**, 1559 (1982).

17. C. Weisbuch, "Fundamental Properties of III-V Semiconductor Two-Dimensional Quantized Structures: The Basis for Optical and Electronic Device Applications," in Applications of Multiquantum Wells, Selective Doping, and Superlattices, Semiconductors and Semimetals vol 24, ed. by R. Dingle, (Academic, San Diego, 1987), pp. 78-91.

18. R. Dingle, "Confined carrier Quantum States in Ultrathin Semiconductor Heterostructures," Festkorperprobleme 15, 21 (1975).

19. D.S. Chemla and D.A.B. Miller, "Room Temperature Excitonic Nonlinear-Optical Effects in Semiconductor Quantum-Well Structures," J. Opt. Soc. Am. B 2, 1155 (1985).

20. D.A.B. Miller, D.S. Chemla, T.C. Damen, A.C. Gossard, W. Wiegmann, T.H. Wood, and C.A. Burrus, "Electric Field Dependence of Optical Absorption Near the Band Gap of Quantum Well Structures," Phys. Rev. B 32, 1043 (1985).

21. T.H. Wood, C.A. Burrus D.A.B. Miller, D.S. Chemla, T.C. Damen, A.C. Gossard, and W. Wiegmann, "High Speed Optical Modulation with GaAs/GaAlAs Quantum Wells in a p-i-n Diode Structure," Appl. Phys. Lett. 44, 16 (1984).

22. D.A.B. Miller, J.S. Weiner, and D.S. Chemla, "Electric-Field Dependence of Linear Optical Properties in Quantum Well Structures: Waveguide Electroabsorption and Sum Rules," IEEE J. Quant. Electron. QE-22, 1816 (1986).

23. D.A.B. Miller, D.S. Chemla, T.C. Damen, A.C. Gossard, W. Wiegmann, T.H. Wood, and C.A. Burrus, "The Quantum Well Self-Electro-Optic Effect Device," Appl. Phys. Lett. 45, 13 (1984).

24. H.C. Casey and M.B. Panish, <u>Heterostructure Lasers</u>, (Academic Press, San Diego, 1978).

25. Y. Arakawa and A. Yariv, "Quantum Well Lasers - Gain, Spectra, Dynamics," IEEE J. Quant. Electron. **QE-22**, 1887 (1986).

26. W.T. Tsang, "Quantum Confinement Heterostructure Semiconductor Lasers," in <u>Applications of Multiquantum Wells, Selective Doping, and Superlattices</u>, Semiconductors and Semimetals vol 24, ed. by R. Dingle (Academic, San Diego, 1987).

27. E.E. Mendez, "Electronic Mobility in Semiconductor Heterostructures," IEEE J. Quant. Electron. **QE-22**, 1721 (1986).

28. The literature of this field is immense; several reviews may be found in <u>Applications of Multiquantum Wells, Selective Doping, and Superlattices</u>, Semiconductors and Semimetals vol 24, ed. by R. Dingle, (Academic, San Diego, 1987).

29. Y.-C. Chang, L.L. Chang, and L. Esaki, "A New One-Dimensional Quantum Well Structure," Appl. Phys. Lett. **47**, 1324 (1985).

30. J. Cibert, P.M. Petroff, G.J. Dolan, S.J. Pearton, A.C. Gossard, and J.H. English, "Optically Detected Carrier Confinement to One and Zero Dimension in GaAs Quantum Well Wires and Boxes," Appl. Phys. Lett. **49**, 1275 (1986).

31. M.A. Reed, J.N. Randall, R.J. Aggarwal, R.J. Matyi, T.M. Moore, and A.E. Wetsel, "Observation of Discrete Electronic States in a

Zero-Dimensional Semiconductor Nanostructure," Phys. Rev. Lett. **60**, 535 (1988).

32. B. Devaud, J. Shah, T.C. Damen, B. Lambert, and A. Regreny, "Bloch Transport of Electrons and Holes in Superlattice Minibands: Direct Measurement by Luminescence Spectroscopy," Phys. Rev. Lett. **58**, 2582 (1987).

33. B. Devaud, J. Shah, T.C. Damen, B. Lambert, A. Chomette, and A. Regreny, "Optical Studies of Perpendicular Transport in Semiconductor Superlattices," IEEE J. Quant. Electron. **QE-24**, 1641 (1988).

34. T.C.L.G. Sollner, E.R. Brown, W.D. Goodhue, and H.Q. Le, "Observation of Millimeter-Wave Oscillations From Resonant Tunneling Diodes and Some Theoretical Considerations of Ultimate Frequency Limits," Appl. Phys. Lett. **50**, 332 (1987).

35. T.C.L.G. Sollner, W.D. Goodhue, P.E. Tannenwald, C.D. Parker, and D.D. Peck, "Resonant Tunneling Through Quantum Wells at Frequencies up to 2.5 THz," Appl. Phys. Lett. **43**, 588 (1983).

36. S.L. Shapiro, ed., Ultrashort Light Pulses, (Springer, Berlin, 1977).

37. J. Herrmann and B. Wilhelmi, Lasers for Ultrashort Light Pulses, (North-Holland, Amsterdam, 1987).

38. C.V. Shank, E.P. Ippen, and S.L. Shapiro, eds., Picosecond Phenomena I, (Springer, Berlin, 1978).

39. R.M. Hochstrasser, W. Kaiser, and C.V. Shank, eds., Picosecond Phenomena II, (Springer, Berlin, 1980).

40. K.B. Eisenthal, R.M. Hochstrasser, W. Kaiser, and A. Laubereau, eds., Picosecond Phenomena III, (Springer, Berlin, 1982).

41. D.H. Auston and K.B. Eisenthal, eds., Ultrafast Phenomena IV, (Springer, Berlin, 1984).

42. G.R. Fleming and A.E. Siegman, eds., Ultrafast Phenomena V, (Springer, Berlin, 1986).

43. J. Valdmanis, R.L. Fork, and J.P. Gordon, " Generation of Optical Pulses as Short as 27 Femtoseconds Directly from a Laser Balancing Self-Phase Modulation, Group Velocity Dispersion, Saturable Absorption, and Saturable Gain," Opt. Lett. 10, 131 (1985).

44. R.L. Fork, C.H. Brito Cruz, P.C. Becker, and C.V. Shank, "Compression of Optical Pulses to Six Femtoseconds by Using Cubic Phase Compensation," Opt. Lett. 12, 483 (1987).

45. M.C. Adams, W. Sibbett, and D.J. Bradley, "Linear Picosecond Electron-Optical Chronoscopy at a Repetition Rate of 140 MHz," Optics Commun. 26, 273 (1978).

46. R.L. Fork, C.V. Shank, C. Hirlimann, R. Yen, and W.J. Tomlinson, "Femtosecond White-Light Continuum Pulses," Optics Lett. 8, 1 (1983).

47. W.H. Knox, M.C. Downer, R.L. Fork, and C.V. Shank, "Amplified Femtosecond Optical Pulses and Continuum Generation at a 5-kHz Repetition Rate," Opt. Lett. 9, 552 (1984).

48. I.N. Duling III, T. Norris, T. Sizer II, P. Bado, and G.A. Mourou, "KiloHertz Synchronous Amplification of 85-Femtosecond Optical Pulses," J. Opt. Soc. Am. B **2**, 616 (1985).

49. G. Bastard and J.A. Brum, "Electronic States in Semiconductor Heterostructures," IEEE J. Quant. Electron. **QE-22**, 1625 (1986).

50. H.C. Casey and M.B. Panish, *op. cit.* Part A, p. 192.

51. W.I. Wang, E.E. Mendez, and F. Stern, "High Mobility Hole Gas and Valence-Band Offset in Modulation-Doped p-AlGaAs/GaAs Heterojunctions," Appl. Phys. Lett. **45**, 639 (1984).

52. A. Baldereschi and N.O. Lipari, "Energy Levels of Direct Excitons in Semiconductors with Degenerate Bands," Phys. Rev. B **3**, 439 (1971).

53. M. Shinada and S. Sugano, "Interband Optical Transitions in Extremely Anisotropic Semiconductors. I. Bound and Unbound Exciton Absorption," J. Phys. Soc. of Japan **21**, 1936 (1966).

54. R.L. Greene, K.K. Bajaj, and D.E. Phelps, "Energy Levels of Wannier Excitons in GaAs-Ga$_{1-x}$Al$_x$As Quantum-Well Structures," Phys. Rev. B **29**, 1807 (1984).

55. D.S. Chemla, D.A.B. Miller, and P.W. Smith, "Nonlinear Optical Properties of Multiple Quantum Well Structures for Optical Signal Processing," in Applications of Multiquantum Wells, Selective Doping, and Superlattices, Semiconductors and Semimetals vol 24, ed. by R. Dingle (Academic, San Diego, 1987).

56. W. Sha, private communication, 1988.

57. J.E. Fouquet and A.E. Siegman, "Room-Temperature Photoluminescence Times in a GaAs/Al$_x$Ga$_{1-x}$As Molecular Beam Epitaxy Multiple Quantum Well Structure," Appl. Phys. Lett. **46**, 280 (1985).

58. Y. Arakawa, H. Sakaki, M. Nishioka, J. Yoshino, and T. Kamiya, "Recombination Lifetime of Carriers in GaAs-GaAlAs Quantum Wells Near Room Temperature," Appl. Phys. Lett. **46**, 519 (1985).

59. T. Matsusue and H. Sakaki, "Radiative Recombination Coefficient of Free Carriers in GaAs-AlGaAs Quantum Wells and its Dependence on Temperature," Appl. Phys. Lett. **50**, 1429 (1987).

60. H. Sakaki, M. Tanaka, and J. Yoshino, "One Atomic Layer Heterointerface Fluctuations in GaAs-AlAs Quantum Well Structures and Their Suppression by Insertion of Smoothing Period in Molecular Beam Epitaxy," Jpn. J. Appl. Phys. **24**, L417 (1985).

61. R.J. Elliot, "Intensity of Optical Absorption by Excitons," Phys. Rev. **106**, 1384 (1957).

62. R.S. Knox, Theory of Excitons, (Academic Press, New York, 1963), p. 120.

63. D.A.B. Miller, D.S. Chemla, T.C. Damen, A.C. Gossard, W. Wiegmann, T.H. Wood, and C.A. Burrus, "Band-Edge Electroabsorption in Quantum Well Structures: The Quantum-Confined Stark Effect," Phys. Rev. Lett. **53**, 2173 (1984).

64. H. Haug and S. Schmitt-Rink, "Basic Mechanisms of the Optical Nonlinearities of Semiconductors Near the Band Edge," J. Opt. Soc. Am. B **2**, 1135 (1985).

65. G. Tränkle, H. Leier, A. Forchel, H. Haug, C. Ell, and G. Weimann, "Dimensionality Dependence of the Band-Gap Renormalization in Two- and Three-Dimensional Electron-Hole Plasmas in GaAs," Phys. Rev. Lett. **58**, 419 (1987).

66. S. Schmitt-Rink, D.S. Chemla, and D.A.B. Miller, "Theory of Transient Excitonic Optical Nonlinearities in Semiconductor Qauntum-Well Structures," Phys. Rev. B **32**, 6601 (1985).

67. J.E. Fouquet, A.E. Siegman, R.D. Burnham, and T.L. Paoli, "Carrier Trapping in Room-Temperature, Time-Resolved Photoluminescence of a $GaAs/Al_xGa_{1-x}As$ Multiple Quantum Well Structure Grown by Metalorganic Chemical Vapor Deposition," Appl. Phys. Lett. **46**, 374 (1985).

68. J.E. Fouquet and R.D. Burnham, "Recombination Dynamics in $GaAs/Al_xGa_{1-x}As$ Quantum Well Structures," IEEE J. Quant. Electron. **QE-22**, 1799 (1986).

69. E.O. Göbel, H. Jung, J. Kuhl, and K. Ploog, "Recombination Enhancement Due to Carrier Localization in Quantum Well Structures," Phys. Rev. Lett. **51**, 1588 (1983).

70. J. Christen, D. Bimberg, A. Steckenborn, and G. Weimann, "Localization Induced Electron-Hole Transition Rate Enhancement in GaAs Quantum Wells," Appl. Phys. Lett. **44**, 84 (1984).

71. B. Deveaud, T.C. Damen, J. Shah, and C.W. Tu, "Dynamics of Exciton Transfer Between Monolayer-Flat Islands in Single Quantum Wells," Appl. Phys. Lett. **51**, 828 (1987).

72. J. Shah, "Hot Carriers in Quasi-2-D Polar Semiconductors," IEEE J. Quant. Electron. **QE-22**, 1728 (1986).

73. S.A. Lyon, "Thermalization of Hot Carriers in Quantum Wells," Superlattices and Microstructures **3**, 261 (1987).

74. J. Shah and G.J. Iafrate, eds., Hot Carriers in Semiconductors, Solid State Electronics **31** (1988).

75. J.F. Ryan, R.A. Taylor, A.J. Turberfield, A. Maciel, J.M. Worlock, A.C. Gossard, and W. Wiegmann, "Time-Resolved Photoluminescence of Two-Dimensional Hot Carriers in GaAs-AlGaAs Heterostructures," Phys. Rev. Lett. **53**, 1841 (1984).

76. H.-J. Polland, W.W. Rühle, J. Kuhl, K. Ploog, K. Fujiwara, and T. Nakayama, "Nonequilibrium Cooling of Thermalized Electrons and Holes in GaAs/Al$_x$Ga$_{1-x}$As Quantum Wells," Phys. Rev. B **35**, 8273 (1987).

77. C.V. Shank, R.L. Fork, R. Yen, J. Shah, B.I. Greene, A.C. Gossard, and C. Weisbuch, "Picosecond Dynamics of Hot Carrier Relaxation in Highly Excited Multi-Quantum Well Structures," Solid State Commun. **47**, 981 (1983).

78. W.H. Knox, C. Hirlimann, D.A.B. Miller, J. Shah, D.S. Chemla, and C.V. Shank, "Femtosecond Excitation of Nonthermal Carrier Populations in GaAs Quantum Wells," Phys. Rev. Lett. **56**, 1191 (1986).

79. A. Seilmeier, H.-J. Hübner, G. Abstreiter, G. Weimann, and W. Schlapp, "Intersubband Relaxation in GaAs-$Al_xGa_{1-x}As$ Quantum Well Structures Observed Directly by an Infrared Bleaching Technique," Phys. Rev. Lett. **59**, 1345 (1987).

80. W.H. Knox, R.L. Fork, M.C. Downer, D.A.B. Miller, D.S. Chemla, and C.V. Shank, "Femtosecond Dynamics of Resonantly Excited Excitons in Room Temperature GaAs Quantum Wells," Phys. Rev. Lett. **54**, 1306 (1985).

81. A. Mysyrowicz, D. Hulin, A. Antonetti, A. Migus, W.T. Masselink, and H. Morkoc, ""Dressed Excitons" in a Multiple-Quantum-Well Structure: Evidence for an Optical Stark Effect with Femtosecond Response Time," Phys. Rev. Lett. **56**, 2748 (1986).

82. A. Von Lehmen, D.S. Chemla, J.E. Zucker, and J.P. Heritage, "Optical Stark Effect on Excitons in GaAs Quantum Wells," Optics Lett. **11**, 609 (1986).

83. See, for example, P.L. Knight and P.W. Milonni, "The Rabi Frequency in Optical Spectra," Phys. Rep. **66**, 22 (1980).

84. S. Schmitt-Rink and D.S. Chemla, "Collective Excitations and the Dynamical Stark Effect in a Coherently Driven Exciton System," Phys. Rev. Lett. **57**, 2752 (1986).

85. M. Tsuchiya, T. Matsusue, and H. Sakaki, "Tunneling Escape Rate of Electrons From a Quantum Well in Double-Barrier Heterostructures," Phys. Rev. Lett. **59**, 2356 (1987).

86. J.F. Whitaker, G.A. Mourou, T.C.L.G. Sollner, and W.D. Goodhue, "Picosecond Switching Time Measurement of a Resonant Tunneling Diode," Appl. Phys. Lett. **53**, 385 (1988).

;

87. T. Tada, A. Yamaguchi, T. Ninomiya, H. Uchiki, T. Kobayashi, and T.Yao, " Tunneling Process in AlAs/GaAs Double Quantum Wells Studied by Photoluminescence," J. Appl. Phys. **63**, 5491 (1988).

88. J.F. Whitaker, "Ultrafast Electrical Signals: Transmission on Broadband Guiding Structures and Transport in the Resonant Tunneling Diode," Ph.D. Thesis, University of Rochester, 1988, (unpublished).

89. J.S. Blakemore, "Semiconducting and Other Major Properties of Gallium Arsenide," J. Appl. Phys. **53**, R123 (1982).

CHAPTER II

EXPERIMENTAL DEVELOPMENT

The experiments discussed in this thesis are of two kinds: time-resolved photoluminescence spectroscopy and time-resolved absorption spectroscopy. The former is useful to investigate dynamical processes in the temporal range 20 ps - 1 ns. The latter is capable of giving a time resolution of less than 100 fs. In this chapter I describe in detail the experimental apparatus used to take the data presented in chapters III and IV. Needless to say, the major proportion of an experimental thesis consists of the development and refinement of experimental equipment and techniques. Indeed the laser developed for the femtosecond absorption spectroscopy in our laboratory was of a novel design, which has since been duplicated in several laboratories around the world. However, in this chapter I will discuss only the final setup used to perform the experiments described in this thesis, and will not discuss the innumerable studies and permutations of dye lasers and amplifiers which culminated in the femtosecond absorption spectroscopy setup presented here. Many details of the early experimental development in our laboratory can be found in the dissertations of J.D. Kafka,[1] I.N. Duling,[2] and T. Sizer.[3]

II.A.   Time-Resolved Photoluminescence

II.A.1.   Laser Oscillator

The dye laser used in the time-resolved photoluminescence (PL) experiments was of a standard design. The pump source was a cw mode-locked Nd:YAG laser (Quantronix model 116, mounted on a Super-Invar slab for high thermal and mechanical stability). The Nd:YAG laser was acousto-optically mode-locked with a 50 MHz RF source, and the laser repetition rate was 100 MHz. Typical output parameters were 7-watt average power, 80-ps pulse width, and 1% peak-to-peak power fluctuations. The output was frequency-doubled in a 5mm KTP crystal, giving an average green power of 0.8-1.0 watt. As was first shown by Sizer *et.al.*,[4] the frequency-doubled cw mode-locked Nd:YAG laser is a nearly ideal pump source for picosecond dye lasers because of its high stability, short pulse width, and, as I will discuss later, it makes possible high gain synchronous amplification of short pulses.

The dye laser cavity was a standard folded astigmatically compensated design,[5] with cavity length equal to that of the Nd:YAG pump laser, so the repetition rate was also 100 MHz. The laser setup is shown in Fig. 2.1. Laser dyes LDS 721 or LDS 698 (Pyridine 1) were used depending on the desired pump wavelength. The laser was tuned with a single-plate birefringent filter (Lyot) and (if necessary to force the laser to operate at a
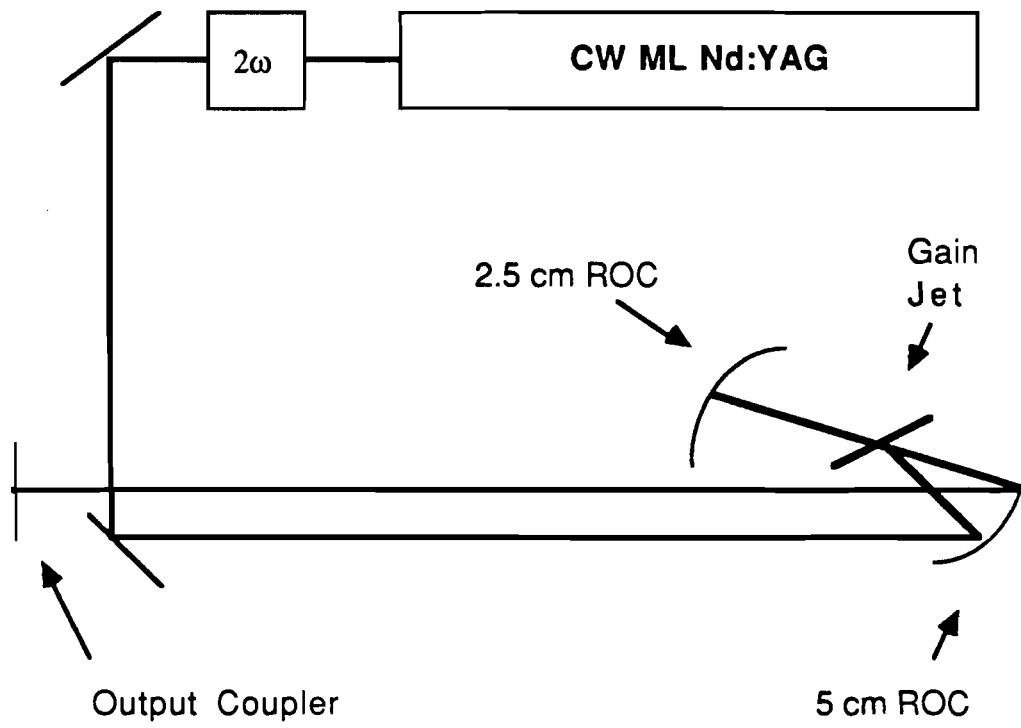
Figure 2.1. Synchronously pumped near-infrared dye laser used for time-resolved photoluminescence studies.

single wavelength near the edge of its tuning range), a 5 μm uncoated pellicle. The output power and pulse width depended of course on the laser wavelength and tuning elements in the cavity. What is important for the PL experiments, however, is that the pulse width was always shorter than the 20 ps time resolution of the streak camera, and the output power generally had to be kept lower than about 60 mW to avoid the generation of satellite pulses.

II.A.2   Cryogenics

The PL experiments were always carried out with the sample held at 6K. This was required for two reasons: (i) low temperatures were required for the PL signal level to be strong enough to be detectable by the streak camera detection system with reasonable signal integration times, and (ii), I wanted to avoid as much as possible complications that arise at higher temperatures, such as phonon effects and the effects due to broad carrier distribution functions.

The cryostat was a TRI Research model RC110 flow cryostat. The sample was held in vacuum on an oxygen-free copper cold finger. Electrical vacuum feedthroughs were provided so that a bias voltage could be applied to the sample. A calibrated silicon diode (Cryocal model DT-500) was used to monitor the

temperature of the cold finger near the sample; for all the experiments reported here the temperature was 6K.

The laser beam was focussed onto the sample surface, usually with a 152 mm focal length lens. The spot size of the pump beam at focus was measured by scanning a 12.5 μm pinhole across the beam at the same position as the sample. The pinhole was scanned using a computer-controlled stepper with 1 μm resolution. The light passing through the pinhole was detected with a PIN diode, integrated on an A/D converter, and stored in the computer. (A description of the data acquisition software may be found in ref. 6). The spot diameter was typically 30-60 μm, though the error in the measurement was about -5%, +40%, due primarily to the difficulty of positioning the pinhole at precisely the location of the sample in the cryostat.

II.A.3.   Time-Integrated PL Spectroscopy

Luminescence from the sample was collected by an f3 lens. For time-integrated (cw) PL spectroscopy, the luminescence was imaged through a .32m grating monochromator with 300 l/mm grating (Instruments SA model HR320) onto an optical multichannel analyzer (OMA). The OMA detector head was an EG&G PAR model 1420R, which is an intensified 1024-element diode array with extended red sensitivity. The OMA was controlled using an EG&G model 1461 controller interfaced to the

PDP-11 computer via a direct-memory-access (DMA) board. A shutter in the pump beam was used to enable subtraction of background noise from the spectrum. The spectral resolution of the system was 7 Å (1.3 meV), and the spectral range covered on a single spectrum was 2160 Å (365 meV).

II.A.4. Time-Resolved PL Spectroscopy

The PL spectroscopy system is shown in Fig. 2.2. A mirror on a kinematic mount was used so that the PL could be directed to either the OMA for cw spectroscopy, or the streak camera for time-resolved studies. The streak camera was a Hamamatsu model C1587 with model M1955 synchroscan drive unit. The output of a PIN photodiode monitoring the output of the Nd:YAG laser oscillator was amplified, and this 100 MHz RF was used to drive the deflection plates of the synchroscan streak camera. Thus the PL signal arriving at the streak camera photocathode at 100 MHz was synchronized to the voltage driving the deflection plates (hence the term "synchroscan"). The jitter between the deflection plate voltage and the dye laser output is the principal limitation on the time resolution of the streak camera system. For typical signal integration times (1 second to a few minutes) this jitter limits the time resolution to about 20 ps.

The photocathode was an extended-red S-1 type, which covers the spectral region 300-1500 nm. The streak camera
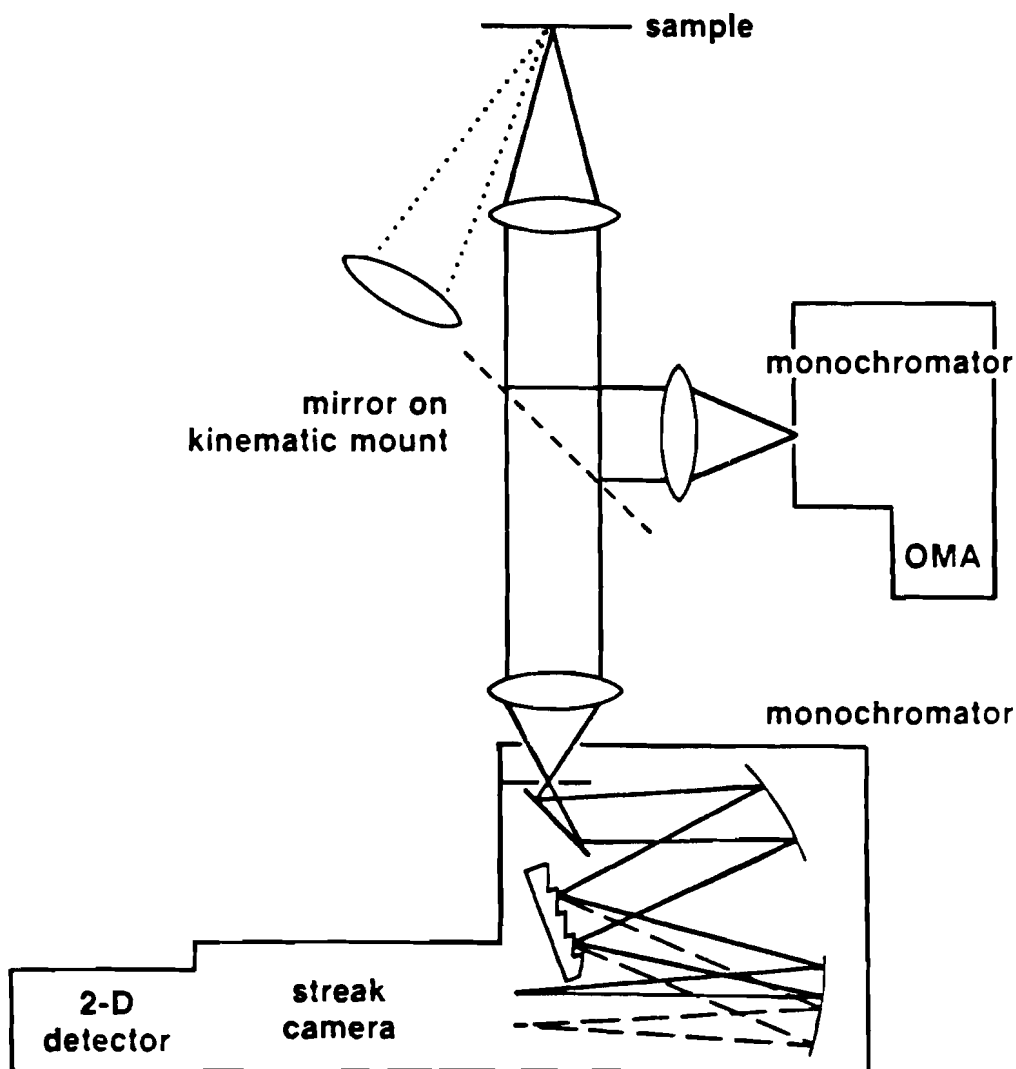
Figure 2.2.   Photoluminescence spectroscopy system.   The dye
laser pump beam is focussed on the sample as shown by
the dotted line.   The dashed line indicates a mirror on a
kinematic mount.   The optical beam path through the
streak camera monochromator is detailed to show how
the luminescence is dispersed across the entrance slit of
the streak camera.

images the output of the photocathode onto a detector, and this imaging capability was used to enable us to do time-resolved spectroscopy. The luminescence from the sample was dispersed through an 0.32m monchromator with 300 l/mm grating across the entrance slit of the streak camera. A spectral resolution of about 3 meV could be achieved, with a total coverage of about 110 meV on a single spectrum. The streaked image was integrated on a two-dimensional intensified SIT detector (Hamamatsu model C1000) and stored on floppy disk for later analysis. It should be noted that the temporal dispersion of the luminescence signal by the grating was only about 0.5 ps over the entire detected spectrum, so no correction of the spectra for the group-velocity dispersion of the grating was necessary.

The results of the PL spectroscopy are discussed in chapters III and IV.B below.

II.B. Subpicosecond Absorption Spectroscopy

In this section I describe in detail the laser system we have developed in our laboratory over the last several years that is now capable of performing time-resolved absorption (or reflectivity) spectroscopy over the entire visible spectrum with 100-fs resolution, and with kHz data acquisition rates. Such experimental capabilities have been developed only in the last few years; a good recent review of the state-of-the-art techniques

of amplified femtosecond lasers has been provided by Knox.[7] I will first discuss the laser system components used to generate a white-light continuum pulse, and then describe in some detail the techniques used to perform pump-probe experiments using these short continuum pulses.

II.B.1. Dye Oscillator

The first requirement of a short-pulse white-light laser system is of course an oscillator capable of producing pulses in the 100 fs range or shorter. Such pulses can be achieved using pulse-compression techniques to generate femtosecond pulses from picosecond dye oscillators.[8] However, aside from the fact that such techniques had not been developed much at the time I began work on the dye oscillator, the stability requirements of the short-pulse source for the generation of a stable, useful white-light continuum are extremely stringent, and the usefulness of this technique to generate a stable continuum has yet to be demonstrated. Hence the requirement for a femtosecond dye oscillator.

The most widely used source of femtosecond optical pulses is the colliding-pulse-mode-locked dye laser (CPM),[9] which typically produces pulses in the 60-100 fs range, although pulses as short as 27 fs have been achieved.[10] In its usual ring configuration, the CPM is pumped by a cw argon-ion laser. The

ring contains separate gain and saturable absorber jets. The laser operates in its minimum-loss condition, in which there are two pulses counterpropagating in the ring which collide in the saturable absorber. The pulses interfere in the absorber jet, so the absorber is saturated more deeply. This serves to shorten the pulses and stabilize the laser ouput. The pulses can be amplified by pumping a dye amplifier with nanosecond pulses from a frequency-doubled Q-switched Nd:YAG laser[11] or from a copper-vapor laser.[12]

In our laboratory, however, we have taken an alternate approach to amplification of ultrashort dye laser pulses, in which we pump the dye amplifier with short (<100 ps) pulses.[13-15] Pumping with short pulses results in an efficient high-gain amplifier with good contrast between the amplified pulse and amplified spontaneous emission, and also makes the further amplification of the white-light continuum straightforward. This scheme of amplification requires that the dye oscillator and amplifier pump pulses be synchronized to within a few tens of picoseconds, hence we term this "synchronous" amplification. Synchronous amplification requires that the dye oscillator be synchronously pumped. The dye oscillator I describe here is synchronously pumped, but has the additional advantage of being colliding-pulse mode-locked. I have further discussed the design and development of this laser in references 16 and 17.

A necessary condition for a dye laser to be both synchronously pumped and colliding-pulse mode-locked is that the critical position of the saturable absorber be unaffected by adjustments of the cavity length. The use of an antiresonant ring as one end mirror of a linear cavity[18] enables this condition to be satisfied. An antiresonant ring consists of a 50% splitter and a ring to return the beams to the splitter. An incoming pulse from the linear part of the cavity is split into two equal parts by the 50% splitter; when the two pulses recombine on the splitter, they interfere so that the entire pulse is returned to the cavity. In fact, as Siegman has shown,[18] if the splitter reflectivity is R and the transmission T, then the power returned to the cavity is given by 4RT, and the power coupled out of the cavity is $(T-R)^2$. As suggested by Siegman[19] and subsequently demonstrated with Q-switched Nd:YAG[20] and Nd:Glass[21] lasers, colliding-pulse mode-locking may be obtained by situating a saturable absorber exactly opposite the 50% splitter in the antiresonant ring. Our laser represents an extension of this technique to the synchronously-pumped, cw mode-locked regime.

A diagram of the dye laser is shown in Fig. 2.3. The laser consists of a four-mirror linear cavity, for which one end mirror is a 5% output coupler mounted on a translation stage and the other is an antiresonant ring. The gain medium is a 200-μm jet of Rhodamine 6G in ethylene glycol, and the saturable absorber is a 20-μm jet of DODCI (Diethyloxadicarbocyanine Iodide) in ethylene
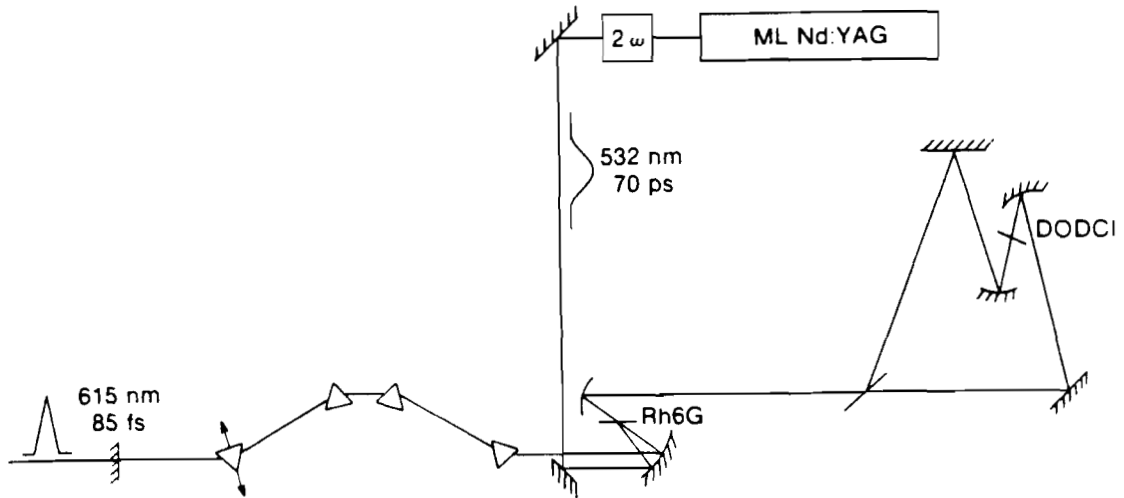
Figure 2.3. Synchronously pumped, colliding-pulse mode-locked antiresonant ring dye laser. The arrows on the first prism indicate how the prism is moved to tune the intracavity dispersion.

glycol. The typical DODCI concentration is 2×10^{-3} M, which causes the laser to operate with a central wavelength of 615-618 nm.

The dye laser is synchronously pumped at 100 MHz by the frequency-doubled output of the cw mode-locked Nd:YAG laser described in section II.A.1 above. Both the Nd:YAG pump laser and the dye laser are mounted on Super-Invar slabs to minimize cavity-length fluctuations. The shortest pulses and greatest stability are obtained when the cavity lengths are properly matched and the Nd:YAG laser cavity length is adjusted so the phase jitter of the Nd:YAG output is minimized. Both the pump and dye lasers also have end-mirrors mounted on piezo-electric transducers to make the required sub-micron cavity length adjustments easy and reproducible. When the cavity lengths are well matched, the dye laser stability is of the order of the pump laser stability, which for frequency-doubled Nd:YAG is about 1% rms.

The dye cavity mirrors have single-stack high-index coatings centered at 620 nm to minimize the effects of unwanted temporal dispersion.[22] In order to control the dispersion in the cavity, four quartz Brewster prisms are situated in the linear part of the cavity. As first demonstrated by Fork *et.al.*[23,10] in a cw-pumped CPM laser, the angular dispersion of the prisms introduces negative group velocity dispersion (GVD), while the prism glass introduces positive GVD. Therefore, by controlling the

amount of glass in the cavity (*i.e.* by moving one of the prisms in or out of the cavity along its axis), one may tune the net GVD of the cavity. The dependence of the pulse width on the intracavity glass is shown in Fig. 2.4. It should be noted that not only is there a sharp minimum in the pulse width but also the pulse shape and spectrum differ qualitatively in two different regions of the graph. When there is too little glass in the cavity, the pulse has negligible wings, the spectrum tails to the yellow, and the time-bandwidth product $\tau_p \Delta \upsilon$ is 0.35. When there is too much glass in the cavity, the pulse has broad wings, the spectrum tails to the red, and $\tau_p \Delta \upsilon$ is 0.5. The minimum pulse width occurs with approximately 50-100 μm less glass than the prism position which yields a symmetrical spectrum. This is consistent with a picture of pulse shaping where the minimum pulse width occurs when positive self-phase modulation (SPM) is balanced by negative GVD to from a stable pulse. The dependence of the laser spectrum on the intracacity glass is shown in Fig. 2.5. Generally the laser is most stable when operated with a slight net negative cavity GVD (*i.e.* with slightly less glass than that which gives the shortest optical pulse). Typically the laser pulse width is about 90 fs (assuming a sech^2 pulse shape), determined by background-free autocorrelation, but pulse widths as short as 45 fs have been obtained.
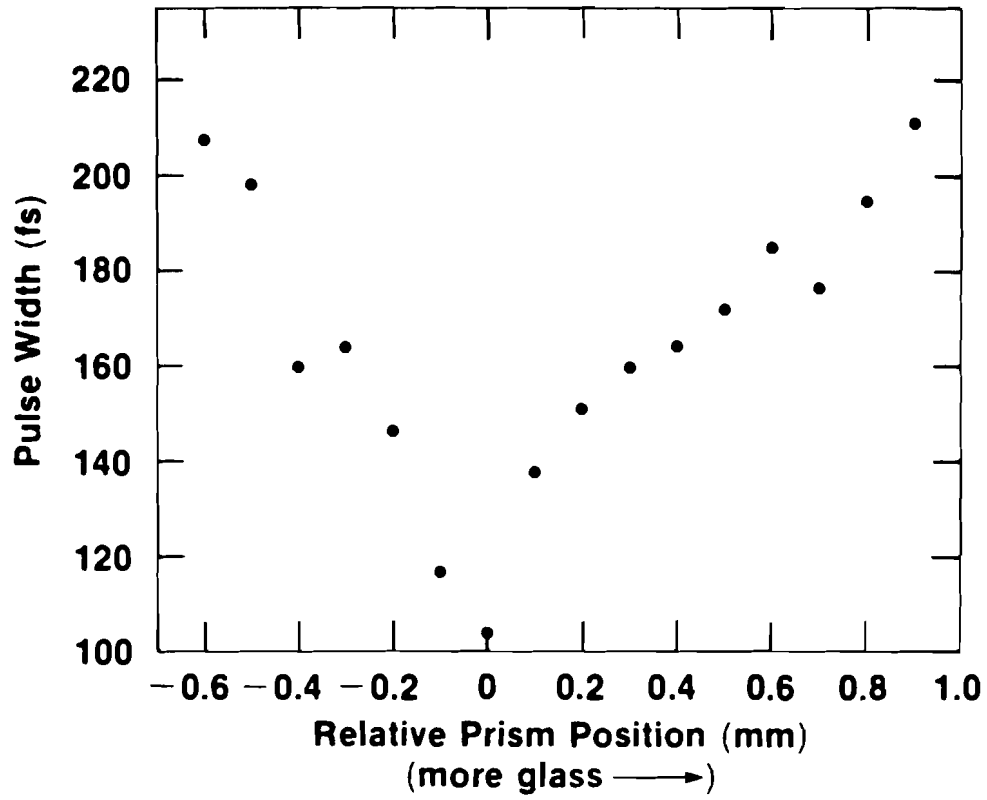
Figure 2.4. Pulse width of the antiresonant ring laser vs. intracavity glass.
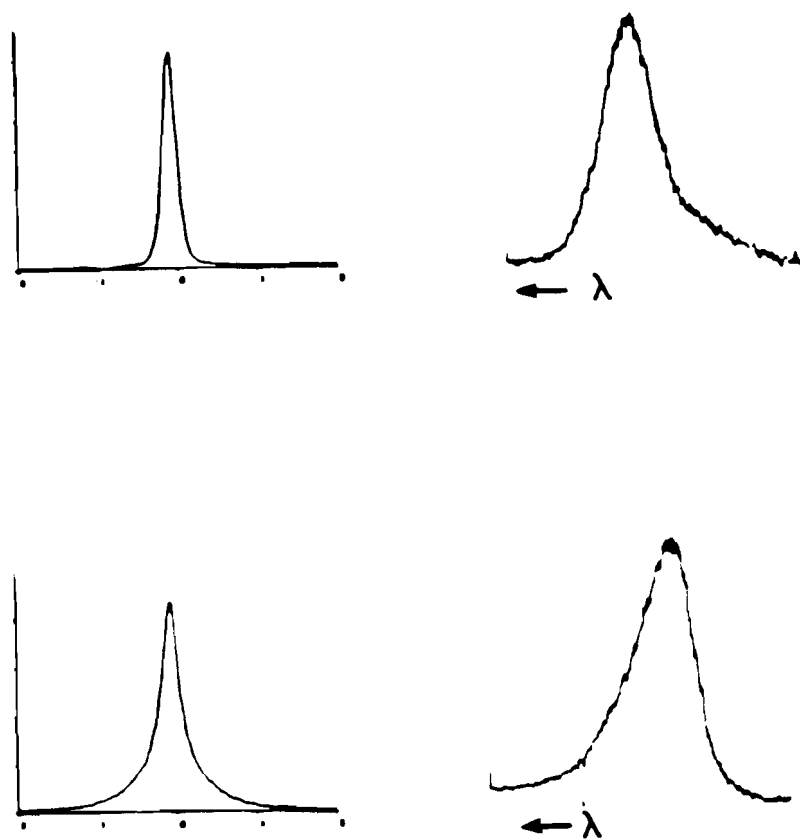
Figure 2.5. Pulse autocorrelations and spectra for two different laser conditions. Top: net negative intracavity group-velocity dispersion (GVD). Bottom: net positive intracavity GVD.

II.B.2 Nd:YAG Regenerative Amplifier

The pump source for the dye laser amplifier is the frequency-doubled output of a Nd:YAG regenerative amplifier. The regenerative amplifier is cw-pumped, so that the laser can be Q-switched, injected with a short (80 ps) seed pulse, and cavity-dumped at a 1 kHz repetition rate. A schematic drawing of the amplifier configuration is shown in Fig. 2.6. The basic idea of the synchronous dye amplifier is to seed the Nd:YAG regenerative amplifier with a pulse from the cw mode-locked Nd:YAG that is the pump source for the dye oscillator. This gaurantees that the amplifier pump pulse and the dye laser pulse will be strictly synchronized. Timing between the pump and signal pulses is then simply accomplished with an optical delay line.

A portion of the 1.06 μm radiation from the Nd:YAG oscillator is injected into an optical fiber. The fiber is used simply to transport the beam across the laboratory to the amplifier, and to decouple the alignment of the Nd:YAG oscillator and regenerative amplifier. After the fiber, a Pockels cell switchout selects a single pulse from the 100 MHz train of pulses. This pulse is injected into the regenerative amplifier off a 4% reflector. The injected pulses are of approximately 100 pJ energy and 80 ps duration.

The regenerative amplifier design is shown in Fig. 2.7. The laser head is a Quantronix model 117 with 3 x 104 mm Nd:YAG
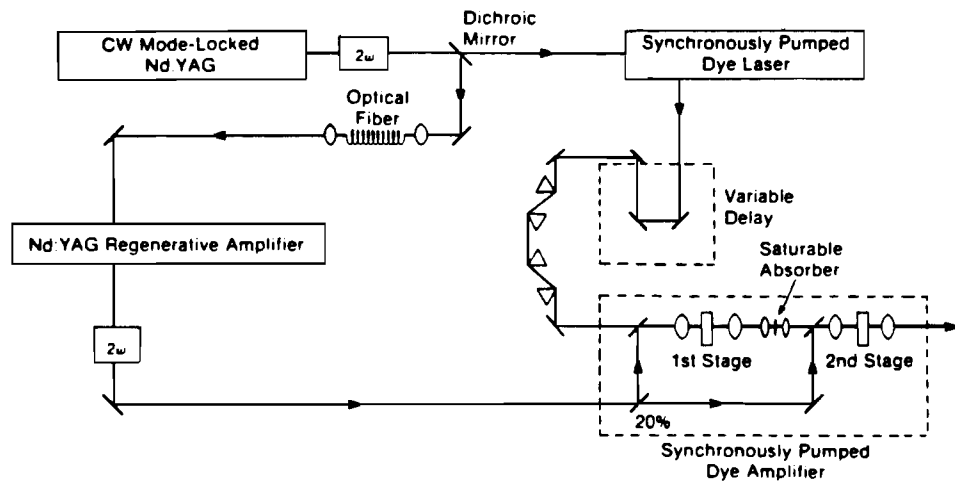
Figure 2.6.   Schematic of the kHz dye laser amplifier system.
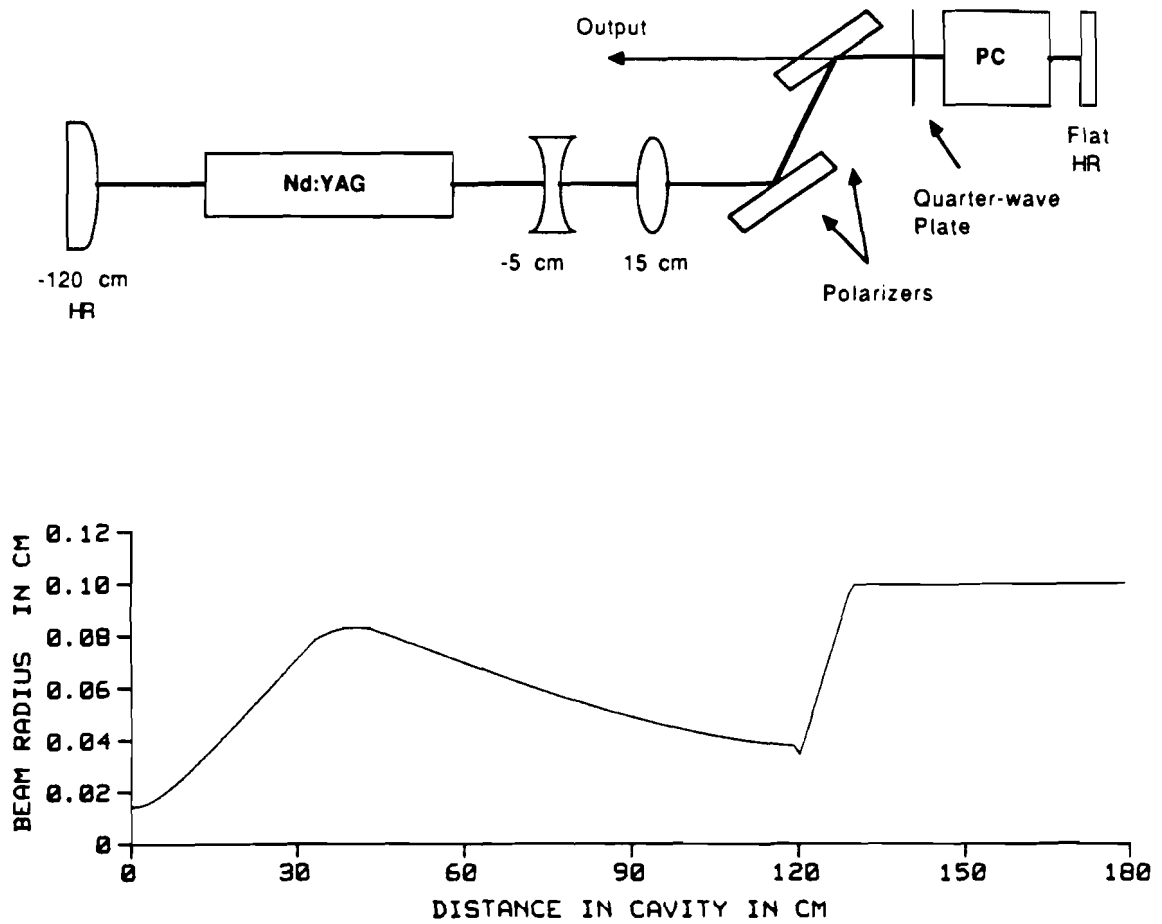
Figure 2.7. Nd:YAG cw-pumped regenerative amplifier. On top is a schematic of the cavity design. Below is the calculated beam diameter in the cavity.

rod. The thermal lensing of this rod is very strong, and a cavity round-trip time of about 12 ns is desirable so that any secondary pulses in the cavity due to injection of unwanted pulses from the oscillator will be well separated in time from the main pulse. Furthermore, ideally the beam in the intracavity Pockels cell should be large enough to prevent damage to the Pockels cell crystal, and be collimated to enhance the switchout contrast ratio. The contrast ratio can be further enhanced by using the thin-film polarizers in reflection mode. The laser cavity shown in Fig. 2.7 satisfies all these requirements.[24]

The operation of the regenerative amplifier is as follows. The quarter-wave plate in the cavity frustrates the cw lasing and rejects any injected light that leaks through the first switchout after two round trips. The amplifier is triggered by applying a voltage step to the lithium niobate Pockels cell sufficient to compensate for the quarter-wave plate. This action not only Q-switches the laser but also traps the injected pulse (selected by the first switchout) in the cavity. Following approximately 40 round trips (480 ns), a second voltage step is applied to the Pockels cell providing an additional quarter-wave rotation, and the pulse is rejected from the cavity.

The result is that the regenerative amplifier output is routinely 1.2 mJ at a repetition rate of up to 1.7 kHz, with a pulse width of 80 ps. The repetition rate is limited entirely by the first switchout; typically the laser is operated at 1 kHz. The pulse

energy is limited by the thermal depolarization in the Nd:YAG rod combined with the use of high-contrast dielectric polarizers in the cavity. Output energy fluctuations are typically less than 2% rms.

The output of the regenerative amplifier is down-collimated by a telescope to a diameter of approximately 500 μm, and is frequency-doubled in a 2.5 cm CD*A crystal which is temperature-tuned to phase match at 50 °C. The second-harmonic energy is 500 μJ per pulse. The second-harmonic is directed by a dichroic mirror to the dye amplifier; the remaining fundamental is again down-collimated and frequency-doubled in an 8-mm KTP (potassium titanyl phosphate) crystal. This second-harmonic, which is used to amplify a portion of the white light continuum, has an energy of 80 μJ per pulse.

II.B.3. Dye Amplifier

The dye amplifier is also displayed in Fig. 2.6. It is configured as a standard two-stage, collinearly pumped amplifier.[13] The stages are 1 cm in length with flowing dye solution. I found the optimum dye solution to be Sulforhodamine 640 dissolved in a 50/50 mixture of methanol and water. This dye solution offers the best combination of high gain but low amplified spontaneous emission (ASE) level, essentially because the ratio of water to methanol can be varied so that the gain spectrum of the amplifier dye matches the dye oscillator

spectrum. (A higher proportion of water, which is a polar solvent, produces a gain spectrum which is shifted to the red). The dye concentration is about 5×10^{-5} M.

The spot sizes and relative pump power for each amplifier stage were carefully optimized so that the maximum gain could be extracted from the amplifier consistent with a minimum of pulse broadening due to gain saturation. The optimized amplifier has a first stage pumped by 20% of the second-harmonic energy from the frequency-doubled Nd:YAG regenerative amplifier. The spot size of the pump and oscillator beams is about 150 μm diameter, and the gain is typically 1000. The amplified dye beam then passes through a 200-μm jet of Malachite Green saturable absorber, which serves to absorb the unamplified 100 MHz dye pulses and most of the ASE from the first stage. The amplified beam suffers a loss of about 2 in the absorber. The second stage is pumped by the remaining second-harmonic. The spot size is about 1 mm diameter, and the gain is typically 100. Thus including the absorber loss the net gain is 5×10^4, so since the input pulse energy from the oscillator is about 200 pJ, the amplified pulse energy is 10 μJ. (This corresponds to the measured average power of 10 mW). The highest pulse energy I have observed with this system without pulse broadening is 15 μJ. If pulse width is not a concern, the spot sizes in the two stages can be reduced so the amplifier will be driven farther into saturation.

This can produce amplified pulses with energy in excess of 40 μJ, but the pulse then broadens to about 200 fs FWHM.

The ratio of the amplified short pulse energy to ASE at the output of the amplifier is typically 1000:1, though this figure varies significantly with the age of the amplifier dye and the relative water to methanol content of the solvent. This figure is of concern only when a pump-probe experiment is being performed where a pump pulse near 615 nm is necessary, in which case the effect of the ASE portion of the pump pulse must be considered. In all the experiments reported in this thesis, the amplified dye pulse was used to generate a white light continuum, from which a pump pulse far to the red of 615 nm was selected, so the ASE from the amplifier was not an important consideration.

Aside from avoiding saturation of the amplifier to maintain a short dye laser pulse, it is necessary to compensate for the GVD of the amplifier chain. This is accomplished by passing the oscillator output through a flint (SF-10) prism pair in a double-pass configuration before the amplifier chain. The pulse width at the output of the amplifier is then easily minimized by adjusting the amount of glass the beam travels through in the prism pair (in exactly the same fashion as in the dye oscillator). Thus the prism pair puts a slight negative chirp on the dye pulse that is exactly compensated by the positive GVD of the amplifier chain, and the output of the amplifier is typically 90-120 fs. The prism pair is placed before the amplifier so that the loss due to reflections and

scattering in the prisms can be recovered in the amplifier. (If it were placed after the amplifier, there would be less energy available for the continuum generation). As a further precaution against GVD that cannot be compensated with the prism pair, the mirrors in the amplifier chain all have single-stack dielectric coatings centered at 615 nm.

The stability of the amplified dye pulse is 3% rms (measured by taking a histogram of the pulse energy). It is extremely important for the generation of a stable, useful continuum that the amplified dye stability be less than or of the order of 3%.

II.B.4.   Continuum Generation and Amplification

The amplified dye laser pulse is focussed with a 65 mm lens onto a 1 mm jet of ethylene glycol. A thick optical-quality jet is obtained using a low-pressure flow system with a high-quality sapphire nozzle (Precomp model PRE10N015). The focussed intensity is about 10^{13} W/cm^2. This intensity for a 100 fs pulse is sufficient to produce a white light continuum, which extends over the entire visible range.[25,26] Apart from the effect of GVD, this continuum pulse is as short as the pump pulse, namely 100 fs. The spectrum of the continuum peaks strongly at the pump pulse wavelength and falls off roughly exponentially to each side, though under certain conditions the spectrum shows structure due principally to self-phase modulation.[27] The position of the dye jet

relative to focus is critically important for obtaining a smooth, unmodulated, stable spectrum. Usually the optimum glycol jet position is just beyond focus. The focal length of the pump lens is also critical; a longer lens will produce a modulated spectrum since the continuum generation will be closer to threshold. A shorter lens will produce an intensity that is too high, and the dye laser beam will actually atomize the front and back surfaces of the glycol jet, and a mist of ethylene glycol will be blown off the surfaces. This scatters the laser beam, destroying the beam quality and introducing instabilities in the continuum spectrum and energy.

A portion of the white light spectrum used in my experiments is shown in Fig. 2.8. (The spectrum is not corrected for the responsivity of the OMA detector). This spectrum is an integration of 5000 laser shots. When the laser system is running properly, the shot-to-shot fluctuations of any given spectral portion of the continuum are about 8-12% rms.

The white light is collimated by a 38-mm achromatic lens after the glycol jet. A beamsplitter reflects about 50% of the light into the pump arm of the pump-probe setup, as is shown in Fig. 2.9. A filter selects a 10 nm bandwidth portion of the spectrum. This beam is sent through a computer-controlled delay line (1 μm resolution), and amplified in a 1 cm dye flow cell. The 80-μJ second-harmonic from the second (KTP) frequency-doubling of the Nd:YAG regenerative amplifier is used to pump this amplifier.
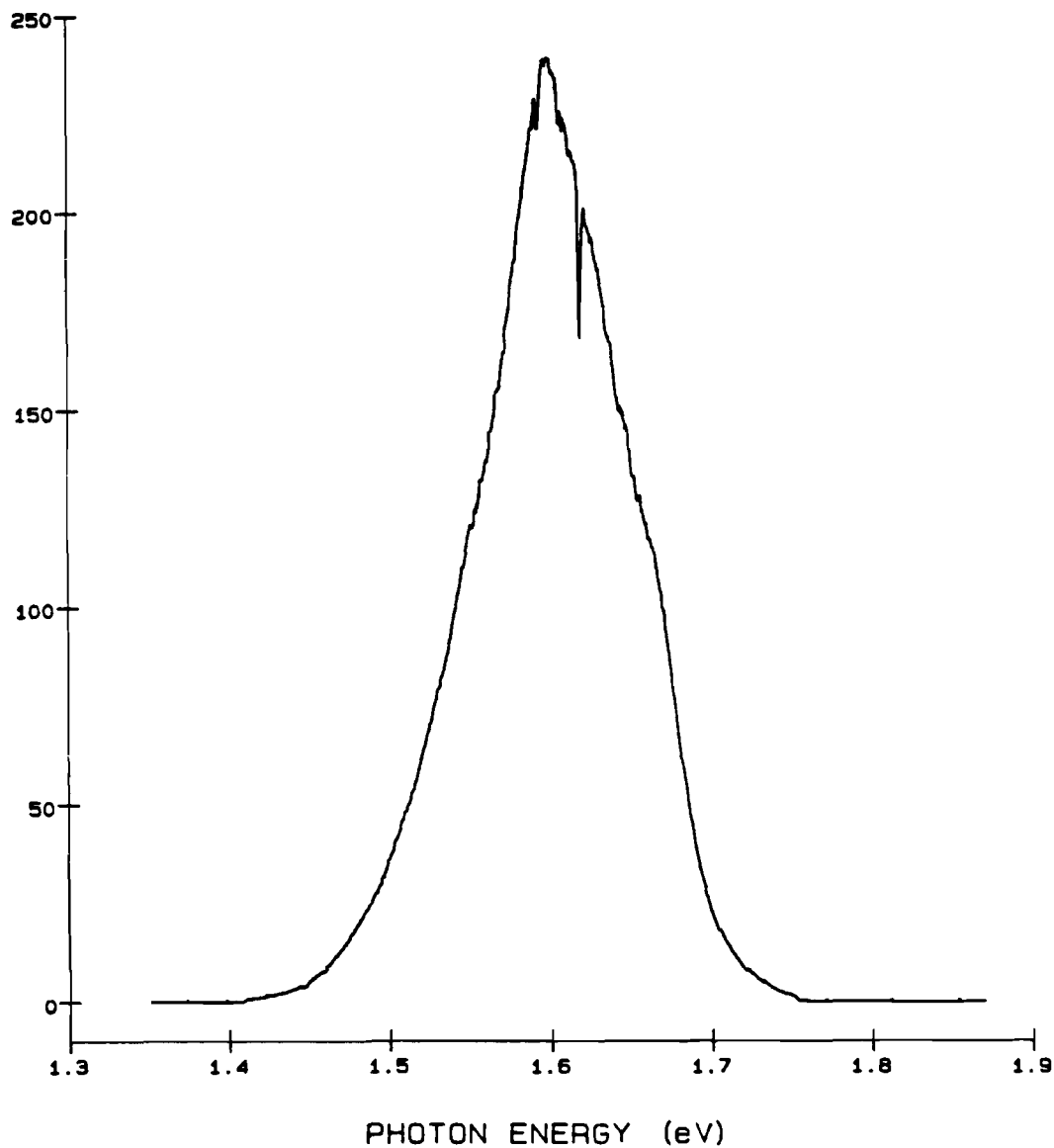
Figure 2.8. Typical white light spectrum over the probe range
1.4-1.8 eV. An RG780 filter (with transmission edge
between 1.6 and 1.7 eV) was used to block the intense
portion of the continuum at higher photon energies.
(The glitch in the center of the spectrum is due to a dead
diode in the OMA detector array).
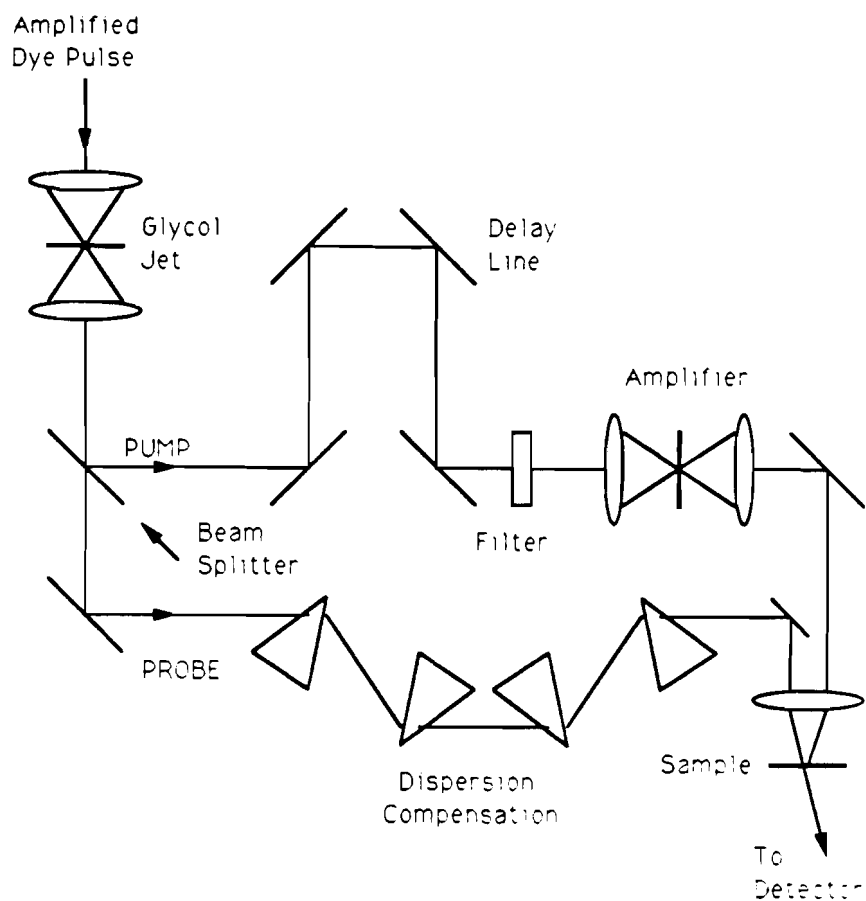
Figure 2.9. Schematic of the pump-probe setup. Not shown are the pump beam for the continuum amplifier, the neutral density filters in the probe beam, or the probe reference beam detector.

A filter after the amplifier is used to block any remaining pump light (and, when possible, ASE from the amplifier). The amplified continuum energy is typically in the 10-70 nJ range in the spectral region of interest in my experiments (690-820 nm). The ASE is at least 100 x below the amplified pulse energy.

The remaining portion of the white light after the splitter is attenuated and used as a probe beam. Typically the probe energy is below the pump energy by at least 100 x. I discuss how pump-probe experiments are performed in the next section.

II.B.5. Pump-Probe Experiments

The basic idea of a pump-probe experiment is very simple. A short optical pulse is used to pump the sample and induce a change in its optical properties, such as its reflectivity or absorption spectrum. A much weaker pulse is delayed in time and used to probe the change in optical properties of the sample due to the pump. The time resolution is obtained by varying the time delay between the pump and probe. Since the pump and probe pulses are derived from the same source by using a beamsplitter, there is no temporal jitter between the pump and probe; hence the time resolution is limited only by the optical pulse width.

When a spectral continuum is available for the probe, then the change in the entire spectral region of interest due to the

pump can be accumulated at once by using parallel detection: the probe beam after passing through the sample is dispersed through a monochromator and integrated on an OMA. Thus we can do time-resolved spectroscopy. When the change in optical properties due to the pump is small and higher sensitivity is required, the OMA may be replaced with a narrow slit and photomultiplier or photodiode detector. Then the detection is at a single wavelength, but the detectors are fast, so that if the probe beam is simultaneously monitored before it goes through the sample, energy fluctuations may be normalized out on every single laser shot, and a substantial sensitivity increase may be obtained.

The time origin, *i.e.*, the delay line position for which the pump and probe beams arrive at the sample at the same time, is precisely determined by cross-correlating the pump. pulse with the probe pulse. A nonlinear crystal ($LiIO_3$) is placed at the same position as the sample. The pump and probe beams are aligned so they are parallel and about two beam diameters apart. They are focussed on the crystal, which is aligned to generate the sum frequency of the pump and probe pulses. The sum frequency beam is dispersed in a monochromator before being detected by a photomultiplier tube. By tuning the monochromator wavelength, one may easily select which spectral portion of the probe is to be correlated with the pump. The sum frequency signal is detected as a function of time delay, the result being the cross-correlation;

a typical example is given in Fig. 2.10. The FWHM is 180 fs. The pump and probe pulse widths are likely very close, so to a good approximation the cross-correlation may be deconvolved to get the real pulse width in the same fashion as an autocorrelation. For sech^2 pulse shape, the deconvolution factor is 0.6482,[28] so the pulse width is 120 fs.

It is particularly important when doing time-resolved spectroscopy to avoid systematic error due to GVD, since the entire probe spectrum must arrive at the sample at the same time. If the continuum spectral range of interest is very broad, then the temporal shift due to GVD in the glycol jet, lenses, and filters between the red and blue portions of the probe spectrum can be significant. This temporal shift can be directly measured by cross-correlating the probe with the pump over the probe spectral range of interest. The result is displayed in Fig. 2.11 (squares). The pulse width of any given portion (of approximately 10 nm width) of the spectrum is 140 fs, but there is an approximately linear chirp that leads to a 500 ps temporal dispersion over the 120 nm probe spectrum.

This dispersion may be corrected by inserting a prism pair in double pass arrangement in the probe beam. The white light dispersion when quartz prisms are used is shown in Fig. 2.11 (circles). The pulse width for each spectral component is 120 fs and the dispersion over the 120 nm bandwidth is 30 fs. Unfortunately the quartz prisms are not useful since to obtain the
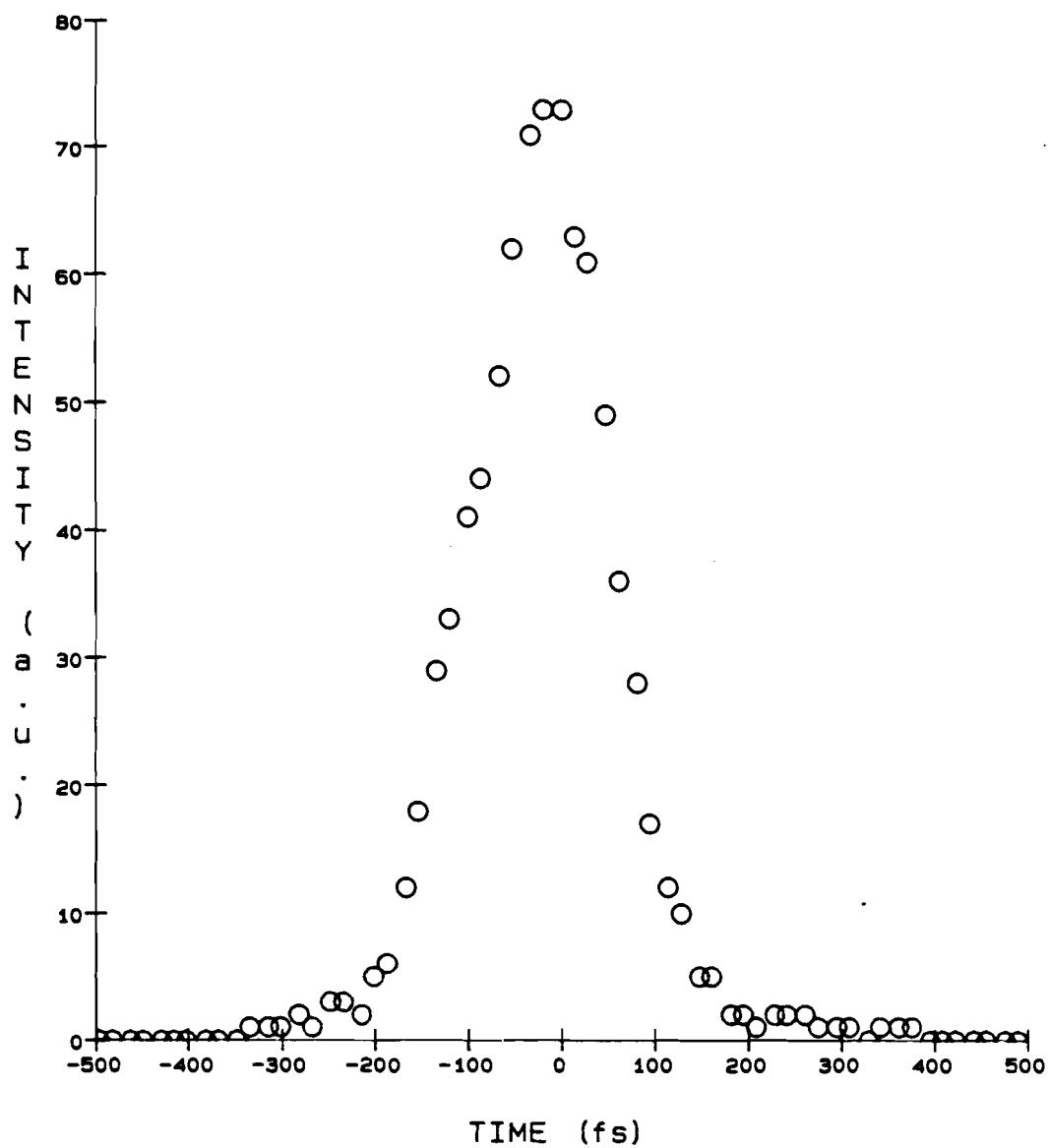
Figure 2.10. Cross-correlation of the 770 nm portion of the probe with the 790 pump beam. The correlation width is 180 fs, which corresponds to a pulse width of 120 fs.
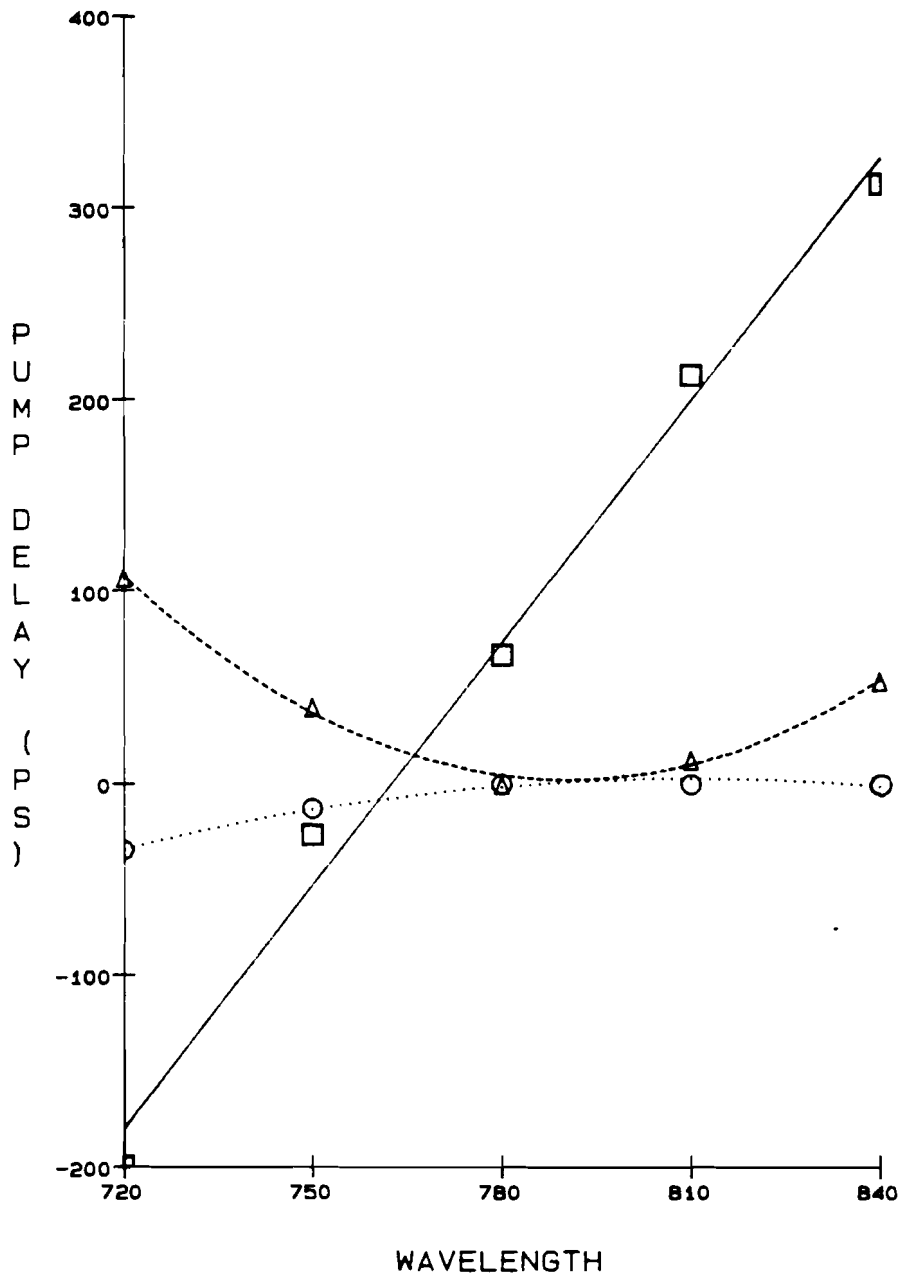
Figure 2.11. Temporal dispersion of the white light continuum pulse. The squares show the positive linear dispersion of the uncompensated continuum. The circles (triangles) show the dispersion when quartz (SF-10 flint) prisms are used to compensate for the linear chirp of the continuum.

necessary negative chirp, the prisms must be far apart and the beams must go through the prisms as close to the tip as posssible. However in this case the beam suffers from vignetting (due to the several-mm beam diameter), and the probe beam quality is destroyed and energy lost. Possibly this problem could be overcome by focussing the beam through the prism arrangement, with the focal position just beyond the second prism. However, a simpler solution is to use flint prisms, which give a much higher dispersion. Thus the necessary prism separation is smaller, and the vignetting problem is eliminated. The continuum dispersion for flint (SF-10) prisms is shown in Fig. 2.11 (triangles). The pulse width at each spectral component is 110 fs, and the dispersion over the 120 nm bandwidth is 100 fs. This dispersion is somewhat worse than that for quartz prisms, since the flint prisms have a higher quadratic as well as linear dispersion. In fact, to show that the minimum achievable dispersion is limited by the quadratic dispersion of the prisms, I have fitted the dispersion data to parabolas. The result is the dotted curves of Fig. 2.11. It is important to note that each time the central probe wavelength of interest is changed, it is necessary to adjust the amount of glass the beam passes through in the prism pair to minimize the continuum dispersion.

A further consideration in doing pump-probe experiments is that the probe beam must be centered on the pump beam at the position of the sample. Ideally, the pump beam will be larger

than the probe so that the pump intensity is roughly constant over the area of the probe spot. This is accomplished by down-collimating the pump beam after the continuum amplifier. The pump and probe spots are then overlapped by putting a small (12.5 μm) pinhole adjacent to the sample. The sample is then placed precisely at the focus by maximizing the throughput of the probe beam through the pinhole; the overlap is then easily obtained by aligning the pump through the pinhole. The overlap may be verified and the spot sizes measured by scanning the pinhole through the beams and detecting the transmitted light through the pinhole. For the experiments reported in this thesis, the spot sizes were typically a pump diameter of 48 μm and a probe diameter of 26 μm. After the alignment and focus are optimized, the sample is simply translated into place.

II.B.6. Data Acquisition

All the white light time-resolved spectroscopy experiments reported in this thesis measured the so-called differential absorption of the sample. What is measured is $\Delta T/T$, where T is the transmitted probe energy with no pump beam incident on the sample, and ΔT is the change in transmission due to the pump, *i.e.*, the transmitted probe with pump incident minus the transmitted probe with no pump incident on the sample.

As I mentioned at the beginning of the previous section, the differential absorption spectrum may be accumulated using an OMA. The readout of the OMA diode array is synchronized to the laser by triggering the readout with a pulse timed to the laser amplifier. The kiloHertz trigger from the amplifier timing electronics is divided down typically by 50x, so that the OMA will integrate 50 laser shots and be read out at 20 Hz. Shutters are placed in both pump and probe beams, which may be triggered by the OMA controller. The shutter sequence used to accumulate the differential absorption spectrum is as follows. Both shutters are initially open, and one scan of the transmitted probe is accumulated into memory A. The pump shutter is then closed, and one scan of the probe is subtracted from A. The probe shutter is then closed and a background (dark current) spectrum is added to A. The pump shutter is then opened, and any pump light that is scattered onto the OMA is subtracted from A. (For very high quality samples and large signal levels the last two steps are not necessary). The transmitted spectrum without pump is then accumulated into memory B. An ignored scan is performed between each accumulated scan since a scan readout does not completely reset the OMA diode array. The cycle is repeated as often as necessary to achieve the desired signal-to-noise ratio. Once the data is acquired, it is transferred to the PDP-11 computer and memory A is normalized to memory B; the result is the $\Delta T/T$ spectrum.

For reasonable (5-30 min.) integration times, the typical minimum $\Delta T/T$ signal observable (*i.e.* for a signal-to-noise ratio of one) is about 0.5%. This is limited by continuum fluctuations and the cavity-length stability of the dye oscillator. It may be possible to improve the sensitivity substantially by stabilizing the dye oscillator cavity length with a feedback loop.

For experiments where it is not necessary to accumulate the entire differential absorption spectrum at once, photodiodes or photomultipliers may be used to monitor the probe light. For these experiments, a portion of the probe is split off before the sample and used as a reference beam. Both transmitted probe ("A") and reference ("B") beams are passed through monochromators to select the wavelength of interest, and detected with photodetectors. For the experiments reported here, the probe energies were so low that photomultipliers with extended red multialkali photocathodes (Hamamatsu type R2066) were required. For each laser shot, A and B are integrated and digitized using a LeCroy 2249W pulsed A/D. The computer acquires A and B, checks to see that B is within an acceptable energy range, and computes the signal $S=(A-B)/B$. This yields the differential absorption of the sample up to a factor due to the chosen signal level of B. The signal S may be calibrated to yield the quantitative value of $\Delta T/T$.

The attainable sensitivity for these single-wavelength experiments is limited by two things. First, the sample surface

must be of high quality and the probe beam directionality must be stable. Otherwise the detectors A and B will not observe exactly the same signal and random fluctuations will be introduced. (It is also extremely important that the two detectors be monitoring exactly the same wavelength portion of the spectrum). Secondly, in order to avoid saturating the photocathode output, it is necessary to limit the incident photon flux. I have found it necessary to limit the flux such that only about 625 photoelectrons are emitted from each photocathode for each laser shot. Thus the shot noise fluctuations will be about 4%. For a reasonable experiment, about 20000 laser shots may be accumulated at each data point, so the shot noise limit to the sensitivity is about 3×10^{-4}. In practice the sensitivity limit is about 0.1%.

The results of the sub-picosecond differential absorption spectroscopy are presented in chapter IV.C.

II.C. References

1. J.D. Kafka, Ph.D. Thesis, University of Rochester, 1983.

2. I.N. Duling III, Ph.D. Thesis, University of Rochester, 1985.

3. T. Sizer II, Ph.D. Thesis, University of Rochester, 1985.

4. T. Sizer II, G. Mourou, and R.R. Rice, "Picosecond Dye Laser Pulses Using a CW Frequency Doubled Nd:YAG as the Pumping Source," Optics Commun. **37**, 201(1981).

5. H.W. Kogelnik, E.P. Ippen, A. Dienes, and C. Shank, "Astigmatically Compensated Cavities for CW Dye Lasers," IEEE J. Quant. Electron. **QE-8**, 373 (1972).

6. T. Sizer II, "Fast and Flexible Forth Programming in a Femtosecond Laser Lab," J. Forth Application and Research **3**, 25 (1985).

7. W.H. Knox, "Femtosecond Optical Pulse Amplification," IEEE J. Quant. Electron. **QE-24**, 388 (1988).

8. B. Nikolaus and D. Grischkowsky, "90-fs Tunable Optical Pulses Obtained by Two-Stage Pulse Compression," Appl. Phys. Lett. **43**, 228 (1983).

9. R.L. Fork, B.I. Greene, and C.V. Shank, "Generation of Optical Pulses Shorter Than 0.1 psec by Colliding Pulse Mode Locking," Appl. Phys. Lett. **38**, 671 (1981).

10. J. Valdmanis, R.L. Fork, and J.P. Gordon, "Generation of Optical Pulses as Short as 27 Femtoseconds Directly from a Laser

Balancing Self-Phase Modulation, Group Velocity Dispersion, Saturable Absorption, and Saturable Gain," Opt. Lett. **10**, 131 (1985).

11. R.L. Fork, C.V. Shank, and R.T. Yen, "Amplification of 70-fs Optical Pulses to Gigawatt Powers," Appl. Phys. Lett. **41**, 223 (1982).

12. W.H. Knox, M.C. Downer, R.L. Fork, and C.V. Shank, "Amplified Femtosecond Optical Pulses and Continuum Generation at 5-kHz Repetition Rate ," Opt. Lett. **9**, 552 (1984).

13. T. Sizer II, J.D. Kafka, A. Krisiloff, and G. Mourou, "Generation and Amplification of Sub-Picosecond Pulses Using a Frequency-Doubled Neodymium YAG Pumping Source," Opt. Commun. **39**, 259 (1981).

14. T. Sizer II, J.D. Kafka, I.N. Duling III, C.W. Gabel, and G.A. Mourou, "Synchronous Amplification of Subpicosecond Pulses," IEEE J. Quant. Electron. **QE-19**, 506 (1983).

15. I.N. Duling III, T. Norris, T. Sizer II, P. Bado, and G.A. Mourou, "Kilohertz Synchronous Amplification of 85-Femtosecond Optical Pulses," J. Opt. Soc. Am. B **2**, 616 (1985).

16. T. Norris, T. Sizer II, and G. Mourou, "Generation of 85-fsec Pulses by Synchronous Pumping of a Colliding-Pulse Mode-Locked Dye Laser," J. Opt. Soc. Am. B **2**, 613 (1985).

17. T. Norris, I.N. Duling III, M. Pessot, T. Sizer II, J. Dawes, and G.A. Mourou, "Generation of Microjoule 65-fsec Pulses at High Repetition Rate ," in Digest of the Conference on Lasers and Electro-Optics (Optical Society of America, Washington, D.C., 1985), paper TUE4.

18. A.E. Siegman, "An Antiresonant Ring Interferometer for Coupled Laser Cavities, Laser Output Coupling, Mode Locking, and Cavity Dumping," IEEE J. Quant. Electron. **QE-9**, 247 (1973).

19. A.E. Siegman, "Passive Mode Locking Using an Antiresonant-Ring Laser Cavity," Opt. Lett. **6**, 334 (1981).

20. H. Vanherzeele, J.L. Van Eck, and A.E. Siegman, "Colliding Pulse Mode Locking of a Nd:YAG Laser with an Antiresonant Ring Structure," Appl. Opt. **20**, 3484 (1981).

21. J.M. Buchert, D.K. Basa, L. Tzu, and R.R. Alfano, "Colliding Pulse Mode Locking for an Antiresonant Cavity of a Nd:Glass Laser," J. Appl. Phys. **55**, 683 (1984).

22. S. De Silvestri, P. Laporta, and O. Svelto, "Effects of Cavity Dispersion on Femtosecond Mode-Locked Dye Lasers," in Ultrafast Phenomena IV, ed. by D.H. Auston and K.B. Eisenthal, (Springer-Verlag, Berlin, 1984), p. 23.

23. R.L. Fork, O.E. Martinez, and J.P. Gordon, "Negative Dispersion Using Pairs of Prisms," Opt. Lett. **9**, 150 (1984).

24. The computer code I used to design the regenerative amplifier cavity was provided by J. Scott Coe.

25. R.R. Alfano and S.L. Shapiro, "Emission in the Region 4000-7000 Å via Four-Photon Coupling in Glass," Phys. Rev. Lett. **24**, 584 (1970).

26. R.L. Fork, C.V. Shank, C. Hirlimann, R. Yen, and W.J. Tomlinson, "Femtosecond White-Light Continuum Pulses," Optics Lett. **8**, 1 (1983).

27. J.T. Manassah, M.A. Mustafa, R.R. Alfano, and P.P. Ho,"Spectral Extent and Pulse Shape of the Supercontinuum for Ultrashort Laser Pulse," IEEE J. Quant. Electron. **QE-22**, 197 (1986), and references therein.

28. K.L.Sala, G.A. Kenney-Wallace, and G.E. Hall, "CW Autocorrelation Measurements of Picosecond Laser Pulses," IEEE J. Quant. Electron. **QE-16**, 990 (1980).

CHAPTER III

TUNNELING FROM A SINGLE QUANTUM WELL

III.A. Introduction

In this chapter I describe a set of experiments performed to investigate what might be called the "tunneling-out" problem in GaAs/AlGaAs quantum well (QW) structures. An electron is initially confined in a thin QW, where the well is coupled to a continuum through a thin barrier (Fig. 3.1).
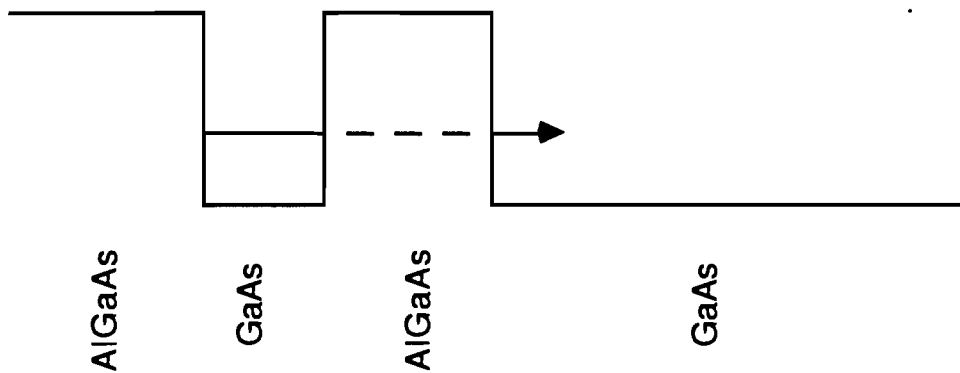
Figure 3.1. Conduction band diagram for the electron tunneling-out problem. The electron is initially confined in the QW, but decays via tunneling into the bulk GaAs region.

Hence the QW electronic state is really metastable, since the electron can tunnel out of the well into the continuum. This tunneling is irreversible, since after the electron escapes from the well it relaxes to the band edge of the continuum and hence cannot return to the well. The goal, of course, is to determine the tunneling decay rate of the electron, and the dependence of this rate on the barrier width, height, and an applied electric field. The tunneling of the heavy hole may be neglected; its effective mass is so large that the tunneling rate is orders of magnitude slower than that of the electrons.

The tunneling-out problem has been around in various forms for many years; among the famous manifestations of this problem are nuclear alpha decay[1] and the cold emission of electrons from a metal surface[2] (the so-called Fowler-Nordheim tunneling). The problem has been understood in principle since the early days of quantum mechanics; a comprehensive discussion of the theory of irreversible tunneling through a barrier has been given by Landau and Lifshitz.[3]

As I mentioned in chapter one, semiconductor heterostructures offer a rich field for the study of tunneling in condensed-matter systems. In the GaAs/AlGaAs system, the barrier width may be controlled to monolayer tolerances, and the barrier height may be controlled by varying the aluminum composition of the AlGaAs barrier. Diode structures may be used to study the effects of an electric field. For this study, we have

tuned the sample parameters so that the tunneling decay time falls within a range accessible by the time-resolved photoluminescence (PL) system described in the previous chapter. Thus we have been able to perform a fairly comprehensive study of the tunneling-out problem in QW structures using time-domain optical techniques. At the time we commenced this study, no such studies had been done. Recently, however, Tsuchiya, et.al., published a similar study[4] in which they investigated the tunneling escape rate of electrons from a QW through very thin AlAs barriers. The principal differences between our study and theirs is that we used thicker AlGaAs barriers, where we could vary the Al composition to study the effect of varying the barrier height, and our samples had the QW region placed in a diode structure so that the effect of an electric field could be studied. We also had a single barrier instead of double barrier structure. For a double barrier structure, the electron can tunnel out of the well in either direction. Thus when an electric field is applied, the tunneling rate through one barrier increases, but the rate through the other barrier decreases. We used a single barrier structure so that the effect of the field on a single barrier could be isolated.

Aside from the question of principle regarding the nature of the tunneling-out problem, there is an additional, practical reason for studying this problem. As I discussed in chapter one, the semiconductor heterostructure that has attracted the most interest for tunneling studies is the double-barrier diode (DBD).

The operation of this structure was shown in Fig. 3.7 of chapter one. This structure is of particular interest for two reasons. First, from a practical point of view, because they display negative differential resistance (NDR) with large peak-to-valley ratios, DBD's are useful for millimeter and submillimeter wave devices, such as oscillators and mixers. Oscillations at frequencies up to 56 GHz have been reported,[5-7] and detection and mixing at frequencies up to 2.5 THz.[8] Secondly, there are outstanding questions regarding the quantum-mechanical nature of the resonant tunneling in this structure.

There are two related questions of particular interest. The first is, what is the time dependence (or conversely, the frequency response) of the tunneling in these structures? Secondly, what is the mechanism of the tunneling in real structures, where the effects of scattering must be considered? The latter question is relevant both to understanding the time dependence of the tunneling and the current-voltage (I-V) characteristic of DBD's.

Considerable theoretical effort has been directed towards answering these questions. The first calculations considered an ideal double-barrier structure with no scattering, interface disorder, or other mechanism by which the resonant energy level in the QW could be broadened. In this case (most thoroughly discussed by Ricco and Azbel[9]), the structure is completely analogous to a Fabry-Perot etalon, where one need only consider the transmission coefficients of each barrier to determine the I-V

characteristic. The frequency response is determined by the requirement that for resonant enhancement of the tunneling, the electron probability amplitude must peak in the well. The buildup time for this peak is expected to be of the order of the resonant state lifetime.

In a fundamental paper, Luryi[10] pointed out that the Fabry-Perot picture of resonant tunneling fails to account for the observed frequency response and I-V characteristics of real DBD's. The observed frequency response is much too fast and the I-V curves display smaller peak-to-valley ratios than predicted. He proposed an additional mechanism for resonant tunneling, namely "sequential" tunneling. The Fabry-Perot picture requires that the electron wavefunction be coherent over the entire DBD structure. However, any scattering process in the well will destroy this coherence. Hence the tunneling process may be viewed as a two-step process, where the electron tunnels first into the well where it is localized by scattering, and then it tunnels out of the well. Many authors[11-24] have considered the time dependence of resonant tunneling when each of these tunneling mechanisms is operating. Capasso *et.al.*,[25] have reviewed the roles of coherent and incoherent tunneling in DBD structures. The important thing to note here, though, is that in either case, one of the most important parameters is the resonance width Γ_r of the confined electron state; whether the tunneling proceeds in a coherent or sequential fashion depends on the relative magnitude of Γ_r to the

scattering width of the state Γ_s. The width Γ_r is related to the tunneling decay time τ_T of the state by the Uncertainty Principle: $\tau_T = \hbar/\Gamma_r$. Our experiment directly measures in the time domain the dependence of this tunneling time and hence the resonance width on the applied electric field.

III.B. EXPERIMENTAL RESULTS

III.B.1.   Sample Structure

The structure of the samples used for this study is shown in Fig. 3.2. A single 30 Å GaAs QW is bounded on top by a thick (0.2 μm) $Al_xGa_{1-x}As$ barrier, and on the bottom by a thin $Al_xGa_{1-x}As$ barrier and 0.1-μm thick GaAs region. This undoped structure is clad between an 0.1-μm p^+ cap layer and a 1-μm n^+ buffer layer grown on top of the semi-insulating (SI) substrate. It should be noted that the photon energy of the luminescence from the QW lies below the $Al_xGa_{1-x}As$ band edge, so there are no effects due to reabsorption of the luminescence from the QW.

Tunneling is possible only through the thin barrier beneath the QW. The barrier width b and Al composition x were varied to study the effect of these on the tunneling rate. In all five samples were studied. One set of samples had an Al composition x of 30%, and nominal barrier widths b of 85, 111, and 121 Å. A second set

p+	AlxGa1-xAs	2000 Å
i	AlxGa1-xAs	2000 Å
i	GaAs	30 Å
i	AlxGa1-xAs	b
i	GaAs	1000 Å
n+	GaAs	1 μm
	S.I. Substrate	

Figure 3.2. Sample structure for the tunneling-out experiments. The barrier is the layer of width b, and the Al composition x was varied from 30 to 50% (see text).

had a barrier width b=86 Å, and Al compositions x of nominally 38% and 50%. A 600-μm diameter mesa was etched down to the n+ buffer and ohmic contacts were made on both n+ buffer and p+ cap, except a 200-μm diameter hole was left for optical access.[26] The p-i-n diodes were operated in reverse bias. Typical current-voltage characteristics are shown in Fig. 3.3, with and without laser light incident on the sample. The reverse bias breakdown voltage was typically about -4V.
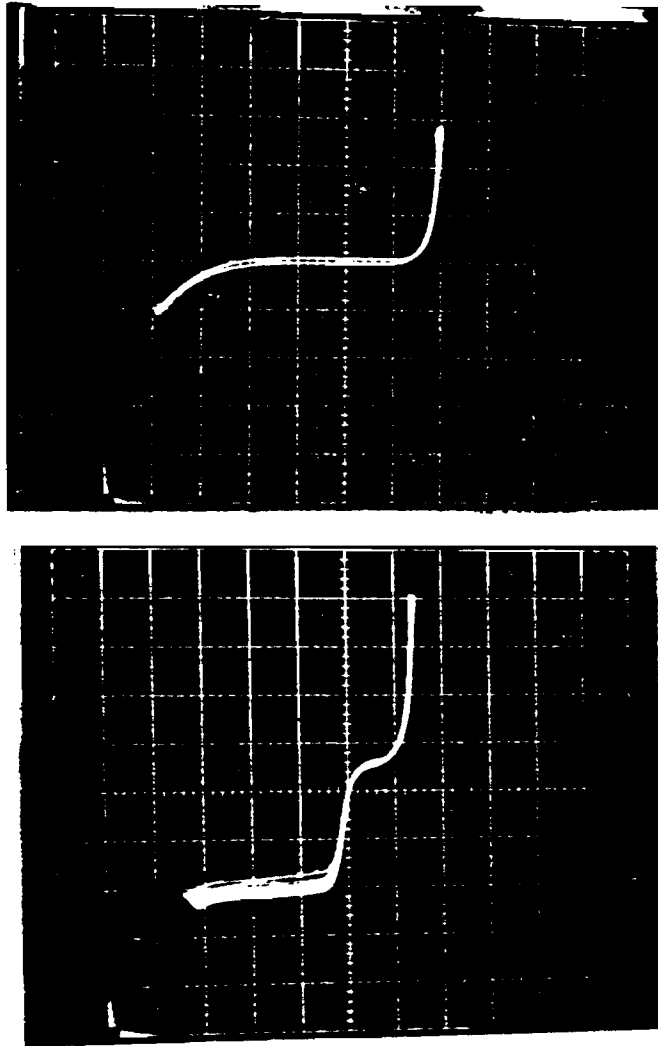
Figure 3.3. Current-voltage (I-V) characteristic for the sample shown in Fig. 3.2. On top is the I-V curve with no light incident on the sample. Below is the I-V curve with the laser pump beam incident. The horizontal scale is 1 V/division; the vertical scale is 20 μA/div.

III.B.2.   Excitation and Luminescence

Electron-hole pairs were injected into the QW at t=0 by a picosecond pulse from a dye laser. The laser system was described in section II.A.1. The laser dye was Pyridine 1; the laser was tuned so only electron-heavy hole pairs were generated. This was to avoid complications due to light hole tunneling through the barrier. However, I found that there was no difference in the results when light holes were also generated; evidently the light hole-heavy hole relaxation time is fast enough so the observed PL decay rates are unaffected.

The samples were held in a cryostat at a temerature of 6 K. At this temperature virtually all the electron-hole pairs are bound in excitons. The strong exciton luminescence spectrum was detected and time-resolved using the setup described in section II.A.4. A typical time-resolved PL spectrum is shown in Fig. 3.4. The advantage of performing time-resolved spectroscopy is that the Stark shift of the PL line with applied electric field can also be simultaneously measured, along with the time dependence of the luminescence. Furthermore, the scattered pump light is also accumulated on the spectrum, so the precise time origin is given.
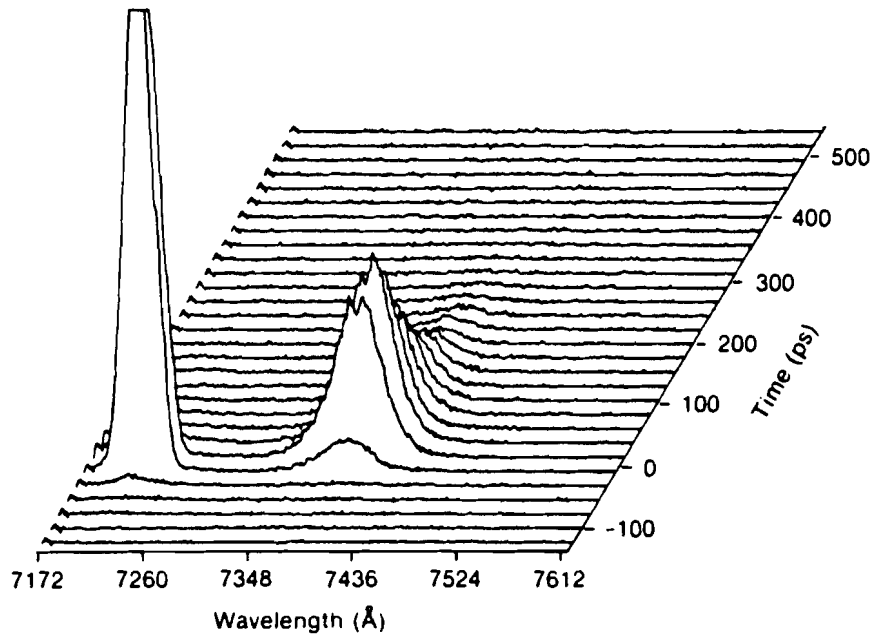
Figure 3.4. Typical time-resolved photoluminescence spectrum. On the left is the scattered laser pump light; on the right is the luminescence from the quantum well.

III.B.3.   PL Decay Times

The PL decay rate can be expressed as

$$\frac{1}{\tau} = \frac{1}{\tau_T} + \frac{1}{\tau_R} , \qquad\qquad (1)$$

where τ_R is the electron-hole recombination (radiative and nonradiative) time, which is of the order of a few hundred picoseconds.   (The actual value depends on the density of trap levels and the injected carrier density).   However, the escape time τ_T is quite independent of those effects and would be equivalent to the measured PL decay time if it were much faster than τ_R.

The PL decays were therefore fitted with single exponential decays.   For decay times much longer than the streak camera response time of 20 ps this was done by simply performing a least-squares fit on the PL decay at t>20 ps.   For decay times close to the streak camera resolution, the data was fitted by using a simple rate equation model so that the effect of the risetime and finite streak camera resolution could be included.   The model assumes that electrons are generated with a rate g (described by a Gaussian pulse with FWHM and time origin determined by the measured pump pulse) into the QW conduction band.   The occupation of the initially populated state is described by n_1.   The

electrons relax to the conduction band origin, where they may bind with the holes to form excitons; this state is described by n_2. (The hole relaxation is assumed to be extremely fast[27]). Thus the combined subband relaxation and exciton formation time are included in a rate k_{sr}. The electron tunneling rate is k_T and the recombination rate is k_R. Hence the rate equations are

$$\frac{dn_1}{dt} = g - (k_T + k_{sr})n_1 \tag{2}$$

$$\frac{dn_2}{dt} = k_{sr}n_1 - (k_T + k_R)n_2 . \tag{3}$$

The observed luminescence is just proportional to n_2.

The equations were numerically integrated, and the rates k_{sr} and k_T varied to give a best fit. (The rate k_R is too small to be important for the case of fast tunneling where the rate equation fit is required). An example of the fit is shown in Fig. 3.5, for the case of the sample with x=0.3, b=85Å at a bias voltage of -1.75V. A good fit is obtained for $1/k_{sr}$=20ps and $1/k_T=\tau_T$=31($\pm$5)ps.

The decay times vs. calculated injected carrier density are plotted in Fig. 3.6. There was no applied electric field for this data. The data show a density-dependent decay time. At low
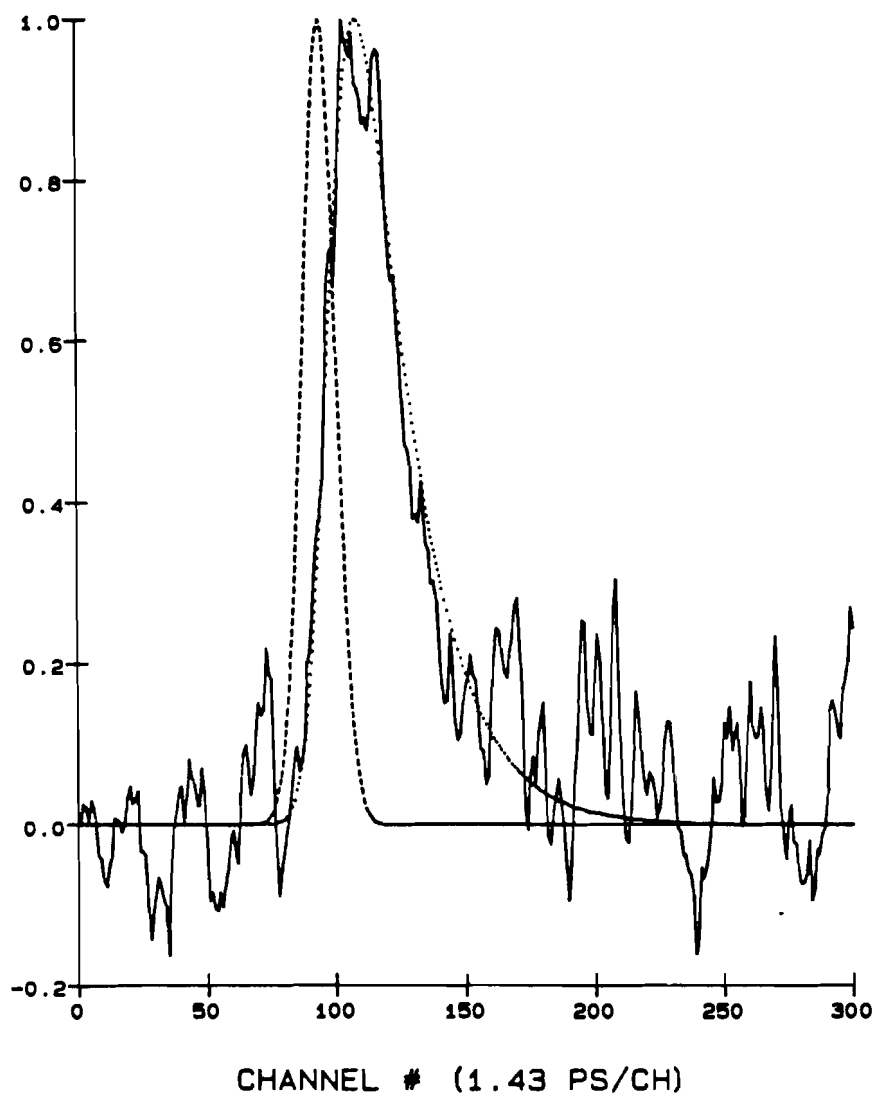
Figure 3.5. Rate equation fit of the luminescence data for the
sample with Al composition x=30% and barrier width
b=85 Å, with an applied bias of -1.75 V. The dashed line
is the laser pulse, the dotted line is the solution for n_2
from the rate equations, and the solid line is the
experimental data. (The time axis is plotted in units of
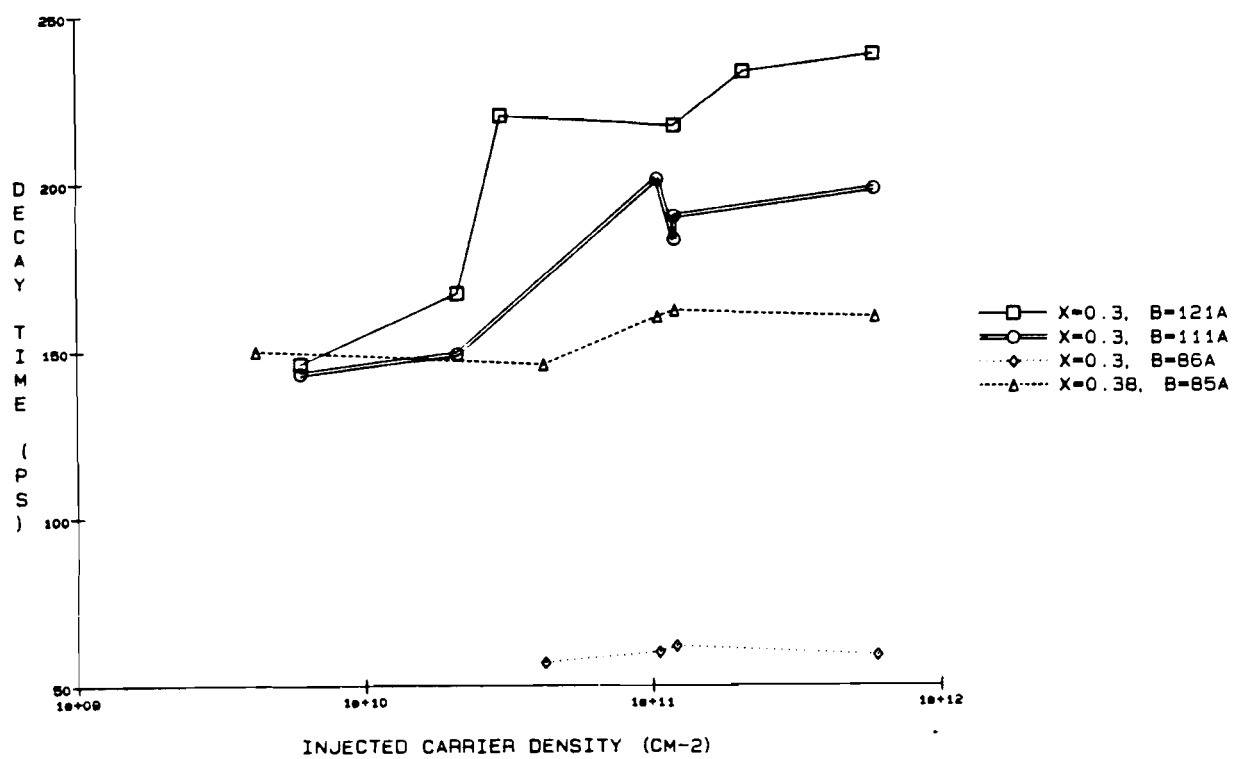the detector channel number).

Figure 3.6. Luminescence decay time vs. injected carrier density.

density, the decay time for all samples is about 150 ps, except for the smallest barrier sample (x=0.3, b=86Å), which has a density-independent decay time of about 60 ps. For larger barrier samples, the decay time increases with density, though this decay time seems to saturate at high density. This behavior has been observed by other workers[28], and is attributed to trap saturation. At low injected density, many carriers (probably holes[28]) fall into traps, thus increasing the observed PL decay rate. At high density, the traps are filled, so the observed PL decay is due only to recombination and tunneling.

III.B.4. Field Dependence of PL Decay

The PL decay as a function of the applied bias is shown in Figs. 3.7 and 3.8 for the various samples. For the data in Fig. 3.7, the Al composition x is 30%, and the barrier width is varied. For Fig. 3.8 the barrier width is constant and the Al composition is varied to study the effect of changing the barrier height. The estimated injected carrier density for these experiments is about 2×10^{10} cm^{-2}. (The observed PL decay times are somewhat longer than observed in the experiment of Fig. 3.6. The discrepancy is likely due to the uncertainty in determining the laser spot size on the sample, and therefore the precise value of the carrier density).
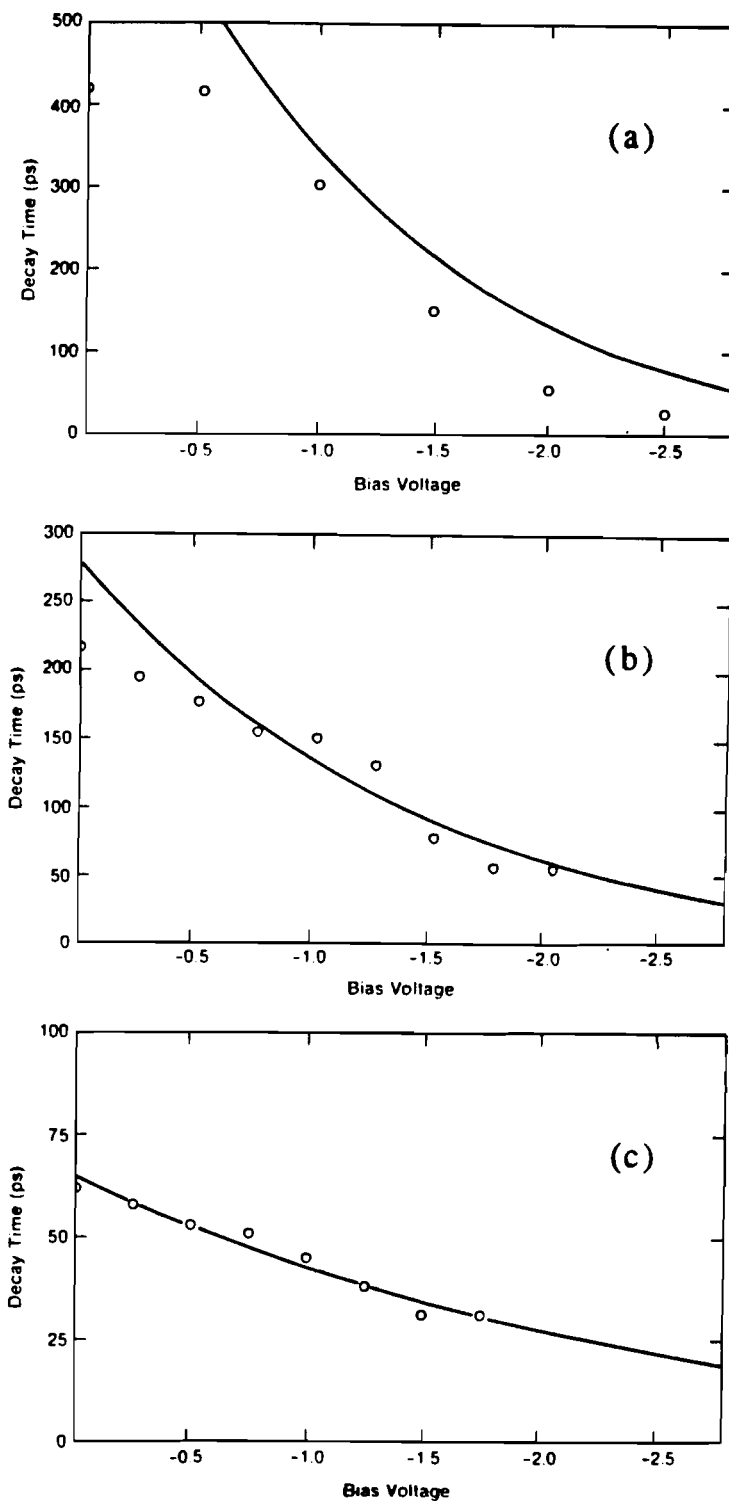
Figure 3.7. Luminescence decay time vs. applied bias for different
barrier widths. The Al composition x=30%. The barrier
widths are (a) 121 Å, (b) 111 Å, and (c) 86 Å. The solid
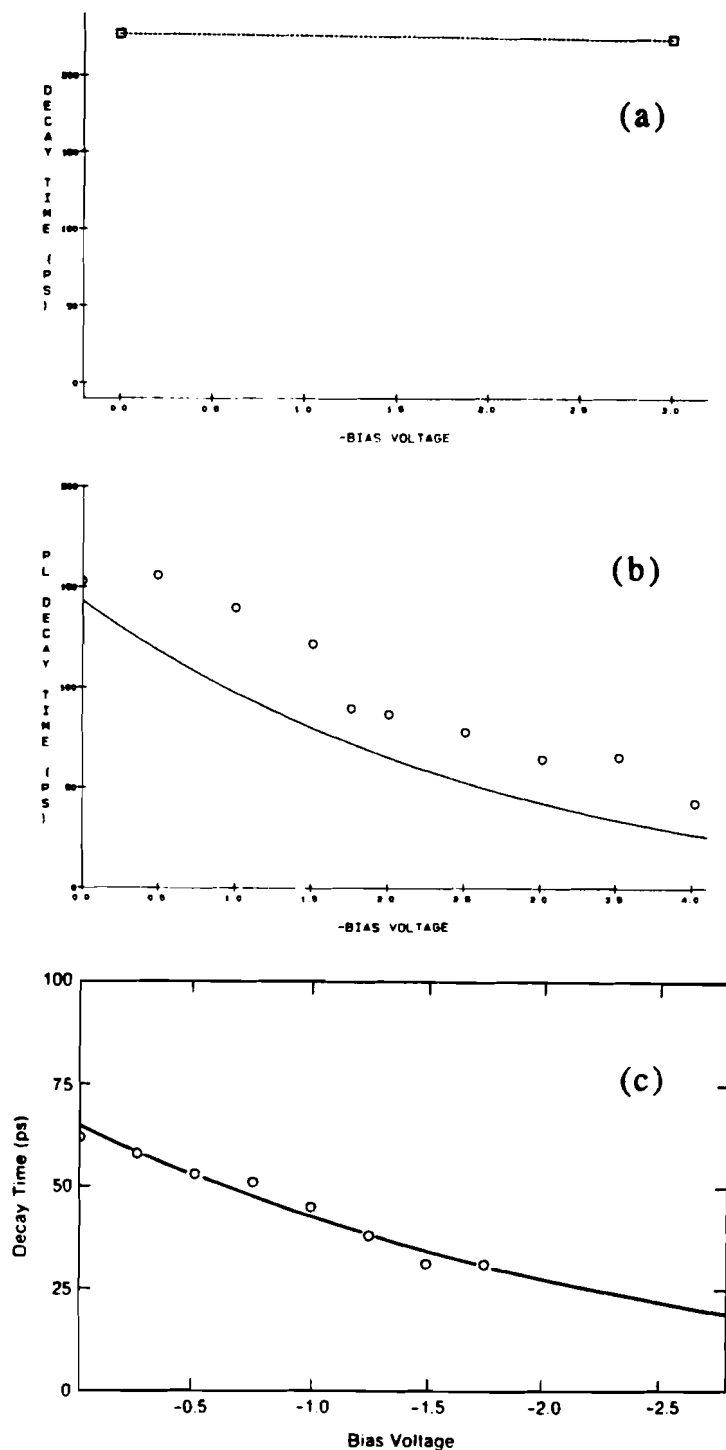lines are the results of the tunneling-out theory
described in section III.C.3.

Figure 3.8.   Luminescence decay time vs. applied bias for different
barrier heights.   The barrier width b=86 Å (85 Å for (c)).
The Al compositions x are (a) 50%, (b) 38%, and (c) 30%.
The dotted line of (a) is simply an aid to the eye; the solid
lines of (b) and (c) are from the tunneling-out theory of
section III.C.3.

The decay time τ at zero bias is strongly dependent on the barrier width (as reported in Ref. 4) and on the height, as expected. Near zero bias, the decrease of τ with applied bias is weak for samples with large barriers; for the data of Figs. 3.7(a) and 3.8(a) the recombination rate dominates at low bias. For higher fields the decay time decreases rapidly with applied field as the tunneling rate begins to dominate, except for 3.8(a), which evidently has such a high barrier that no tunneling is possible. In Fig. 3.7 it is apparent that the rate of decrease in tunneling time with applied field is higher for samples with wider barriers. The reason for this is that as the field increases to tilt the barrier, the effective barrier width to the tunneling electron becomes closer for different samples. A quantitative theory of the tunneling rates is described in section III.C.

III.B.5. PL Stark Shifts

I mentioned previously that the PL spectroscopy system allows the transition energy of the PL to be determined, as well as the time dependence. The resulting Stark shifts are shown in Fig. 3.9. For the sample with x=50%, b=86 Å, which shows no evidence of tunneling, the Stark shift is to lower energy by a few meV. This red shift is typical of previously studied QW structures.[29-31] However, in all other samples the Stark shift appeared as a small blue shift (peaking at about 3 meV for reverse biases in the range
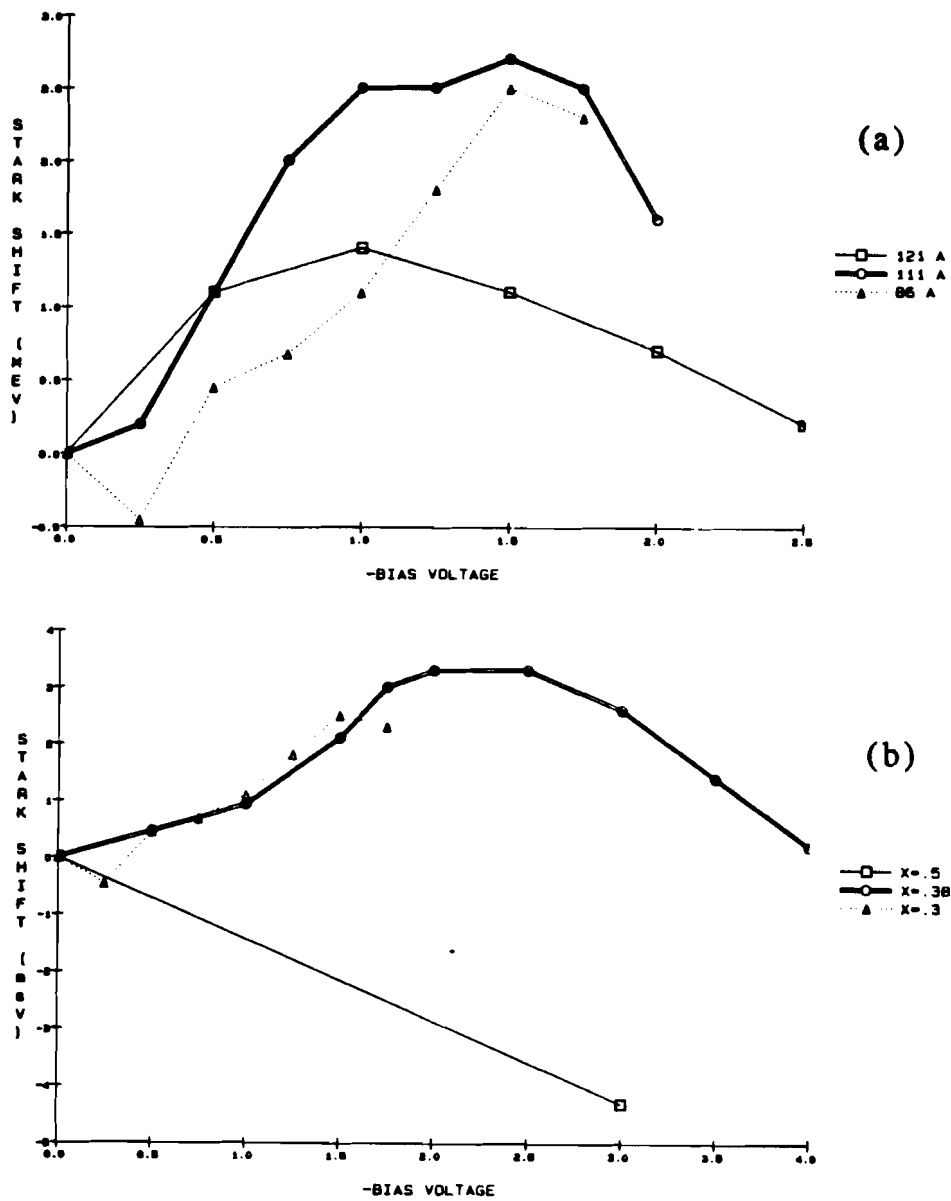
Figure 3.9. Stark shifts of the luminescence lines (a) for samples with different barrier width, and (b), for samples with different height (*i.e.* Al composition x). The error is about ±1 meV.

1-2V). To my knowledge this is the first observation of a blue shift in the PL from a QW with an electric field. I discuss the possible origin of this shift in section III.C.4.

III.C. THEORETICAL INTERPRETATION

III.C.1. Electric Field vs. Bias Voltage

Of course, before any comparison of experiment and theory is possible, it is necessary to determine the relation between the applied bias voltage and the magnitude of the electric field at the location of the QW structure. Sze[32] has calculated the electric field inside a p-i-n diode. The difficulty with applying this calculation to a real MBE-grown AlGaAs p-i-n structure is that the "intrinsic" region in fact has a nonzero background p-type doping.[33] Typically this doping will be in the range 10^{15}-10^{16} cm^{-3}, subject to the precise MBE growth conditions. This background doping will have a strong effect on the field profile inside the diode. Because of the difficulty of determining the doping level in each region of the diode independently, it is not clear how to accurately and self-consistently determine the field profile.[34] To my knowledge only Miller *et.al.*,[35] have attempted to determine the field profile, but they have not published the method they used to determine the (nonuniform) field.

We have taken the simplest approach, determining the depletion region width w by a capacitance-voltage (C-V) measurement,[34] and expressing the field simply as F=V/w where V is the external applied bias. (We find w is in the range of 4000 Å, so for example the field at -2V bias is about 5 x 10⁴ V/cm). Of course this neglects the built-in potential of the diode structure. However, as is shown in Miller *et.al.*,[35] the background p doping tends to reduce the field in the region near the p-i junction, which is where the QW is situated in our samples. Hence our simple approach makes a reasonable first approximation to the field. The good agreement we find between theory and experiment for the tunneling rates provides further confirmation that our approach is reasonable.

III.C.2.   Tunneling Time at Zero Field

In a semiclassical model, the tunneling rate $1/\tau_T$ can be expressed as the product vT of the frequency v of the electron collisions with the barrier and the transmission probability T through the barrier. The oscillation frequency of the electron in the well under flat band conditions is

$$v = \frac{1}{d}\sqrt{\frac{E}{2m_w}} \, , \tag{4}$$

where E is the electron energy (relative to the band edge), d is the well width, and m_W is the electron effective mass inside the well. For our structure v is 1.3×10^{14} s^{-1}.

The transmission coefficient T of the barrier is calculated in the usual way by matching the wavefunctions and probability current across the barrier. The only refinement necessary is that because the electron effective mass is different in the barrier from that in the well and continuum regions, continuity of probability current requires that $(1/m^*)(d\psi/dz)$ instead of just $d\psi/dz$ be continuous across the boundaries. The expression for T under flat band conditions is then

$$T = \frac{4r\,(V-E)E}{\left[(r-1)E+V\right]^2 \sinh^2\left(\frac{b}{\hbar}\sqrt{2m_B\,(V-E)}\right) + 4r\,(V-E)E} \tag{5}$$

where $r=m_b/m_w$, and $m_b\,(m_w)$ is the effective mass in the barrier (well). The calculated tunneling times for the five samples are shown in Table 1, where I have assumed that 65% of the total band offset is in the conduction band.

Table 3.1. Calculated tunneling times for the samples with no applied electric field. The results for the set of samples with Al composition x = 0.3 and different barrier width b are shown in the first column. The results for different Al compositions at fixed b are shown in the second column.

x = 0.3		b = 86 Å	
b (Å)	τ_T(ps)	x	τ_T(ps)
85	17	0.38	143
111	277	0.5	3400
121	809		

III.C.3. Field Dependence of the Tunneling Time

When an electric field is applied to the tunneling structure, both the electron oscillation frequency ν and the transmission coefficient T will change. For the electric fields we are concerned with, ν is essentially constant. This is easily shown by calculating the oscillation period T in the presence of a field from

$$T = 2 \int_{\frac{d}{2}}^{\frac{d}{2}} \frac{dz}{v(z)} , \qquad (6)$$

where $v(z)$ is the instantaneous velocity $\hbar k(z)/m$. The result for

the oscillation period is equation (4) above (with $T = 1/v$), but with a correction term from the field $(eFd/E)^2/32$, which shows that even at a field of 10^5 V/cm the oscillation period changes only by 0.2%.

The transmission coefficient, however, has a very strong dependence on the field. Landau and Lifshitz[3] show that the dependence of the transmission coefficient on the evanescent wavevector κ of a particle inside a potential barrier is

$$T = \exp\left(-2\int_0^b \kappa\, dz\right). \tag{7}$$

Thus we may account for the tilting of the barrier by the electric field by writing the tunneling time as

$$\tau_T = c\exp\left(\frac{2}{\hbar}\int_0^b \sqrt{2m(V-E-eFz)}\, dz\right) \tag{8}$$

where c is a constant. I make the approximation that c and E do not change appreciably with the electric fields considered here. The proportionality constant is obtained by calculating the tunneling time at zero bias as described above.

The results of this calculation are shown as the solid curves in Figs. 3.7 and 3.8. I did not plot the result in Fig. 3.8(a), since for this high barrier, the tunneling time is always much greater than the recombination rate, consistent with experimental observations. For the curve of Fig. 3.7(c), I used a zero-bias tunneling time of 65 ps instead of the calculated value of 17 ps.

This was because I want to show that the expression (8) properly displays the field <u>dependence</u> of the tunneling time, even if it is difficult to calculate the absolute magnitude of the rate accurately.

The difficulty of calculating the precise values of the tunneling time is due to the exponential dependence of the time on the effective mass and barrier width and height. Thus small uncertainties in the sample parameters will produce very large changes in the calculated tunneling time. One might consider fitting the data by varying the sample parameters (*e.g.*, the barrier width), but there are too many degrees of freedom to produce a unique fit. Hence I have assumed that the nominal sample parameters are correct, and have adjusted only the conduction band offset ratio. To illustrate the strong dependence of the tunneling time on the band offset ratio, I note the following. Suppose the conduction band offset. ratio is in the range 62±3%. Then the tunneling time for the sample of Fig. 3.8(a) will be 1.3, 2.1, and 3.2 ns for 59%, 62%, and 63% respectively. The 59% value yields results that are inconsistent with experimental observations at high applied bias. Using a ratio of 65% produces a reasonable fit for all the data except for Fig. 3.7(c).

III.C.4. Luminescence Blue Shift

In section III.B.5 I noted that the Stark shift of the PL line appears as a blue shift for all structures which display tunneling.

This is in contrast to the usually observed red shift. Thus the blue shift is intimately connected with the tunneling. I believe that considerable further experimental and theoretical work will be necessary to understand the cause of this shift. Nevertheless, in this section I will make a few remarks on its possible origin.

One possibility is that as the electrons tunnel from the well, a dipole field builds up that raises the potential barrier seen by the remaining electrons in the well. The higher barrier increases the confinement energy of the electrons in the well; hence the shift in PL to higher energy. This explanation turns out not to be reasonable, since the electrons that have tunneled out of the well will be swept away from the barrier region in about a picosecond. Thus a dipole field cannot build up. Furthermore, the possibility of a transient dipole field can be ruled out, since this would produce a dynamic Stark shift, contrary to observations.

Another possibility is that the shift is due to the holes that are left behind in the well. The holes are strongly confined in the well. Therefore when most of the photogenerated electrons tunnel from the well, the hole lifetime becomes very long since there are no electrons with which they may recombine. If the lifetime is comparable to or longer than the 10 ns time between pump pulses, a substantial positive charge density will build up in the well. Thus the QW will behave in a manner very similar to a p-doped QW.

It is well known that free carriers screen the electron-hole coulomb interaction, thus reducing the exciton binding energy.[36] In fact, Sanders and Chang[37] have calculated the exciton binding energy as a function of dopant charge density for p-type modulation-doped wells. Such a reduction in binding energy would of course produce a blue shift in PL energy. However, a competing effect is band-gap renormalization, which shifts the band edge to lower energy with increasing density.[38] There have been some calculations of the optical properties of doped QW's, but they have principally concentrated on the absorption spectrum.[37,39,40] Obviously, further theoretical and experimental study is required to determine if the blue shift is in fact a many-body effect.

III.D. References

1. G. Gamow, "Zur Quantentheorie des Atomkernes," Zeits. f. Physik **13**, 117 (1923).

2. R.H. Fowler and W. Nordheim, "Electron Emission in Intense Electric Fields," Proc. Roy. Soc., A **119**, 173 (1928).

3. L.D. Landau and E.M. Lifshitz, Quantum Mechanics, Non-Relativistic Theory, 3rd ed. (Pergamon Press, New York, 1977), pp. 178-181.

4. M. Tsuchiya, T. Matsusue, and H. Sakaki, "Tunneling Escape Rate of Electrons From Quantum Well in Double-Barrier Heterostructures," Phys. Rev. Lett. **59**, 2356 (1987).

5. T.C.L.G. Sollner, P.E. Tannenwald, D.D. Peck, and W.D. Goodhue, "Quantum Well Oscillators," Appl. Phys. Lett. **45**, 1319 (1984).

6. E.R. Brown, T.C.L.G. Sollner, W.D. Goodhue, and C.D. Parker, "Millimeter-Band Oscillations Based on Resonant Tunneling in a Double-Barrier Diode at Room Temerature," Appl. Phys. Lett. **50**, 83 (1987).

7. T.C.L.G. Sollner, E.R. Brown, W.D. Goodhue, and H.Q. Le, "Observation of Millimeter-Wave Oscillations From Resonant Tunneling Diodes and Some Theoretical Considerations of Ultimate Frequency Limits," Appl. Phys. Lett. **50**, 332 (1987).

8. T.C.L.G. Sollner, W.D. Goodhue, P.E. Tannenwald, C.D. Parker, and D.D. Peck, "Resonant Tunneling Through Quantum Wells at Frequencies up to 2.5 THz," Appl. Phys. Lett. **43**, 588 (1983).

9.   B. Ricco and M. Ya. Azbel, "Physics of Resonant Tunneling. The One-Dimensional Double-Barrier Case," Phys. Rev. B **29**, 1970 (1984).

10.   S. Luryi, "Frequency Limit of Double-Barrier Resonant-Tunneling Oscillators," Appl. Phys. Lett. **47**, 490 (1985).

11.   A.D. Stone and P.A. Lee, "Effect of Inelastic Processes on Resonant Tunneling in One Dimension," Phys Rev Lett. **54**, 1196 (1985).

12.   D.D. Coon and H.C. Liu, "Time-Dependent Quantum-Well and Finite-Superlattice Tunneling," J. Appl. Phys. **58**, 2230 (1985).

13.   D.D. Coon and H.C. Liu, "Frequency Limit of Double Barrier Resonant Tunneling Oscillators," Appl. Phys. Lett. **49**, 94 (1986).

14.   W.R. Frensley, "Transient Response of a Tunneling Device Obtained from the Wigner Function," Phys. Rev. Lett. **57**, 2853 (1986).

15.   H.C. Liu, "Tunneling Time Through Heterojunction Double Barrier Diodes," Superlattices and Microstructures **3**, 379 (1987).

16.   T. Weil and B. Vinter, "Equivalence Between Resonant Tunneling and Sequential Tunneling in Double-Barrier Diodes," Appl. Phys. Lett. **50**, 1281 (1987).

17.   M. Jonson and A. Grincwajg, "Effect of Inelastic Scattering on Resonant and Sequential Tunneling in Double Barrier Heterostructures," Appl. Phys. Lett. **51**, 1729 (1987).

18. H.C. Liu, "Time-Dependent Approach to Double-Barrier Quantum Well Oscillators," Appl. Phys. Lett. **52**, 453 (1988).

19. J.D. Bruno, T.B. Bahder, and C.A. Morrison, "Limiting Response Time of Double-Barrier Resonant Tunneling Structures," Phys. Rev. B **37**, 7098 (1988).

20. P.J. Price, "Theory of Resonant Tunneling in Heterostructures," Phys. Rev. B **38**, 1994 (1988).

21. H. Guo, K. Diff, G. Neofotistos, and J.D. Gunton, "Time-Dependent Investigation of the Resonant Tunneling in a Double-Barrier Quantum Well," Appl. Phys. Lett. **53**, 131 (1988).

22. J.F. Whitaker, G.A. Mourou, T.C.L.G. Sollner, and W.D. Goodhue, "Picosecond Switching Time Measurment of a Resonant Tunneling Diode," Appl. Phys. Lett. **53**, 385 (1988).

23. R. Gupta and B.K. Ridley, "The Effect of Level Broadening on the Tunneling of Electrons Through Semiconductor Double-Barrier Quantum-Well Structures," J. Appl. Phys. **64**, 3089 (1988).

24. S.C. Kan, and A. Yariv, "The Ultimate Frequency Response and Time Evolution of Resonant Tunneling in Double-Barrier Structures," J. Appl. Phys. **64**, 3098 (1988).

25. F. Capasso, K. Mohammed, and A.Y. Cho, "Resonant Tunneling Through Double Barriers, Perpendicular Quantum Transport Phenomena in Superlattices, and Their Device Applications," IEEE J. Quant. Electron. **QE-22**, 1853 (1986).

26. The sample growth and processing were done at Cornell University by Xiao Song, with advice and help from Bill Schaff.

27. J. Shah, A. Pinczuk, A.C. Gossard, and W. Wiegmann, "Energy-Loss Rates for Hot Electrons and Holes in GaAs Quantum Wells," Phys. Rev. Lett. **54**, 2045 (1985).

28. J.F. Ryan, R.A. Taylor, A.J. Turberfield, A. Maciel, J.M. Worlock, A.C. Gossard, and W. Wiegmann, "Time-Resolved Photoluminescence of Two-Dimensional Hot Carriers in GaAs-AlGaAs Heterostructures," Phys. Rev. Lett. **53**, 1841 (1984).

29. D.A.B. Miller, D.S. Chemla, T.C. Damen, A.C. Gossard, W. Wiegmann, T.H. Wood, and C.A. Burrus, "Electric Field Dependence of Optical Absorption Near the Band Gap of Quantum Well Structures," Phys. Rev. B **32**, 1043 (1985).

30. H.-J. Polland, L. Schultheiss, J. Kuhl, E.O. Gobel, and C.W. Tu, "Lifetime Enhancement of Two-Dimensional Excitons by the Quantum-Confined Stark Effect," Phys. Rev. Lett. **55**, 2610 (1985).

31. E.J. Austin and M. Jaros, "Electric Field Induced Shifts and Lifetimes in GaAs-GaAlAs Quantum Wells," Appl. Phys. Lett. **47**, 274 (1985).

32. S.M. Sze, <u>Physics of Semiconductor Devices</u>, 2nd ed., (J. Wiley, New York, 1981).

33. X.J. Song, private communication, 1988.

34. X.J. Song, private communication, 1988.

35. D.A.B. Miller, *et.al., op. cit.,* Figure 2.

36. H. Haug and S. Scmitt-Rink, "Electron Theory of the Optical Properties of Laser-Excited Semiconductors," Prog. Quantum Electron. **9**, 3 (1984).

37. G.D. Sanders and Yia-Chung Chang, "Theory of Photoabsorption in Modulation-Doped Semiconductor Quantum Wells," Phys. Rev. B **35**, 1300 (1987).

38. H. Haug and S. Scmitt-Rink, "Basic Mechanisms of the Optical Nonlinearities of Semiconductors Near the Band Edge," J. Opt. Soc. Am. B **2**, 1135 (1985).

39. G.E.W. Bauer and T. Ando, "Electronic Structure of Free Carriers in Quantum Wells Calculated by Density-Functional Theory," Phys. Rev. B **34**, 1300 (1986).

40. G. Livescu, D.A.B. Miller, D.S. Chemla, M. Ramaswamy, T.Y. Chang, N. Sauer, A.C. Gossard, and J.H. English, "Free Carrier and Many-Body Effects in Absorption Spectra of Modulation-Doped Qauntum Wells," IEEE J. Quantum Electron. **QE-24**, 1677 (1988).

CHAPTER IV

TUNNELING BETWEEN COUPLED QUANTUM WELLS

In this chapter I describe experiments performed to investigate tunneling between weakly coupled quantum wells (QW's) using time-resolved optical spectroscopy. As I discussed in chapter I, the double-well problem is an old problem in quantum mechanics. However, the development of bandgap engineering in semiconductors has made it possible to design the potential well parameters (widths, depths, and barrier width between the two wells), rather than just take what nature provides. This has rejuvenated interest in the double-well problem from a fundamental point of view.[1-3] The study of coupled QW's is of practical as well as basic interest, however. Some workers[4-7] have begun to investigate coupled QW's for use as optical modulators, since the absorption edge Stark shift with an applied electric field is larger than that of an isolated well for the same field strength. The second-order susceptibility of the asymmetric coupled QW system has also been calculated and proposed for electro-optical applications.[9] Most studies have been of strongly coupled wells (*i.e.*, a thin barrier between the wells); the work presented here concerns weakly coupled wells.

The ability to design the potential profile of the double-well system has enabled us to solve a long-standing experimental

problem. The classic formulation of the double-well tunneling problem is to suppose that an electron (or other excitation) is initially localized in one well at time t=0. The question is how long it takes for the electron to tunnel to the other well. The experimental difficulty is how to localize the excitation at t=0. As I will discuss in section C of this chapter, this problem may be solved by using an asymmetric double-well structure, in which a photoexcited electron-hole pair may be injected with a short laser pulse into just one of the wells.

In this chapter I first give (in section A) an introduction to the double-well problem, and provide a background for the interpretation of the experimental results. In section B, I discuss experiments using time-resolved photoluminescence (PL) to observe tunneling in double-QW's. In section C, I present the results of subpicosecond time-resolved absorption spectroscopy performed in an attempt to resolve the fast tunneling from an initially localized state.

IV.A   Introduction to the Double-Well Problem

IV.A.1.   States of the System

If the two QW's are not too strongly coupled, it is possible to determine the wavefunctions and energies of the coupled-well system from the isolated-well wavefunctions ψ_L and ψ_R (which I

refer to as the site basis). Tunneling problems are generally thought of in the site basis, since one considers the tunneling of a particle from one localized state to another. However, the time dependence of the total wavefunction is most easily determined in the eigenstate basis ϕ_i of the total Hamiltonian H of the coupled-well system because the time dependence of these states is simply

$$\Phi_i(t) = \phi_i \, e^{-iE_i t/\hbar} \, , \tag{1}$$

where E_i is the energy of the eigenstate ϕ_i. The tunneling behavior can be determined by simply transforming back to the site basis. Thus we must first calculate the eigenfunctions of H given the site basis wavefunctions.

The eigenfunctions of the double-well potential may be written as

$$\phi_i = c_{Li} \, \psi_L + c_{Ri} \, \psi_R \, , \quad i = 1,2 \, , \tag{2}$$

so the eigenvalue equation is

$$(H - E_i)(c_{Li} \, \psi_L + c_{Ri} \, \psi_R) = 0 \, . \tag{3}$$

Multiplying by ψ_L^*, integrating over all space, and repeating the operation with ψ_R^* yields

$$\begin{bmatrix} H_{LL} - E_i & H_{LR} - E_i S_{LR} \\ H_{RL} - E_i S_{RL} & H_{RR} - E_i \end{bmatrix} \begin{bmatrix} c_{Li} \\ c_{Ri} \end{bmatrix} = 0 , \qquad (4)$$

which must be solved for the eigenvalues E and the mixing coefficients c. The integrals are

$$H_{JK} = \int_{-\infty}^{\infty} \psi_J H \psi_K \, dz \qquad (5)$$

$$S_{JK} = \int_{-\infty}^{\infty} \psi_J \psi_K \, dz , \qquad (6)$$

where J and K label L and R. In the usual formulation of the double-well problem, the S_{JK} integrals are assumed to be zero. In this case the eigenvalue equation becomes the familiar

$$\begin{bmatrix} E_L - E & V \\ V & E_R - E \end{bmatrix} \begin{bmatrix} c_L \\ c_R \end{bmatrix} = 0 , \qquad (7)$$

where V is the tunneling matrix element and $E_{L,R}$ are the isolated well eigenvalues. Including the overlap integrals S_{JK} allows the nonorthogonality of the site-basis wavefunctions to be included.

To illustrate the discussion, I will show the calculations for one of the samples used in the differential absorption spectroscopy experiments (referred to in section IV.C as sample C). The conduction band diagram is shown in Fig. 4.1 for flat band conditions (*i.e.*, with no external electric field). The isolated well energies are also given. Calculation of the states using (4) above reveals that the

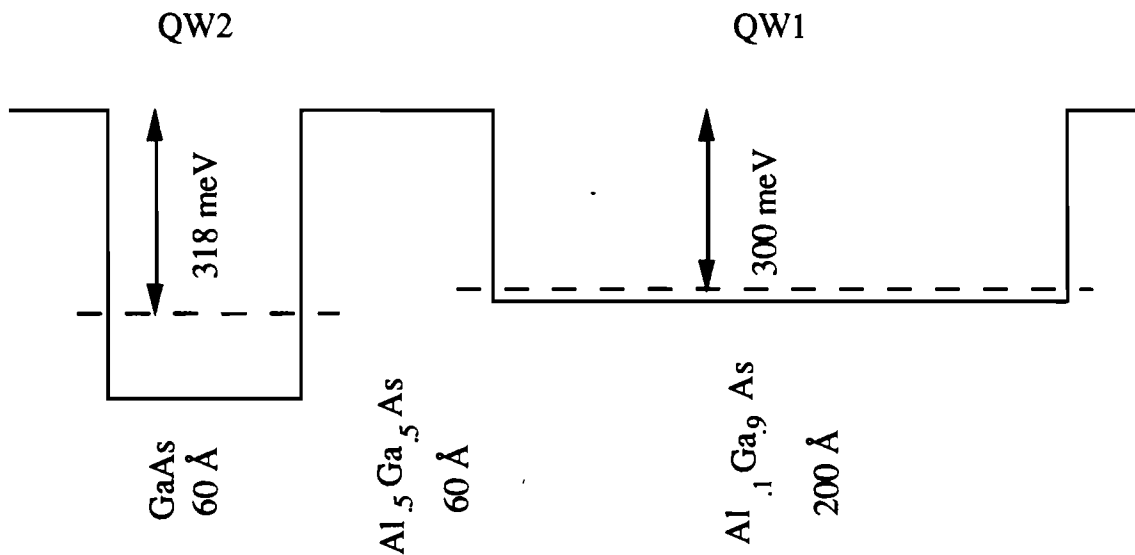QW2   QW1

Figure 4.1.   Conduction band diagram for sample C, showing the lowest electron energies in each well.

states are strongly localized in each well, there being less than 0.03% admixture of the ψ_R state in the ground state ϕ_1, and, correspondingly, less than 0.03% admixture of ψ_L in ϕ_2.

It is necessary to apply a bias voltage for the electron levels of the two wells to be in resonance. In this case, the calculation of the states becomes complicated, since the isolated well wavefunctions and energies shift with the field as I discussed in chapter I. The eigenfunctions and energies can be calculated "exactly" by numerical integration of the Schrödinger equation. Vinter[9] has done this for two of the experimental samples (referred to as A and B); the results are given in section IV.B.2.

An alternative approach is to solve the problem approximately by taking the band edges in the wells and barriers to be flat, and simply take up the voltage difference between the wells at the well/barrier boundaries. The results of such a calculation should not be taken too seriously, but the qualitative conclusions regarding the field-dependent behavior should be reasonably accurate. The results for the energies of the two lowest electron states are shown in Fig. 4.2(a). (The $n \neq 1$ states of the two isolated wells are ignored). The site probabilities for the ground state $|c_{L1}|^2$ and $|c_{R1}|^2$ are shown in Fig. 4.2(b). The most important conclusion is that the wells are weakly coupled so that the state mixing is small over only a narrow range of the electric field. The magnitude of the anticrossing is about 0.2 meV.
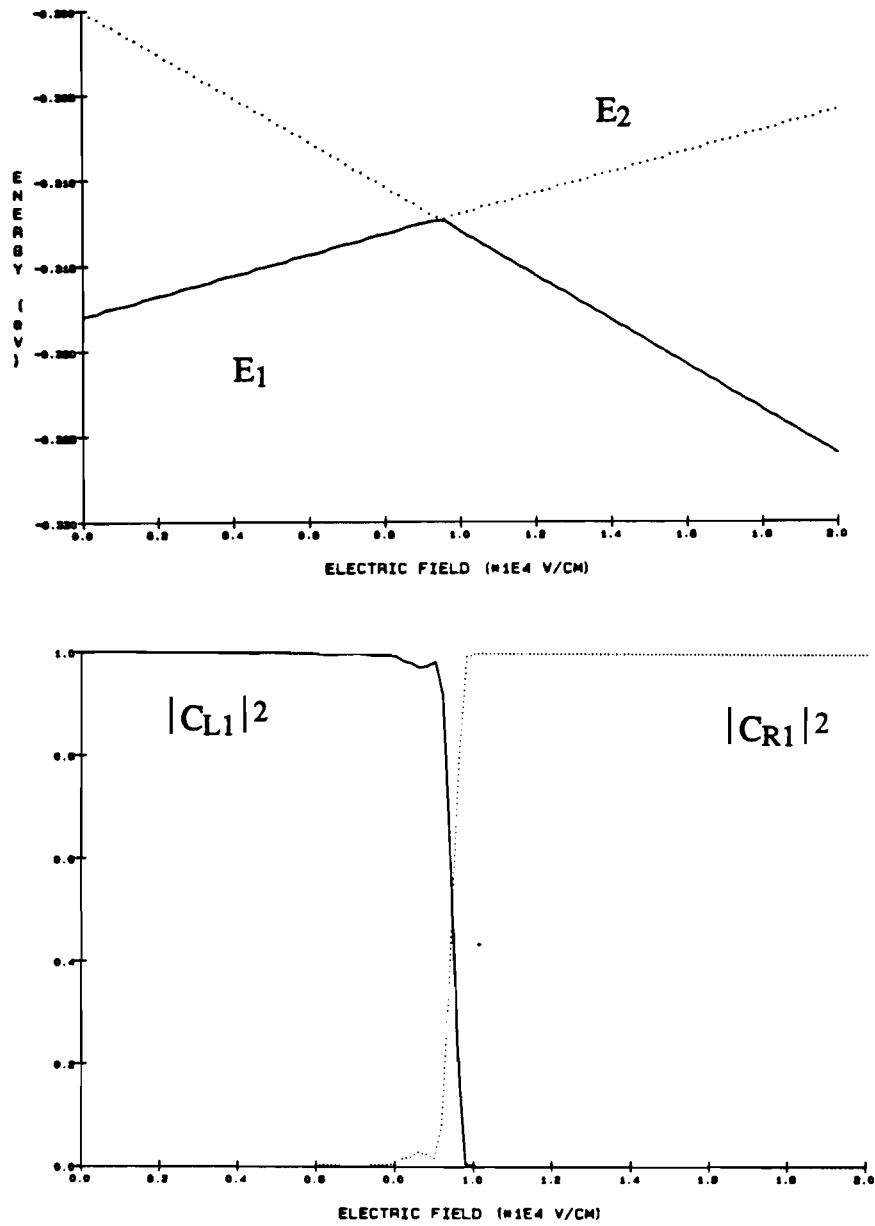
Figure 4.2. The calculated energies of the two lowest states of sample C vs. electric field are shown at the top. Below are the corresponding site probabilities $|c_{L1}|^2$ and $|c_{R1}|^2$ for the lower state.

So far I have discussed the electronic states in the conduction band of the double-QW system. However, the photoexcitation of the QW injects electron-hole pairs, which interact strongly via the Coulomb interaction as I discussed in section I.B.2. The importance of the electron-hole binding for tunneling can be seen as follows. Suppose an electron-heavy-hole pair is injected into the left well (QW2) of the structure shown in Fig. 4.1. The electron may tunnel into QW1, but the heavy hole remains in QW2. However, for the electron to tunnel, it must overcome the strong potential due to the hole in QW2. In effect, what is required is the difference in binding energy between the QW2 exciton (electron and hole both in QW2) and the "charge-transfer" (CT) exciton, in which the electron is in QW1 while the hole is in QW2. The binding energy of the QW2 exciton is about 9 meV.

Knox and Sha[10] have calculated the binding energy of the CT exciton. The essence of their calculation is to extend the Hamiltonian of eqn. (9) of section I.B.2 to include the potentials of both wells. A variational approach similar to that described in section I.B.2 is used, with the addition that the n=2 state of each well is included, the mixing coefficient being a variational parameter. This is done to include the "polarization" of the wavefunctions due to the electron-hole interaction across the barrier. The result for the sample of Fig. 4.1 (sample C) is a binding energy E_{CT} = -3.4 meV. The CT transition oscillator

strength has not been calculated, but is expected to be very small due to the small overlap of the electron and hole wavefunctions.

IV.A.2. Time Development of an Initially Localized State

Suppose that an electron is initially in the left well (QW2) at t=0. The question is, how long does it take to tunnel to the other well? To answer this we follow the program outlined above, and express ψ_L in terms of the ϕ_i. The most convenient way of doing this is to note that normalization of the ψ and ϕ wavefunctions implies that the ϕ's can be written as

$$\phi_1 = \cos\alpha \ \psi_L + \sin\alpha \ \psi_R \tag{8}$$

$$\phi_2 = -\sin\alpha \ \psi_L + \cos\alpha \ \psi_R . \tag{9}$$

From this we can see that the inverse transformation is

$$\psi_L = \cos\alpha \ \phi_1 - \sin\alpha \ \phi_2 \tag{10}$$

$$\psi_R = \sin\alpha \ \phi_1 + \cos\alpha \ \phi_2 . \tag{11}$$

Thus the total wavefunction for an electron that is in state ψ_L at t=0 is

$$\Phi(z,t) = (\cos\alpha\,\phi_1 - \sin\alpha\,\phi_2\,e^{-i\Delta Et/\hbar})\,e^{-iE_1t/\hbar}, \qquad (12)$$

where $\Delta E = E_2 - E_1$ is the eigenstate energy splitting. Thus the probability of finding the electron in the right well is trivially found to be

$$P_R = \left[\int \psi_L^* \Phi\,dz\right]^2 = 1 - \frac{1}{2}\sin^2 2\alpha\,(1 - \cos\frac{\Delta Et}{\hbar}). \qquad (13)$$

(where this time I have neglected the integrals S_{JK}). Thus the electron oscillates between the two wells with a period

$$T = \frac{2\pi\hbar}{\Delta E} \qquad (14)$$

and amplitude

$$A = \sin^2 2\alpha. \qquad (15)$$

This amplitude is equal to unity only for the completely symmetric case. The principal effect of asymmetry is to reduce the amplitude of the tunneling oscillations, even if the isolated

well energies are degenerate. Furthermore, the amplitude is significant only near resonance, since only then are the isolated well wavefunctions strongly mixed.

For example, for sample C at zero bias, the oscillation period is T = 200 fs, and the amplitude A = 2 x 10^{-3}. At resonance (electric field F = 9.5 x 10^3 V/cm) the period is T $\approx$ 20 ps and the amplitude A $\approx$ 0.8.

Of course, the above picture of tunneling in the double-well system is highly idealized. In the real world, the electrons will interact with themselves and with the lattice (through phonons, impurities, interface disorder at the QW boundaries, and alloy disorder in the barrier region). Thus the effect of scattering on the tunneling must be considered. There is a considerable body of literature on the problem of tunneling in the presence of damping.[11-13] The fundamental conclusion is that in the presence of scattering, the discrete states of each well are broadened into a continuum, which destroys the reversibility of the tunneling. In fact, an analogy may be drawn between the tunneling-out problem, which considers the irreversible tunneling from a discrete state into a continuum of states, and the problem of tunneling between sites. In the presence of scattering, the density of final states forms a continuum, and the tunneling becomes irreversible. This point has been elaborated upon by Knox[11] and Duke.[12]

Another way of stating this conclusion is to say that collisions destroy the phase coherence represented by the off-diagonal elements of the density matrix ρ_{12} and ρ_{21}, so the tunneling oscillations are damped. Knox[11] has pointed out that the observability of the coherent tunneling depends on the oscillation period relative to the phase "memory" time. In the limit of strong scattering, the tunneling will appear as a rate process. In fact, it is such rate processes that are generally observed experimentally. To my knowledge there are no time-domain experiments which have observed coherent tunneling oscillations between spatially separated sites. Of course, the two-site coherent tunneling problem is completely analogous to other situations in physics, where a coherent superposition of eigenstates is prepared at t=0, and quantum interferences appear as the system evolves. Two well-studied examples are the phenomenon of quantum beats in atomic resonance fluorescence,[14,15] and K-meson oscillations in particle physics.[16]

Many different scattering mechanisms are possible in QW structures. Weisbuch[17] has given an overview of the various mechanisms and their relative importance. At room temperature, the dominant mechanism is polar optical scattering. At low temperature, impurity scattering is most important, although the scattering rate is also dependent on the carrier density.[18] Capasso et. al.[19] have remarked that a good way to estimate the total scattering time is from mobility measurements on modulation-

doped QW's, since the mobility is related to the average momentum relaxation time by

$$\mu = \frac{e}{m}\tau.$$

At T = 300K the mobility is about 7000 cm^2/Vs, which corresponds to τ = 300 fs. For T < 77K, the mobility is greater than 10^5 cm^2/Vs, so the scattering time is longer than 50 ps. These numbers are typical for the density range of 10^{11} to 10^{12} cm^{-2}, which is the range in which the optical experiments were performed. One additional scattering mechanism to which the mobility measurements are not very sensitive, but which likely will be important for the tunneling experiments, is alloy scattering in the barrier region. This scattering rate will depend on the sample quality, and is very difficult to estimate. The important conclusion is that scattering limits the observability of coherent tunneling at room temperature rather severely, but is not a limiting factor at cryogenic temperatures.

A more serious and unavoidable impediment to the observation of coherent tunneling may be inhomogeneous broadening of the QW energy levels due to well width fluctuations. In this case the real coupled-well system cannot be described by a unique value of ΔE. The inhomogeneous broadening may be estimated by assuming well-width fluctuations of one monolayer. This gives for the 60 Å well of Fig. 4.1 a width of $\Gamma \approx 5$ meV, which implies the tunneling period must

be shorter than 100 fs for any coherence to be observed. The inhomogeneous broadening will be less of a problem for wider wells, but significantly worse for narrower wells. In fact, interface quality appears to be the limiting factor in determining the observability of coherent tunneling.

Although the ultimate goal of observing coherent tunneling is extremely difficult, the tunneling rate between the wells is nevertheless interesting, partly because scattering can not only destroy the coherence of the tunneling, it can also induce transitions between the QW's. In collision-induced tunneling, an electron localized in one well can for example scatter off an impurity, or absorb a phonon, and end up in the other well. This scattering can be elastic (as in the case of ionized impurity scattering), or inelastic (as in the case of phonon-assisted tunneling).

Generally scattering-assisted tunneling is most easily thought of in terms of intersubband scattering; the transition rate for scattering from subband i to subband f is given by the Golden Rule as

$$W_{fi} = \frac{2\pi}{\hbar} \sum_{k_i, k_f, q} \left| < \chi_f |H'| \chi_i > \right|^2 f_i (1-f_f) \delta(E_{k_f} - E_{k_i} \pm E_{col}). \quad (16)$$

In this equation H' is the interaction Hamiltonian, χ is the full three-dimensional wavefunction

$$\chi_i = \frac{1}{\sqrt{A}} e^{i\mathbf{k}\cdot\rho} \phi_i(z) u_{i,\mathbf{k}}(\mathbf{r}), \qquad (17)$$

A is the sample area, ρ is the cylindrical radius in the QW plane, f_i (f_f) is the distribution function of electrons in the initial (final) subband, and $\mathbf{k}$ refers to the momentum parallel to the interface. The energy gained or lost by the electron in a collision is given by E_{col}, which is zero for elastic scattering. The scattering momentum wavevector is $\mathbf{q}$. Once the scattering rate between the subbands is known (in both directions), the population flow between the two wells may be calculated since one knows the projection of the wavefunction on each site. (This is generally rather simple since as we have seen the electronic states are strongly localized on each site except in a narrow resonance region).

· This is the procedure followed by Weil and Vinter[20] in their calculation of LO-phonon-assisted tunneling between coupled quantum wells. (The only additional assumption they require is that the electron gas is nondegenerate, and thus can be described by a Boltzmann distribution). Vinter[21] has performed the calculation for one of our experimental samples (sample A, described in section IV.B.2); the results are given in Fig. 4.3. These results are for a temperature of 77K; the scattering rate will be significantly higher at room temperature (indeed the rate for electrons to scatter from the lowest subband to the second subband via absorption of a phonon will probably increase by
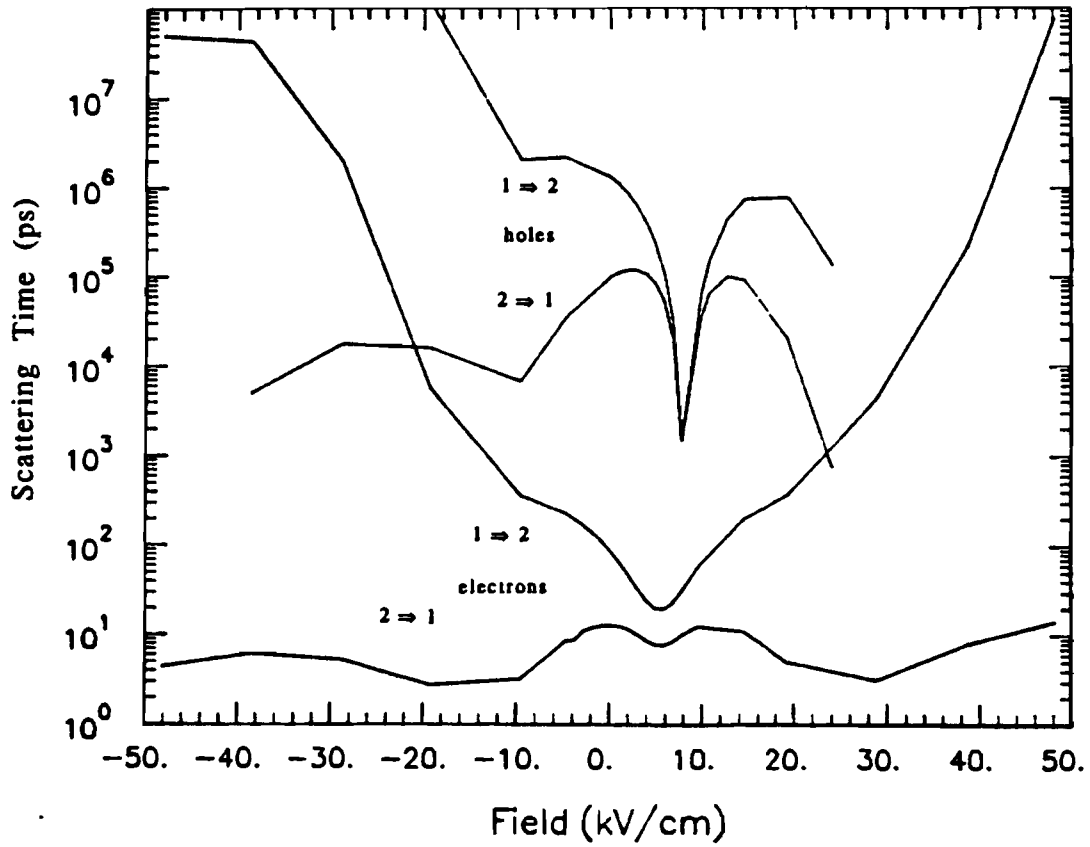
Figure 4.3. Calculated phonon-assisted scattering rates at T=77K for the nominal paramters of sample A (which is described in detail in section IV.B.2). (ref. 21).

over two orders of magnitude[22]). At 6K, all the phonon-assisted scattering rates will be negligible.

A similar calculation of tunneling via ionized impurity scattering has been given by Sawaki *et. al.*[23] A third mechanism which is expected to be important for intersubband scattering is interface roughness scattering,[24] but to my knowledge this calculation has not been performed for the coupled-well system.

IV.A.3. Time Development with Initial Excitation in Both Wells

In chapter II I discussed the two experimental methods we have applied to optically time-resolve tunneling, namely photoluminescence (PL) and absorption spectroscopy. The latter has a time resolution of about 100 fs, and is appropriate for the study of tunneling from an initially localized state. However, the PL time resolution is limited to about 20 ps. Furthermore, in order to monitor the populations of both wells, PL experiments require that electron-hole pairs be injected into both wells by the laser pump. The pump laser is tuned above the exciton lines of both wells so that the scattered laser light will be spectrally separated from the QW PL. Therefore the carriers are injected at $k_{||} \neq 0$, and will scatter and thermalize within a few hundred fs (which is much shorter than the pump pulse width of a few ps). Thus the carriers are injected into both wells with no phase

coherence between the subbands; hence no coherent tunneling can be observed.

Tunneling between the wells via rate processes can certainly occur, however, so the PL experiments can be used to observe tunneling. The signatures of tunneling in these experiments are a decrease in the decay time of the QW PL lines as the tunneling rate increases, and the buildup of a "charge-transfer" state, in which the electrons and holes are in different wells. (This occurs since as an electric field is applied, the electrons and holes will tend to tunnel in opposite directions). The various PL processes relevant to tunneling studies are shown schematically in Fig. 4.4.

IV.A.4.   Concluding Remarks

The tunneling-out experiments of chapter III turned out to be (perhaps surprisingly) quite simple. To a good approximation the rate could be described by a very simple semiclassical model; none of the scattering mechanisms I described in this section had to be invoked to understand the results. The coupled-well problem, however, is considerably more complicated. The simplest theory reveals that the tunneling should be oscillatory, but will only occur with significant amplitude when the energy levels of the two wells are very close to resonance. However, if the two levels are within kT of each other and are weakly coupled, population will certainly transfer from one well to the
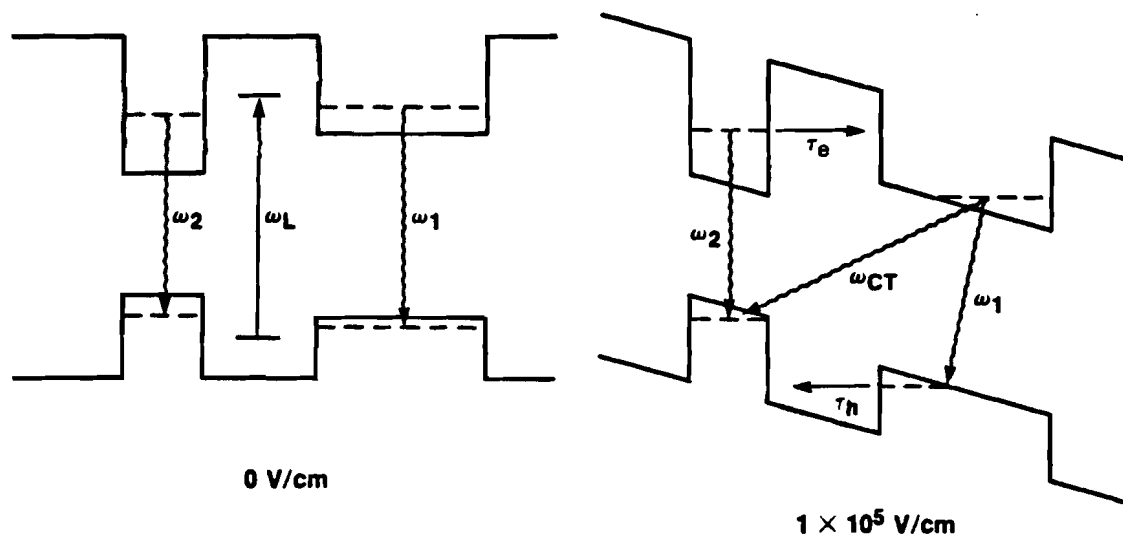
Figure 4.4. Photoluminescence processes in double-quantum-well structures. The charge-transfer (CT) state luminescence comes from recombination of electrons in QW1 and holes in QW2.

other until equilibrium is reached. It is not a simple matter to determine *a priori* what the tunneling rate will be, given the number of possible mechanisms (and equally importantly, the strong dependence of the tunneling rate on the precise sample parameters). Nevertheless, tunneling in double-QW's is well worth studying experimentally, partly because the theoretical picture is far from obvious.

IV.B.   Photoluminescence Experiments

In this section I present the results of time-resolved and continuous (cw) photoluminescence (PL) spectroscopy experiments we performed to observe tunneling in asymmetric DQW structures. As I mentioned in section II.A.4 earlier, the time resolution of the streak-camera PL system is about 20 ps; hence one cannot observe coherent resonant tunneling with this system. Nevertheless, many interesting tunneling rate processes are observable.

The DQW structures used in this study are of an entirely novel design. The two QW's are of different widths, but the Al composition of the wider well is adjusted so that under flat band conditions the electron energy levels are near resonance, and the hole energies are sufficiently different so that the PL energies of the two wells are well separated.[25] This is possible because the heavy hole mass is much larger than the electron mass, so the

;

holes sit close to the top of the valence band in each QW. As I will discuss below, this makes possible at reasonable electric fields the existence of a "charge-transfer" (CT) state, in which the electrons and holes are in different wells. In these experiments we have directly observed for the first time the buildup of a CT state via electron and hole tunneling in opposite directions in asymmetric DQW structures.

B.1. Sample Design

The samples used for this study were grown by molecular beam epitaxy at the central research laboratory of Thomson-CSF in Orsay, France. The growth layers are shown schematically in Fig. 4.5.

The nominal growth parameters are as follows. A 74 Å $Al_{.15}Ga_{.85}As$ QW (QW1) is coupled to a 34 Å GaAs QW (QW2) through an $Al_{.45}Ga_{.55}As$ barrier. Two samples were grown for this study; sample A has a thin (50Å) barrier so the electron states are somewhat delocalized over the two wells, and sample B has a thick (100Å) barrier so the electron states are strongly localized in each QW. Twenty-five periods of the DQW structure were grown on an n^+ GaAs substrate and n^+ GaAs buffer layer. The doping level was 5×10^{17} cm^{-3}. (A 20-period n^+ AlAs/GaAs superlattice was used to smooth the substrate surface). A semitransparent Al Schottky contact was evaporated on the top surface so that the

Semitransparent Contact	
GaAs	50 Å
Al$_{.39}$Ga$_{.61}$As	500 Å
GaAs	34 Å
Al$_{.39}$Ga$_{.61}$As	50 Å
Al$_{.10}$Ga$_{.90}$As	74 Å
Al$_{.39}$Ga$_{.61}$As	300 Å
n$^+$ GaAs	2000 Å
superlattice buffer	800 Å
GaAs	3000 Å
n$^+$ substrate	

25x {

Figure 4.5. Double QW sample structure for PL studies. The nominal growth parameters in Å are given. For sample A the barrier width b is 50Å; for sample B b=100Å.

effect of an electric field applied along the growth direction could be studied.

B.2. Electronic States

The electron and hole states for the above-described DQW system have been calculated by B. Vinter.[26] He obtained the exact wavefunctions and energies by numerically integrating the Schrödinger equation for the coupled well system, rather than starting with the localized states as a basis. The band diagram and results for the wavefunctions for sample A are shown in Fig. 4.6, both under flat band conditions and with an applied electric field (reverse bias). The band offset ratio was assumed to be 0.62:0.38. Under flat band conditions the hole states are strongly localized in each well (due to their heavy mass), but the electrons are somewhat delocalized as expected. With a moderate applied electric field, the electron states become localized in each QW. For sample B the electrons are always strongly localized.

The energy levels vs. applied field are shown in Fig. 4.7. The strong level repulsion near resonance due to the coupling of the wells is quite apparent for sample A. Unfortunately, the PL transition energies predicted by this calculation do not agree very well with the observed values (7038Å for QW1 and 7160Å for QW2 at 6 degrees K). Therefore we have had to revise the sample growth parameters in order to fit the observed PL spectra. If we
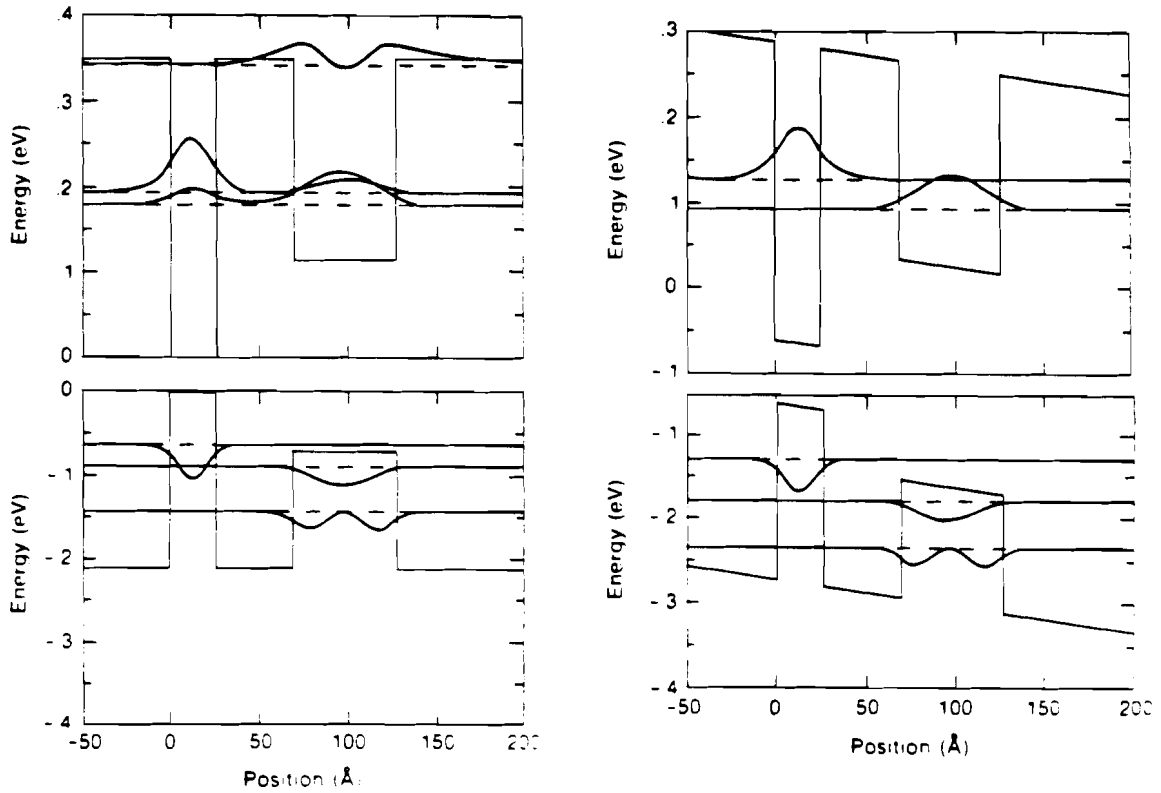
Figure 4.6.   Band diagram and calculated electron and hole states
for sample A (43 Å barrier), (a) with no electric field, and (b),
with an electric field of 30 kV/cm.   Similar results are obtained
for sample B, with the important difference that the electron
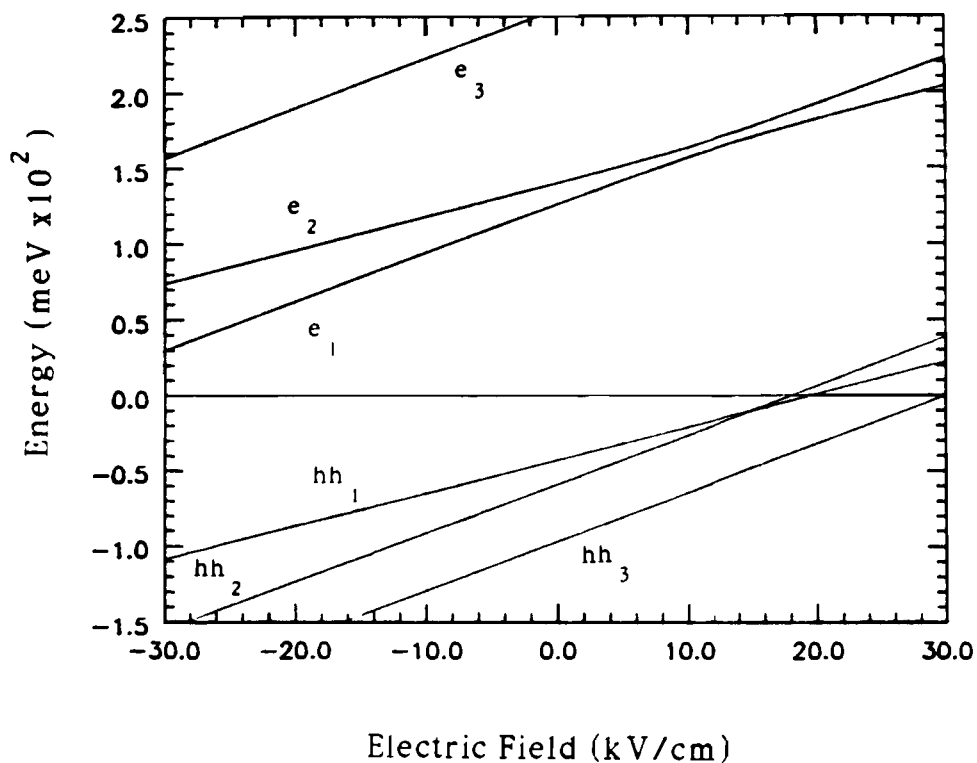states are strongly localized in each QW.

Figure 4.7. Energy levels vs. electric field for sample A. The levels are very similar for sample B, but with a much smaller anticrossing. It should be noted that at zero applied bias voltage, the internal field of the Schottky diode is about 8.2 kV/cm.

assume that the AlAs growth rate R_{Al} was as desired, then the PL energies can be fit by varying the GaAs growth rate R_{Ga}. The thickness of each AlGaAs layer is then given by $(R_{Al}+R_{Ga})t$, where t is the growth time for that layer. The Al composition x is given by

$$x=R_{Al}/(R_{Al}+R_{Ga}).$$

By varying the GaAs growth rate, we determined values of the QW widths and Al compositions that gave a reasonable fit to the PL energies. The results were that QW2 is only 26Å wide, the barrier is 43Å (86Å) for sample A (B) with x=.45, and QW1 is 50Å wide with x=.15.

B.3.   Experimental Setup

The samples were held in a cryostat at a temperature of 6K. The laser and time-resolved PL setup have been described in detail in section II.A. The laser dye used was Pyridine 1; the laser was tuned with a single-plate birefringent filter (Lyot) and an uncoated 5 μm pellicle to 6947Å, so electron-hole pairs were generated in both wells at t=0. For the time-resolved experiments discussed here, I estimate that each laser pulse injected a pair density of approximately 10^{11} cm^{-2} in each well. (This results in a band-filling in the conduction band of 3 meV and in the valence band of 0.4 meV). The resulting PL was dispersed by an 0.32m monochromator with a 300-l/mm grating across the entrance slit of the synchroscan streak camera. The streaked image was

integrated on a 2-D SIT detector, allowing us to obtain PL spectra with a spectral resolution of about 3 meV and a temporal resolution of 22 ps (i.e. the FWHM of the dye laser output).

The time-integrated PL spectra presented here were obtained at Thomson-CSF using a separate system with sub-meV spectral resolution. CW PL spectra are shown for both samples with zero bias voltage in Fig. 4.8. For sample B the ω_1 and ω_2 transitions are about the same magnitude, but for sample A, the ω_1 intensity is much smaller than for ω_2, indicating stronger tunneling processes for this sample as will be discussed below.

B.4. Experimental Results

Time-resolved spectra for sample B (thick barrier) are shown in Figs. 4.9 and 4.10 for reverse bias voltages from 0 to -6V. The spectra show the scattered pump light (defining the time origin) and two PL lines corresponding to recombination within each of the two wells. (The small peaks just after the pump pulse at approximately the same wavelength are due to an unavoidable spurious reflection of the laser onto the streak camera and should be ignored. Also it should be noted that the absolute intensities cannot be compared for different plots). The high energy PL line corresponds to the QW1 transition, and the lower energy line to QW2. The PL rise and decay times change very little with applied bias, as is shown in Fig. 4.11. The Stark
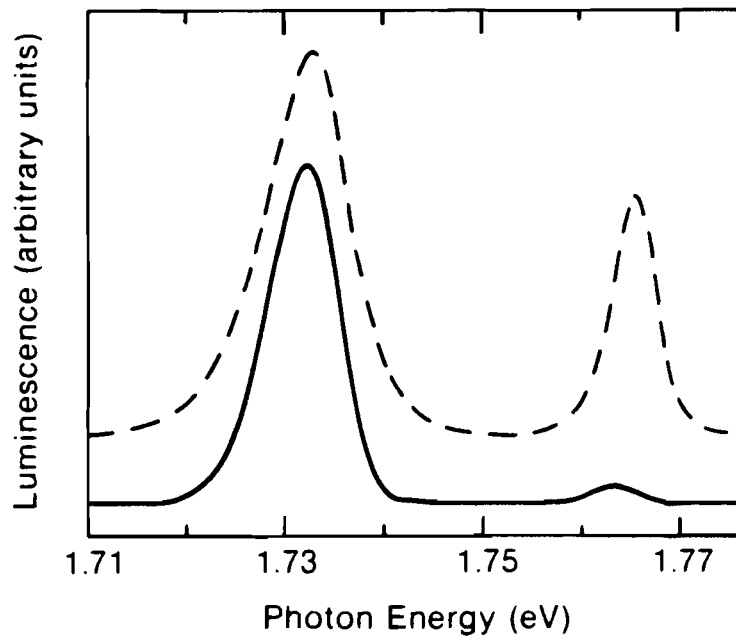
Figure 4.8. Time-integrated (cw) PL spectra for samples A (solid) and B (dashed line) with zero applied bias at a temperature of 6K.
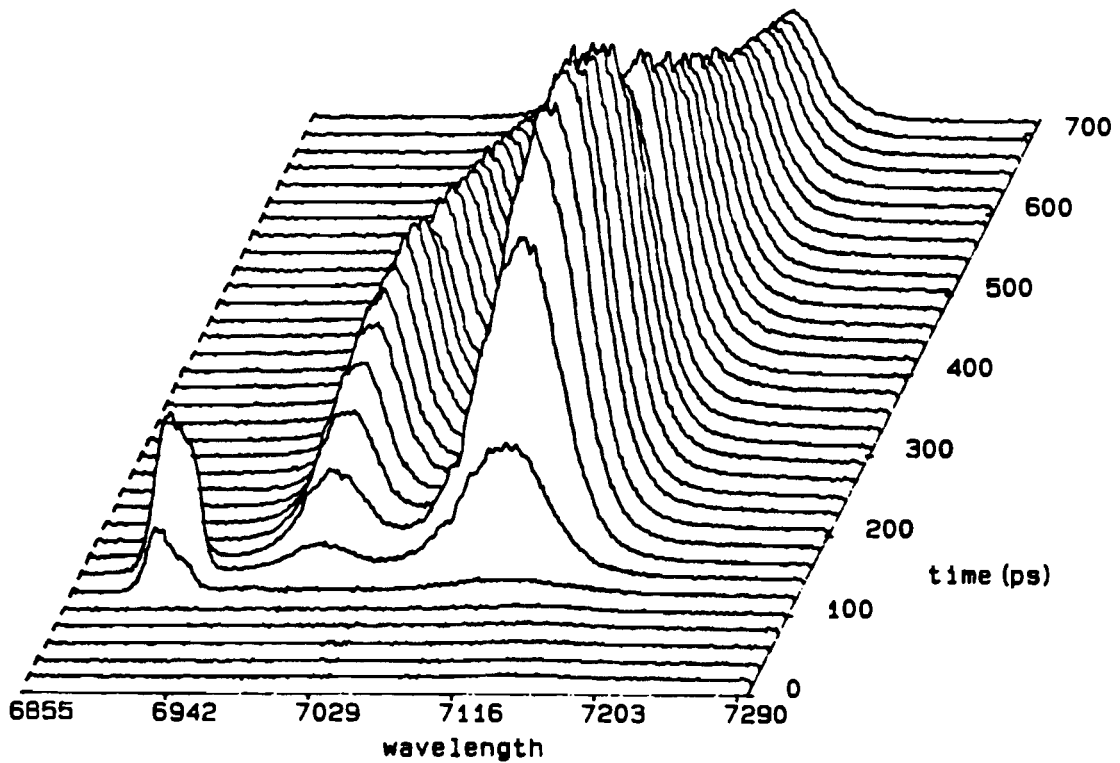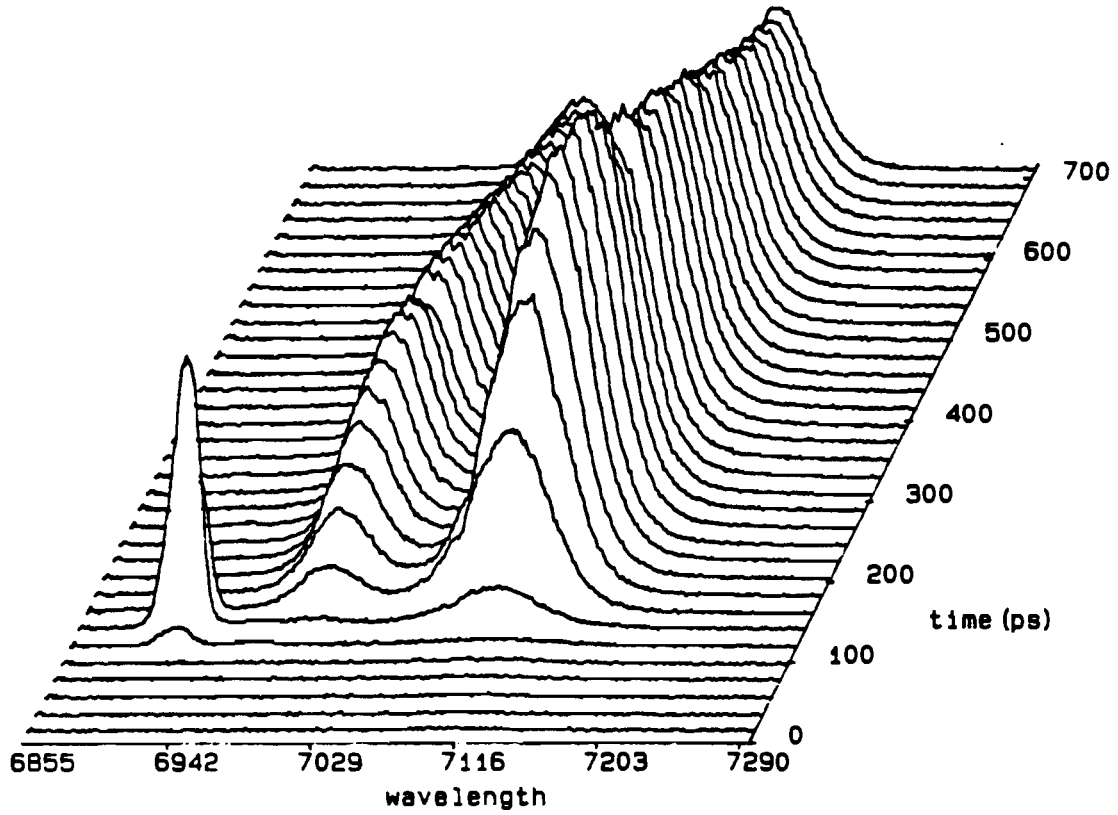
Figure 4.9. Time-resolved PL spectra of sample B for (a) zero applied bias and (b), -2V reverse bias.
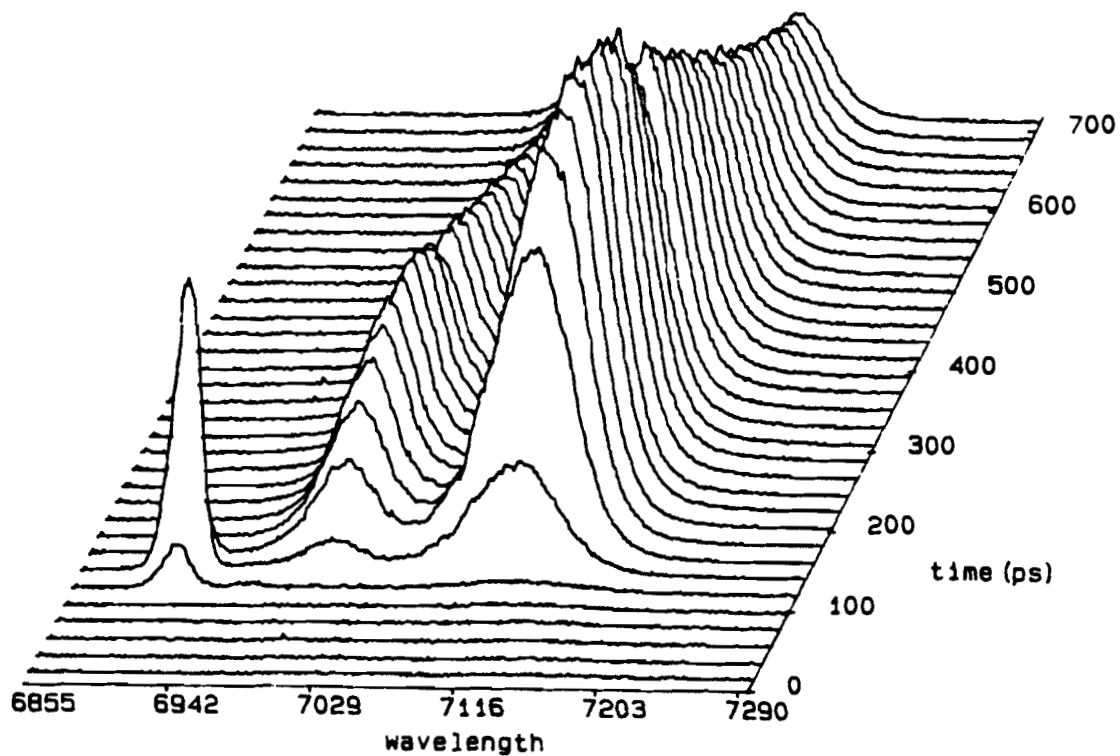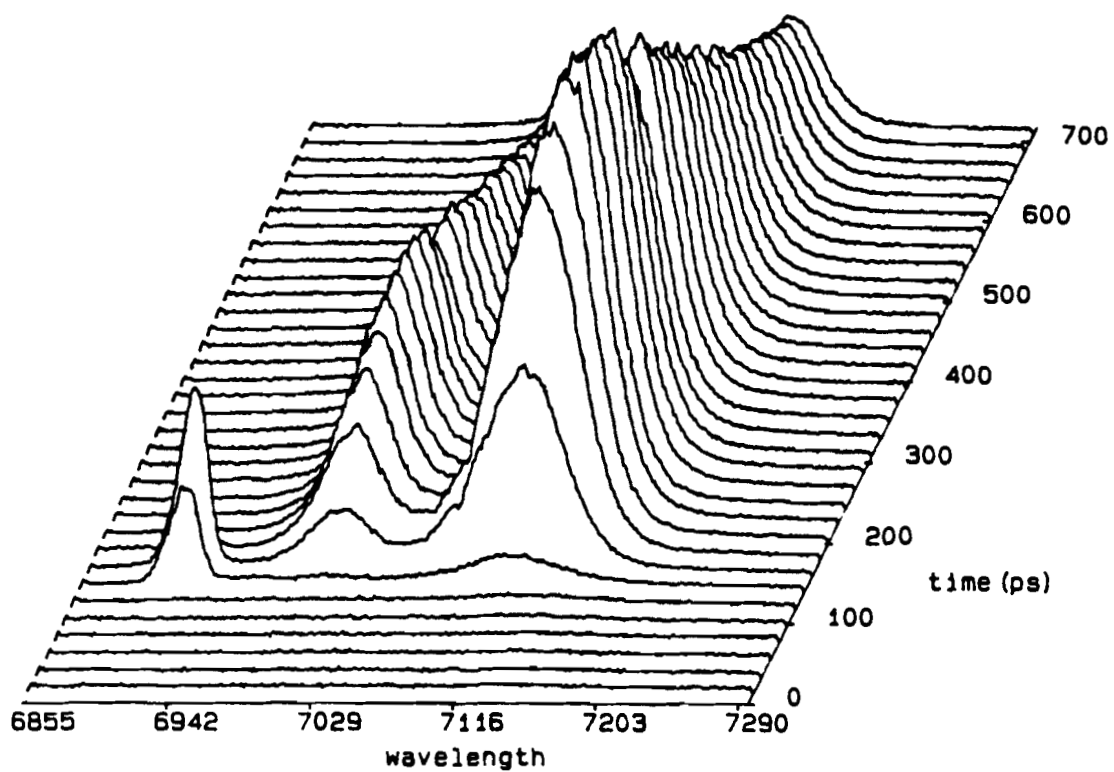
Figure 4.10.   Time-resolved PL spectra of sample B for (a) -4V and (b), -6V bias.
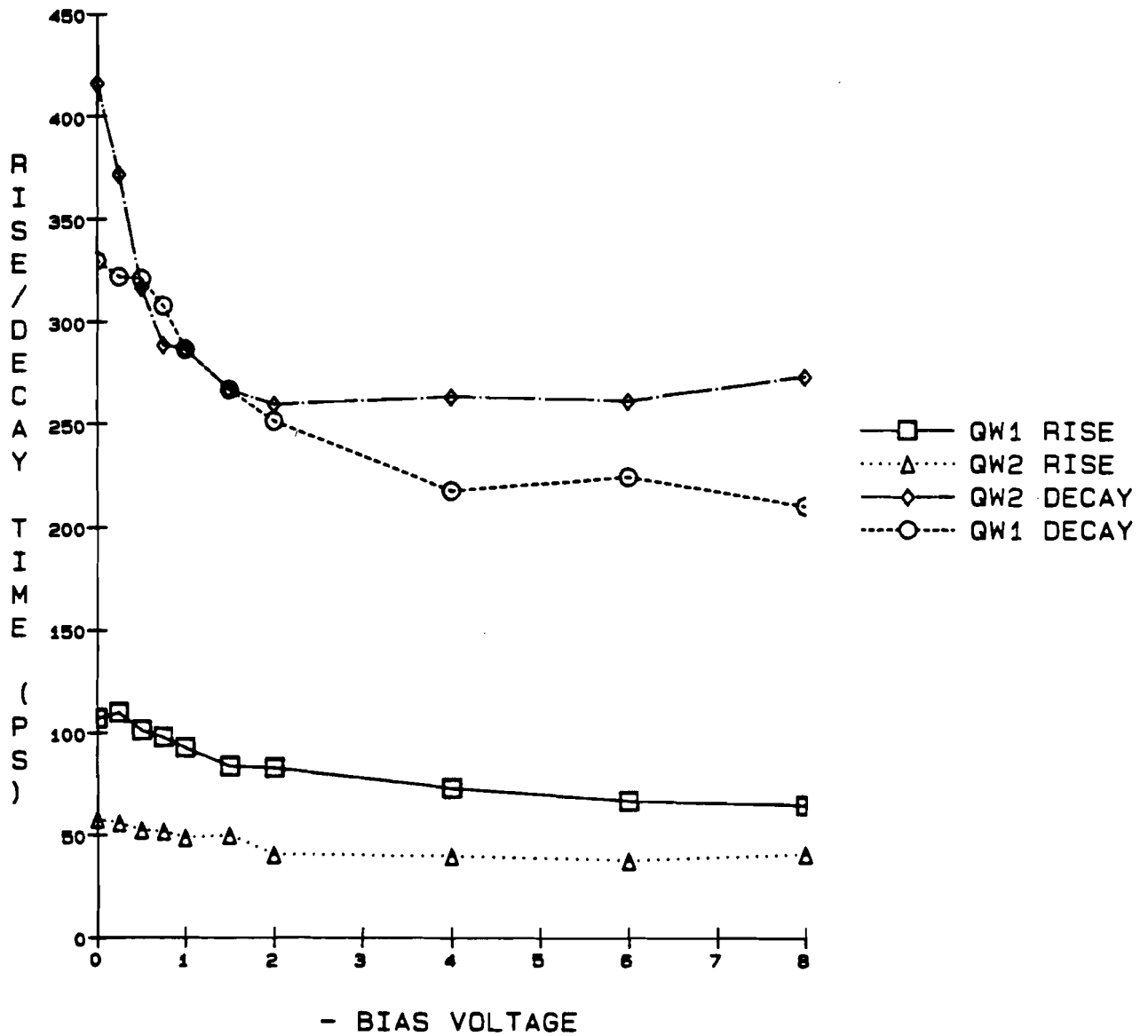
Figure 4.11. Rise times (10-90%) and decay times (1/e single exponential fit) for the two PL lines of sample B.

shift of the PL peaks, plotted in Fig. 4.12, is observed to be a few meV to the red as expected.[27]

In the cw PL spectra shown in Fig. 4.13, however, we observe a third PL peak which shifts strongly and approximately linearly towards the red with applied bias. In the narrow barrier sample (A) this peak appears even more clearly in the cw spectra (Fig. 4.14), and presents a stronger Stark shift. The origin of this peak can be elucidated by examining the time-resolved PL spectra for the thin barrier sample; the line comes from radiative recombination between electrons in QW1 and holes in QW2, which I refer to as the charge-transfer (CT) state.

A selection of the time-resolved PL spectra vs. applied bias is shown in Figs. 4.15-17 for sample A. At low bias one sees the scattered pump light and two PL lines corresponding to the ω_1 and $\omega_1+\omega_{CT}$ transitions of Fig. 4.6. It should be noted that at zero bias the PL of QW2 and the CT state have the same transition energy. As the electric field is increased, the ω_1 and ω_{CT} lines separate and ω_{CT} is strongly Stark shifted to lower energy. This PL has a long lifetime that in fact approaches or exceeds the 10 ns time interval between pump pulses and the synchroscan sweep cycle time; hence the PL signal that appears roughly constant vs. time on the streaked spectrum. (This is clearly seen as a signal at "t<0").

The Stark shifts of the three PL lines vs. bias are shown in Fig 4.18. For bias voltages less than about -3V the ω_2 and ω_{CT} lines are not well separated. The ω_2 wavelength was determined
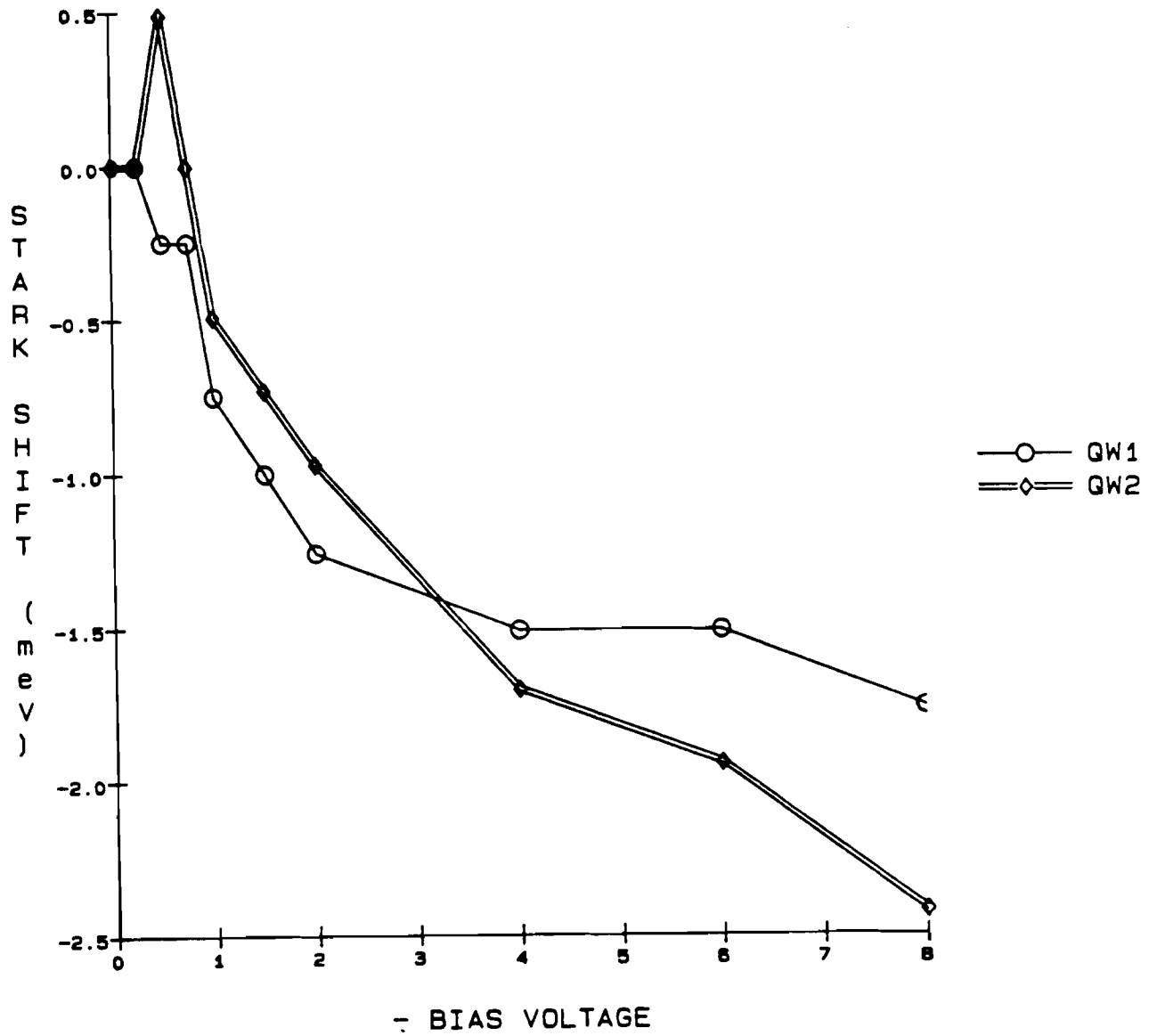
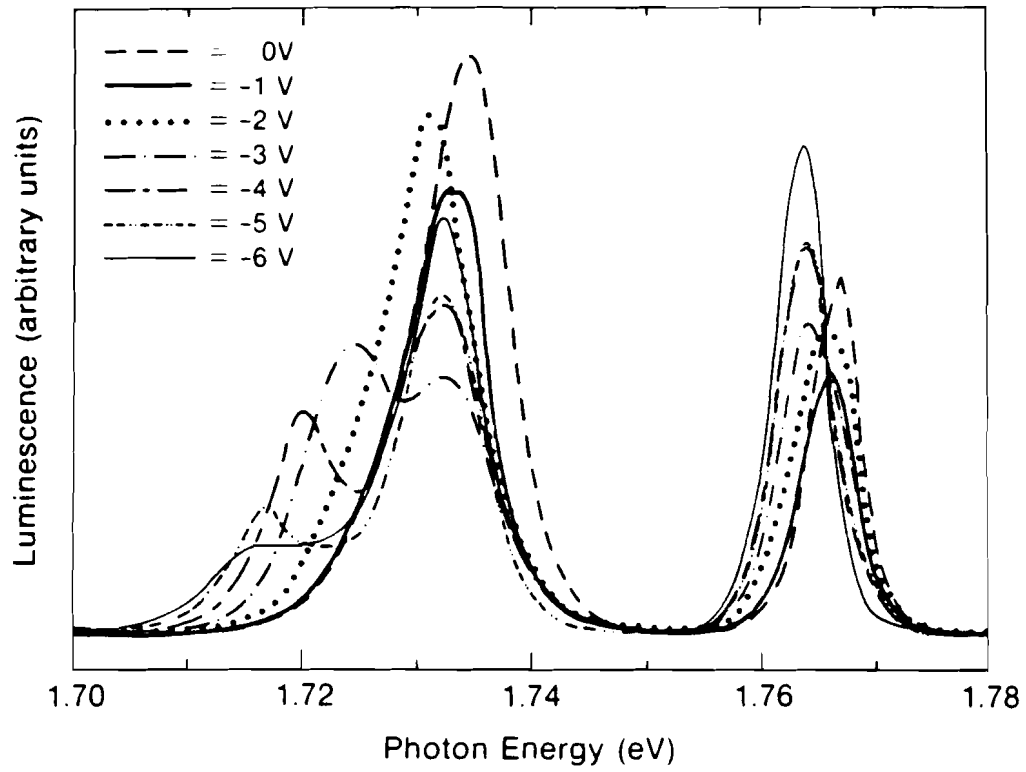Figure 4.12. Stark shifts of the two PL lines of sample B.

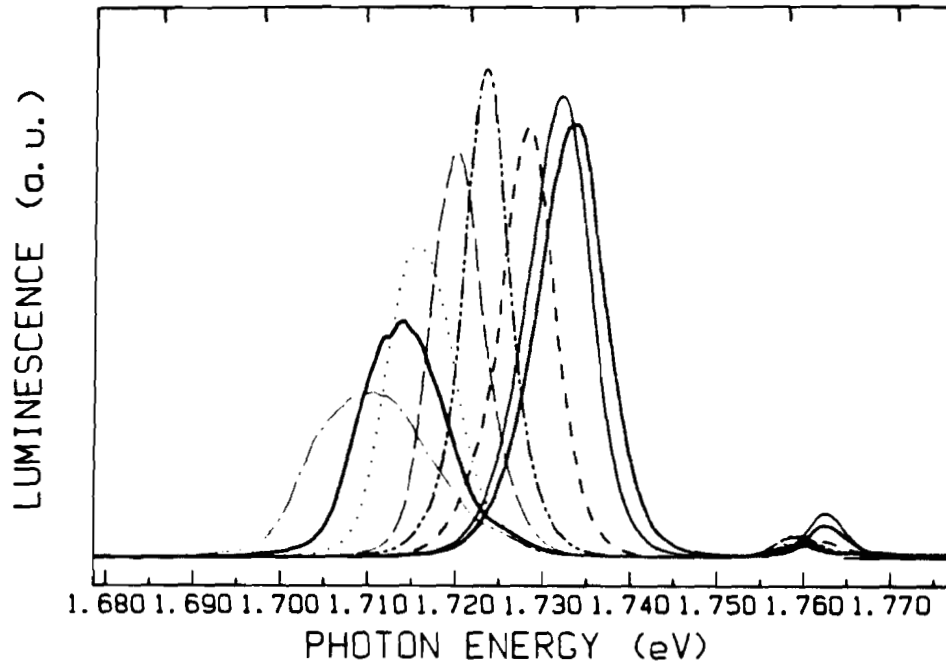Figure 4.13.   CW PL spectra of sample B at different applied voltages.

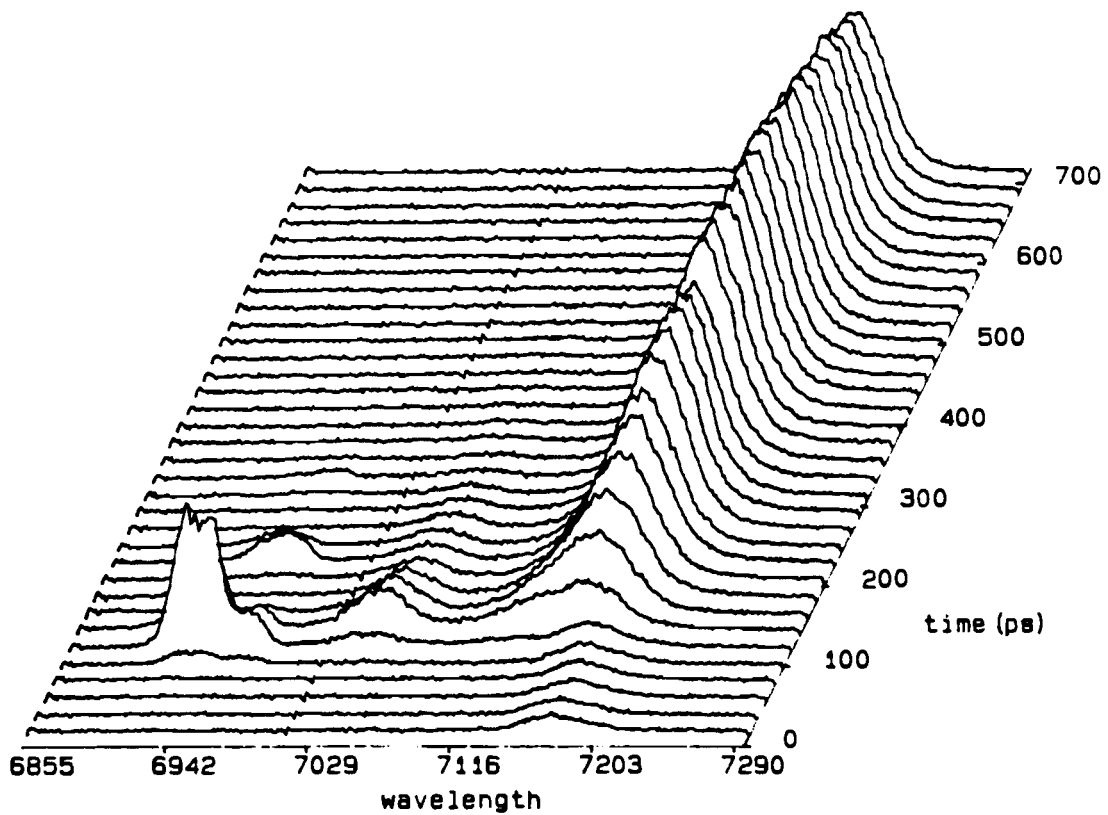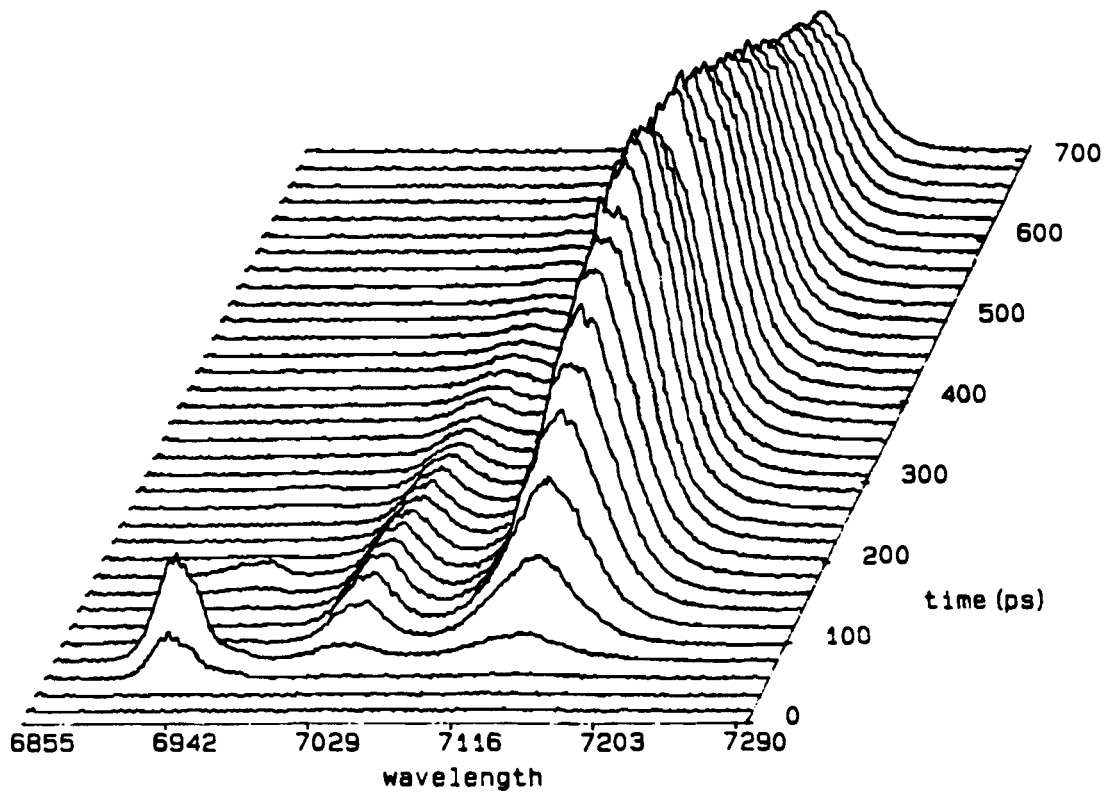Figure 4.14.　CW PL spectra of sample A at different applied voltages.

Figure 4.15. Time-resolved PL spectra of sample A for (a) zero applied bias, and (b), -2V reverse bias.

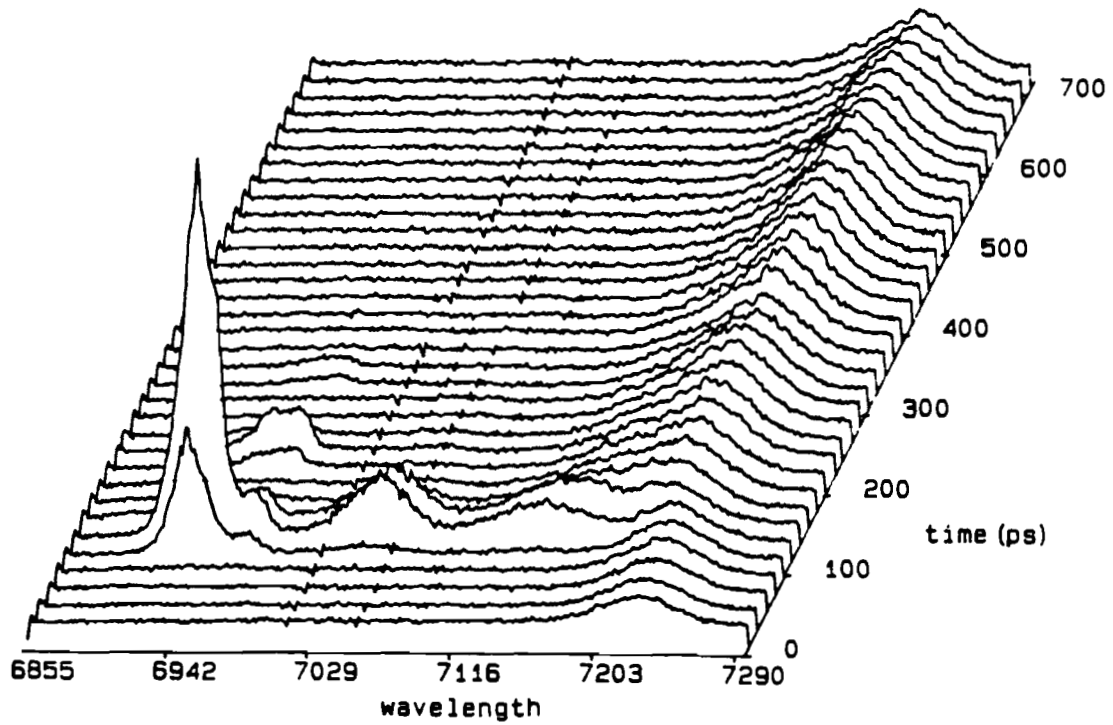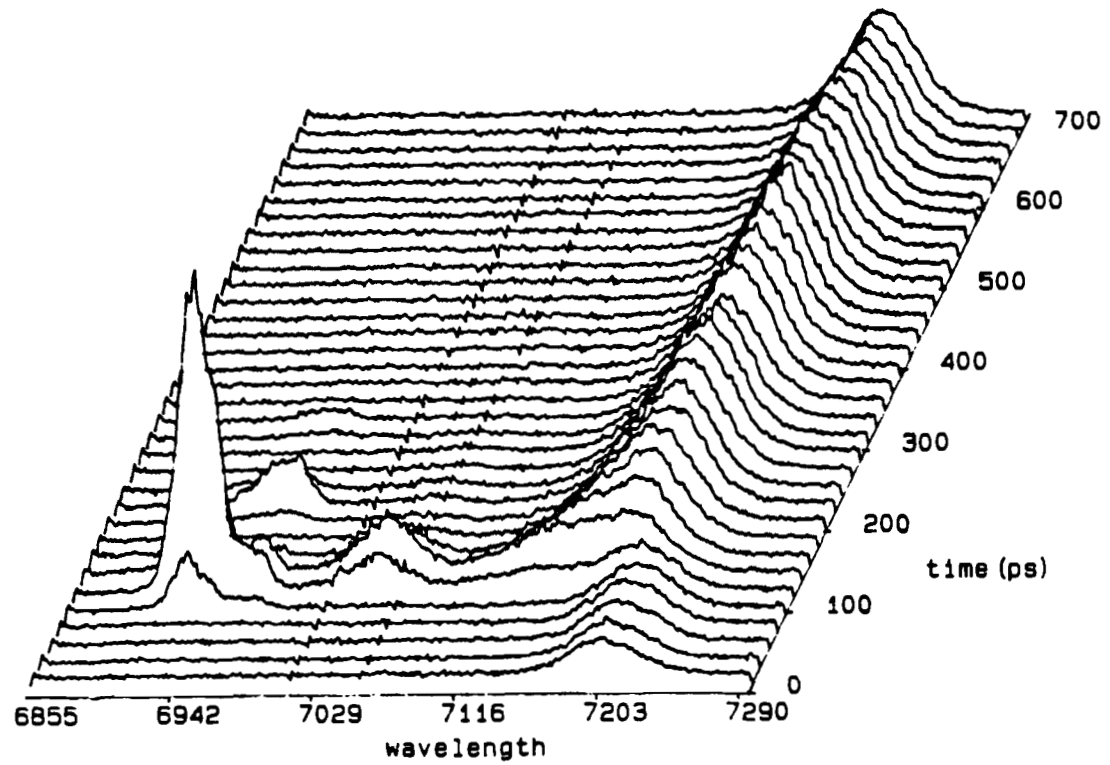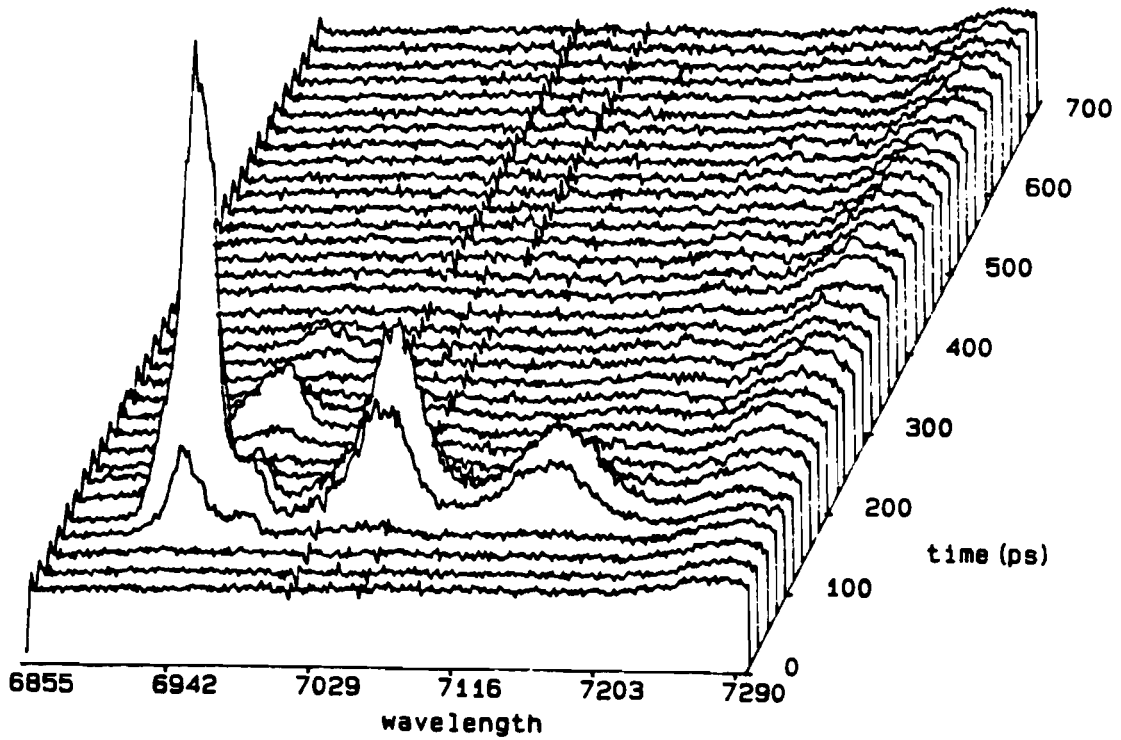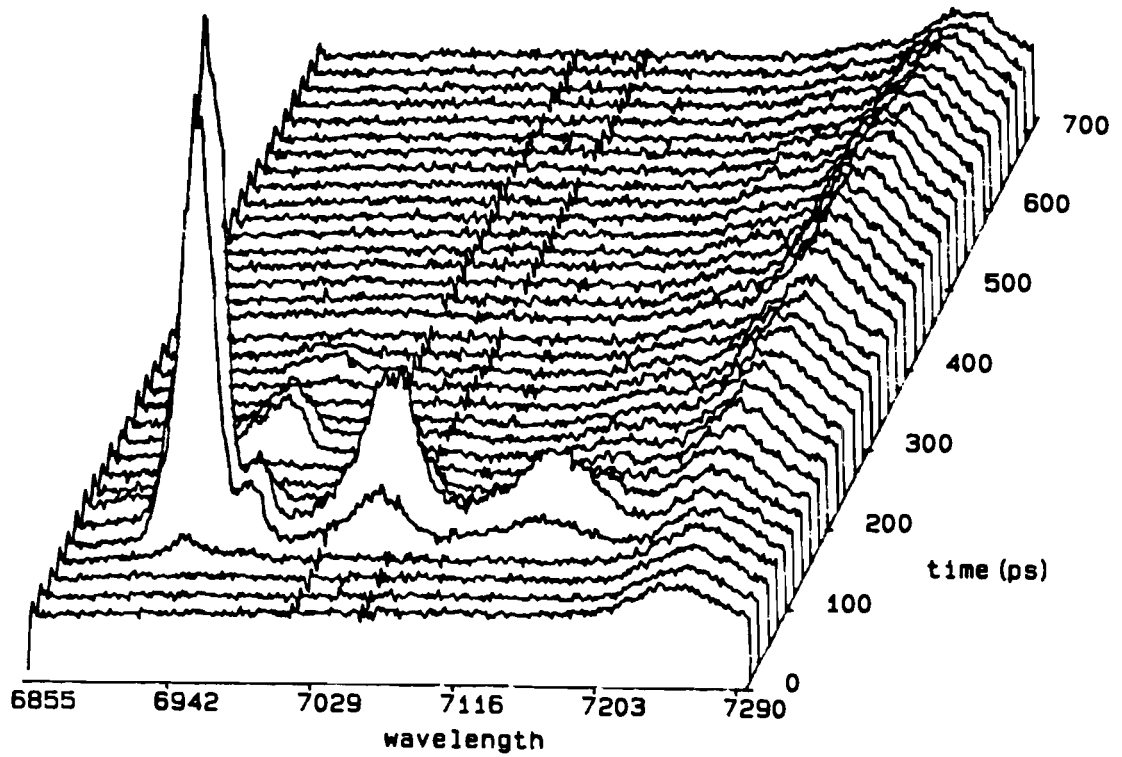Figure 4.16. Time-resolved PL spectra of sample A for (a) -3V, and (b), -4V.

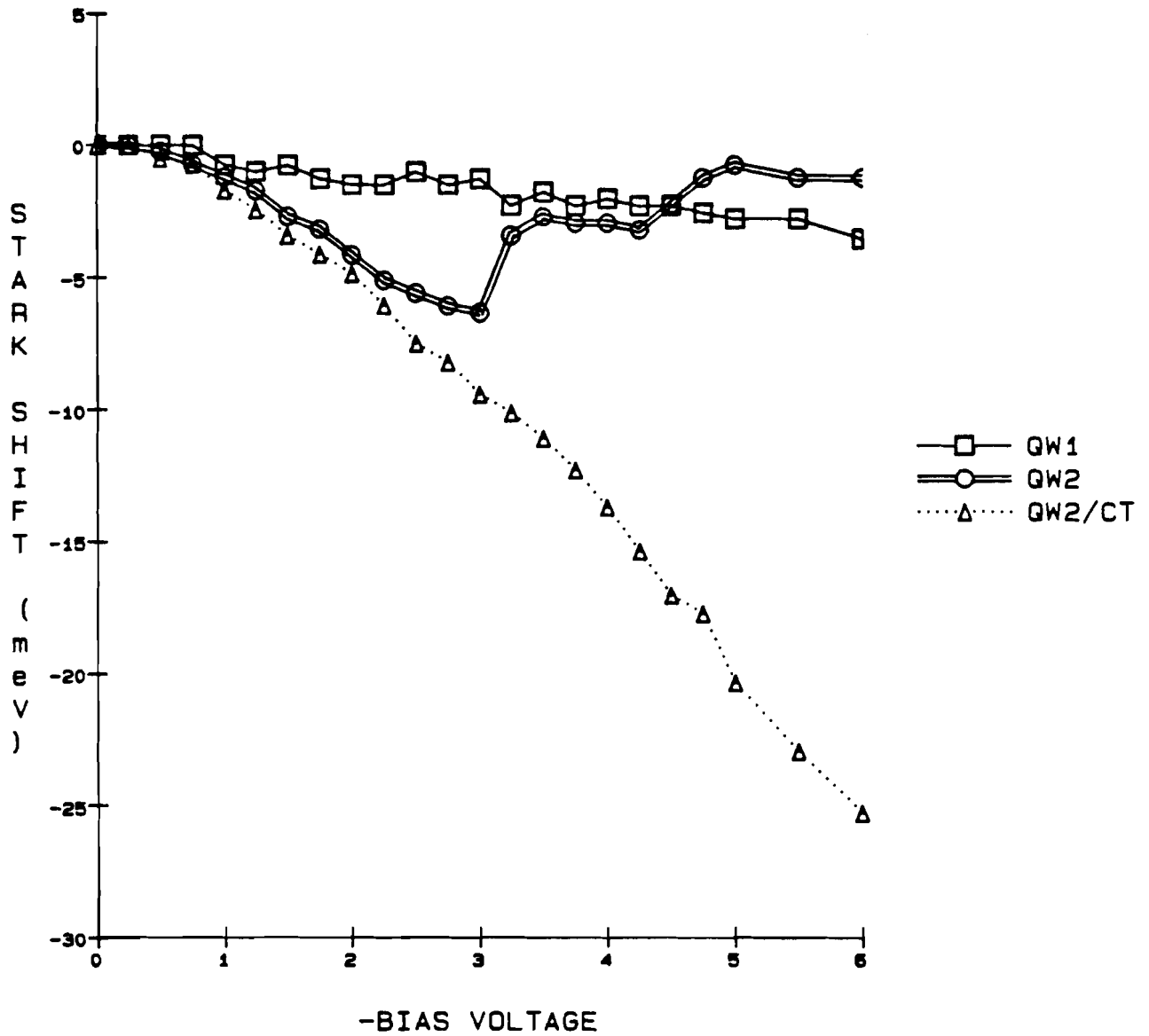Figure 4.17. Time-resolved PL spectra of sample A for (a) -5V, and (b), -6V.

Figure 4.18. Stark shifts of the three lines observed in the time-resolved PL spectra of sample A.

by the peak position near t=0, and the ω_{CT} wavelength by the peak position at "t<0" except where this component did not appear, in which case the position at t≈600 ps was used. The ω_1 and ω_2 lines show a shift of a few meV typical of an exciton confined in a QW. The Stark shift of the ω_{CT} line, however, is much stronger, and is approximately linear with applied bias. The strong red shift and long decay time indicate that this PL in fact is the result of recombination of electrons and holes in the CT state. The CT state is built up by electrons tunneling from QW2 to QW1 and holes tunneling from QW1 to QW2. The long lifetime is the result of the small overlap of the electron and hole wavefunctions, but the CT luminescence is nevertheless observable due to the nearly complete charge separation that takes place. This explains why the CT luminescence is observable in the cw PL spectra but not in the' time-resolved spectra for sample B. In this case the charge separation is not so strong due to the much slower electron and hole tunneling rates between the wells, so although the long-lived radiative recombination is observed as a line in the cw PL spectrum, the instantaneous intensity is low and therefore extremely weak on the time-resolved spectrum.

One further observation confirms that the origin of the strongly red-shifted PL line is from the CT state. The Stark shift of this line is dynamic, since as the carriers recombine the screening of the applied electric field by the CT state is reduced and the red shift increases. This is most easily observed by

comparing the CT wavelength just after the pump pulse with the CT PL wavelength at a very long delay time (which in practice is done by observing the PL at "t<0" on the synchroscan streak image). This is only reliable in the range 2-4V, where the CT lifetime is not so long that the principal part of the signal at t=0 is in fact due to PL emitted at t>>0.

I mentioned previously that the CT state can have a lifetime that can exceed the pump pulse period. As a consequence a d.c. charge can build up in the wells (this is most dramatically apparent in Fig. 4.17, where all the CT luminescence signal comes from these steady-state separated electron-hole pairs). This charge screens the applied field, thus reducing the observed CT Stark shift. Since the CT Stark shift effectively gives the average electric field in the DQW region, the separated charge density can be estimated by comparing the observed PL Stark shift to the calculated electric field in the Schottky diode without the presence of charge carriers. We can then estimate an effective lifetime τ for the separated carriers from $n=g\tau$ where g is the generation rate.

This procedure is accurate for cw experiments, and yields good approximate results for the time-resolved experiments since the lifetime τ is comparable to or longer than the pump pulse period of 10 ns. I make the simplifying assumption that complete charge separation takes place after each pump pulse; this is reasonable for sample A, particularly at voltages greater than about -3V, but is not reasonable for sample B. Since the

separation between the QW's is much less than the laser pump diameter, to a very good approximation the electric field due to the separated charges may be calculated by assuming infinite sheets of charge with areal charge density σ. This screening field is then

$$E=\sigma/\varepsilon\varepsilon_0,$$

where ε is the dielectric constant of GaAs. For example, a pair density of 10^{11} cm^{-2} will give a field of 1.5×10^4 V/cm. The effective cw generation rate for the time-resolved experiments described above was 10^{19} cm^{-2}s^{-1}. The Schottky barrier height of the Al contact on the GaAs surface is 0.8 eV,[28] and the not-intentionally-doped region of sample A is nominally 9710Å; thus the built-in electric field in the DQW region is approximately 8.2×10^3 V/cm. To a good approximation (i.e. ignoring barrier-lowering) the total field under reverse bias is just the sum of the built-in field and the applied field. The results for the carrier density and CT state lifetime for the time-resolved experiments on sample A are given in table 4.1; also given is the band-filling due to the d.c. charge buildup for both electrons and holes.

The lifetimes are surprisingly short. A separate experiment was performed to investigate the dependence of the CT state lifetime on the injected carrier density. Table 4.2 shows the results for the average separated charge densities n and CT lifetime τ vs. injected carrier density n_i (i.e. the electron-hole pair density injected by a single laser pulse). The bias voltage for this

Table 4.1. Separated charge densities, CT state lifetime, and conduction and valence band filling for sample A time-resolved experiments at various reverse bias voltages.

Bias Voltage	$n(cm^{-2})$	τ (ns)	ΔE_c (meV)	ΔE_v (meV)
-1	5.7×10^{10}	5.7	1.7	0.3
-2	1.1×10^{11}	11	3.3	0.6
-4	1.9×10^{11}	19	5.8	1.0
-6	2.5×10^{11}	25	7.6	1.3

data was -6V, so the charge separation should be complete. (There is a discrepancy between the results of this experiment and the results presented in Table 4.1 for the lifetime at an injected carrier density of 10^{11} cm^{-2}; this is most likely due to error in determining the pump laser spot size precisely at the location of the cryostat in the sample, resulting in an error in calculating the injected carrier density).

Apparently there is a strong dependence of the lifetime on the injected carrier density, but the average separated charge density depends only weakly on the initial injected density. This indicates that the observed short lifetime may be due to band-filling. This notion is supported by cw PL experiments performed

Table 4.2.	Average separated charge densities and CT state lifetime vs. injected charge density for sample A, -6 V bias.		

n_i (cm^{-2})	n(cm^{-2})	τ (ns)
6.6×10^{11}	2.4×10^{11}	3.6
9.9×10^{10}	1.8×10^{11}	18
3.2×10^{10}	1.6×10^{11}	50

at Thomson-CSF,[29] where a strong dependence of the lifetime on the pump intensity was also observed: for sample A at -3V bias and 300 W/cm^{-2} pump intensity τ is 20 ns, but at 3 W/cm^{-2} τ is 1.2 μs.

A more refined analysis treating the charged QW's in a self-consistent manner would be required to elucidate the processes that determine the lifetime τ, which it must be noted is not necessarily the radiative lifetime for the CT transition.

The decay rates for sample A of the ω_1 and ω_2 lines vs. bias are also extremely difficult to interpret. The ω_1 decay rate vs. applied bias is plotted in Fig. 4.19. I have not plotted the ω_2 decay rate, since at low bias the situation is complicated by the
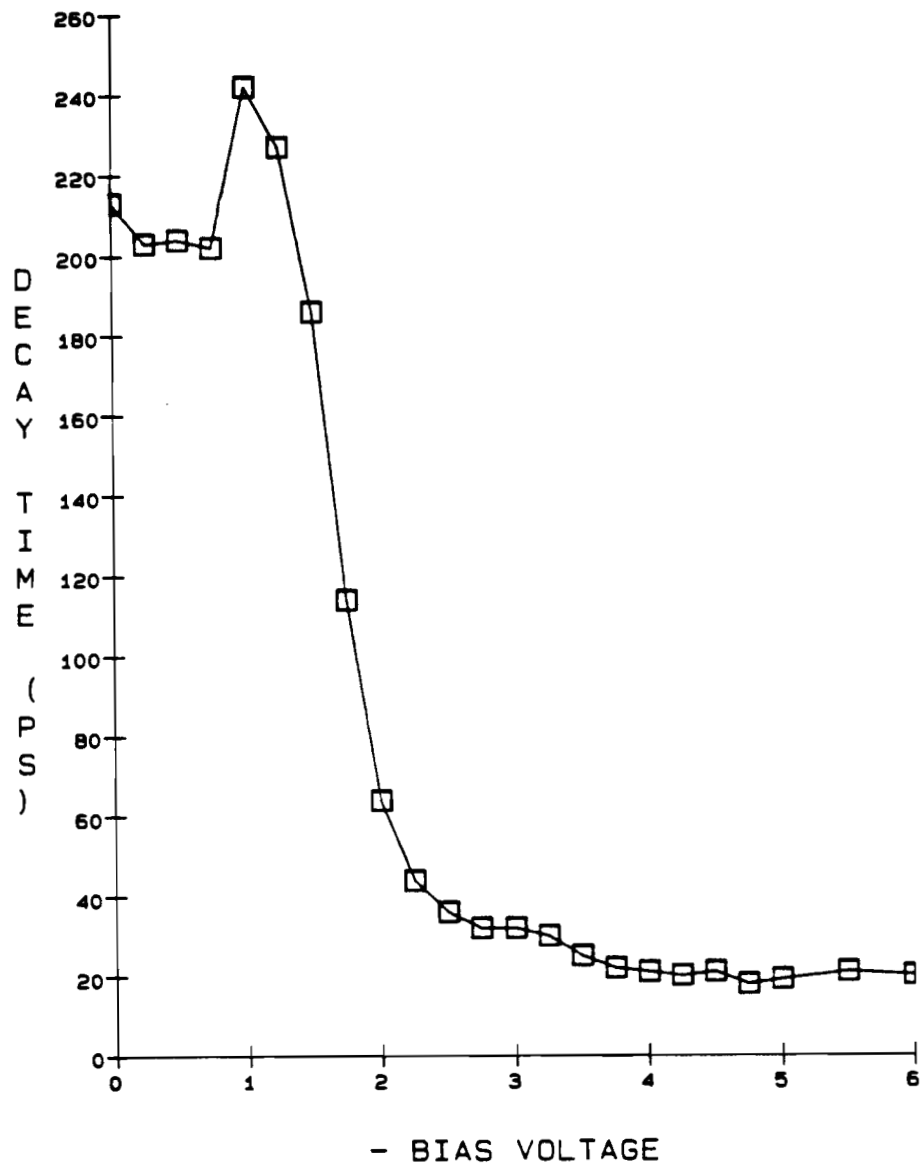
Figure 4.19. Decay time of the ω_1 PL line vs. applied bias for sample A.

fact that the ω_2 and ω_{CT} lines are very close in energy, and therefore are indistinguishable on the PL spectra (see Figs. 4.15 and 4.16). The difficulty of defining a decay rate for the ω_2 line except at high bias is clearly shown in Fig. 4.20, where I have plotted the data of Figs. 4.16(a) and 4.17(a) in a different way, so that the time dependence of the different spectral components may easily be seen. It is obvious that the measured decay time would depend entirely on the spectral window around ω_2 selected. At high bias, where the ω_2 and ω_{CT} lines are well separated and the ω_2 rate can be well-defined, the observed ω_2 decay rate is limited by the streak camera response.

From Fig. 4.6, the simplest interpretation of the rates is that the ω_1 line decays with the hole tunneling rate from QW1 to QW2, and the ω_2 line decays with the electron tunneling rate from QW2 to QW1 (in addition, of course, to the recombination contribution to the total decay rates). The ω_2 decay is always very fast, because the barrier is thin and the electron mass is low, and at low bias the electron wavefunction extends over both wells. The ω_1 decay is at low bias longer than the recombination decay rate, but rapidly increases with electric field, until by -3.5V bias the observed decay is limited by the streak camera response time.

An approximation to the rate for a carrier to tunnel from one QW to another may be obtained by applying the theory developed in section III.C.3 for the tunneling-out problem. A slight modification of the calculation of the transmission
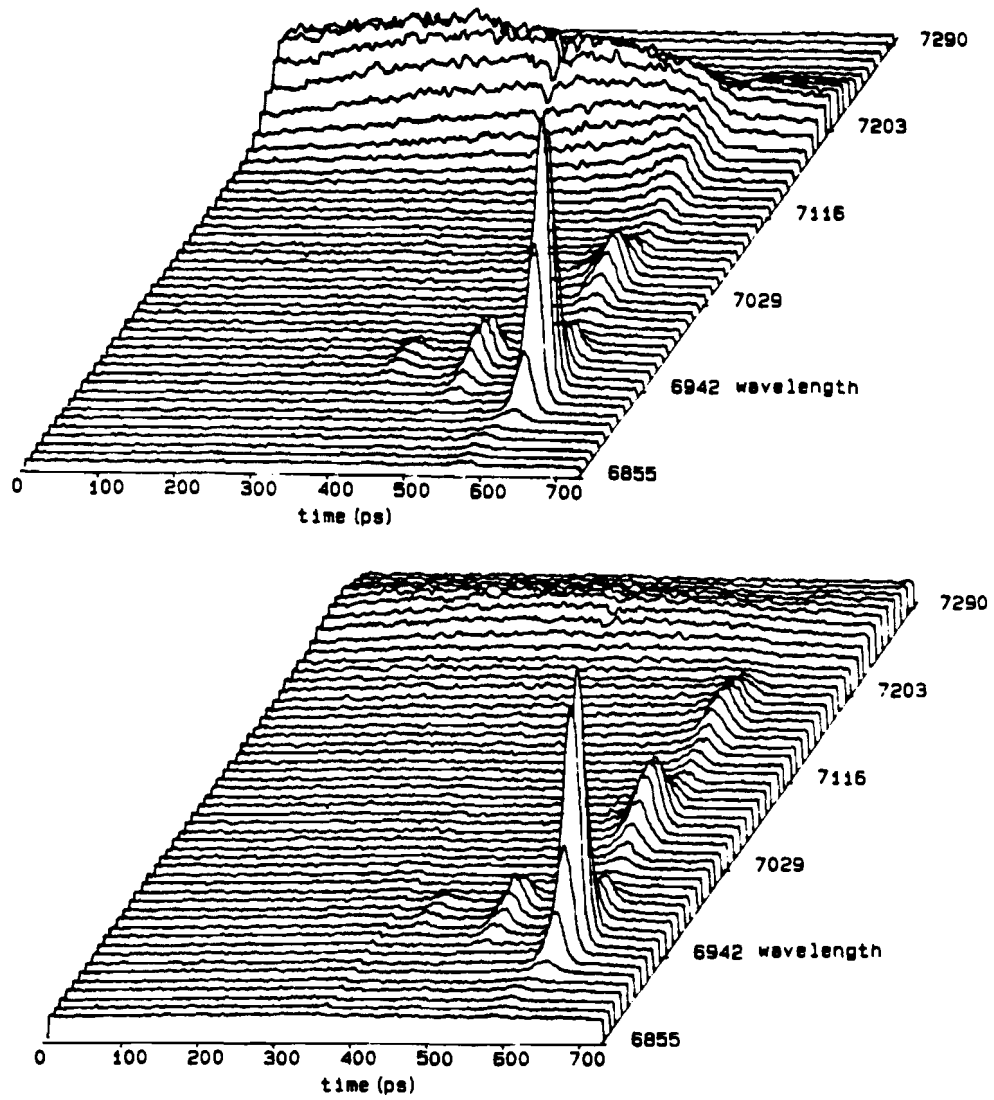
Figure 4.20. Time-resolved PL spectra of sample A at (a), -3V and (b), -5V bias plotted to show the time-dependence of the different spectral components.

coefficients at zero field is necessary due to the misalignment of the band edges of the two QW's; Fig. 4.21 shows the relevant band diagram.   The transmission coefficient at zero field for tunneling from region I to region III is given by

$$T = 4\left\{ \left(1 + \frac{m}{m_3}\frac{k_3}{k_1}\right)^2 \cosh^2 k_2 b + \left(\frac{m}{m_b}\frac{k_2}{k_1} - \frac{m_b}{m_3}\frac{k_3}{k_2}\right)^2 \sinh^2 k_2 b\right\}^{-1},$$

where m is the effective mass in region I, m_b the effective mass in the barrier, m_3 the effective mass in region III, and the k_i are the wavevectors in the three regions (k_2 being the evanescent wavevector in the barrier).   For the heavy holes tunneling from QW1 to QW2 the k's are

$$k_1 = \sqrt{\frac{2m(E-V_1)}{\hbar^2}}$$

$$k_2 = \sqrt{\frac{2m_b(V_2-E)}{\hbar^2}}$$
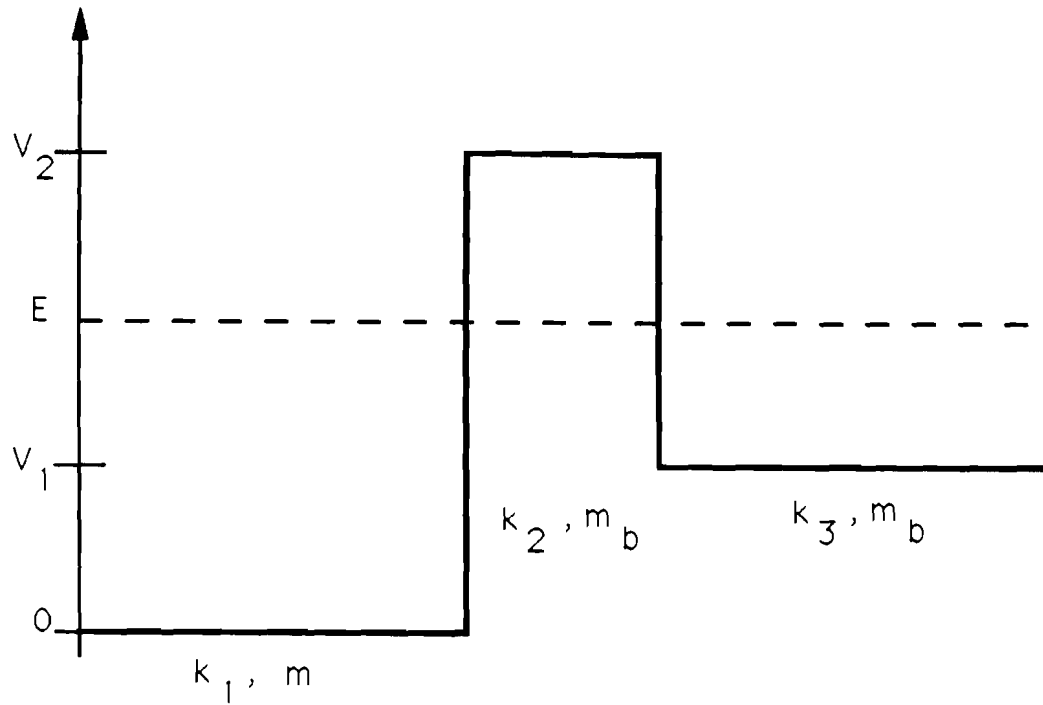
$$k_3 = \sqrt{\frac{2m_3E}{\hbar^2}}$$

Figure 4.21. Band diagram for the tunneling-out theory applied to the DQW problem.

For the electrons tunneling from QW2 to QW1 the k's are

$$k_1 = \sqrt{\frac{2mE}{\hbar^2}}$$

$$k_2 = \sqrt{\frac{2m_b(V_2 - E)}{\hbar^2}}$$

$$k_3 = \sqrt{\frac{2m_3(E - V_1)}{\hbar^2}}$$

The results for the tunneling rates vs. electric field for a 43 Å barrier, assuming a conduction to valence band offset ratio of 62:38, are shown in Figs. 4.22 and 4.23. The electron tunneling rate is much faster than the streak camera response, and so will not be resolved, which is consistent with the experimental results (remembering that at low bias ω_2 and ω_{CT} are indistinguishable). The hole tunneling rate, however, is always much slower than the recombination rate (which is a few hundred ps); thus an interpretation of the ω_1 decay as the hole tunneling rate requires an anomalously fast decay.

The results for the electron tunneling for the 86 Å barrier are shown in Fig. 4.24. These calculated rates appear to be too fast to be consistent with the experimental observations. If the tunneling time at high bias were as short as 50 ps, then a
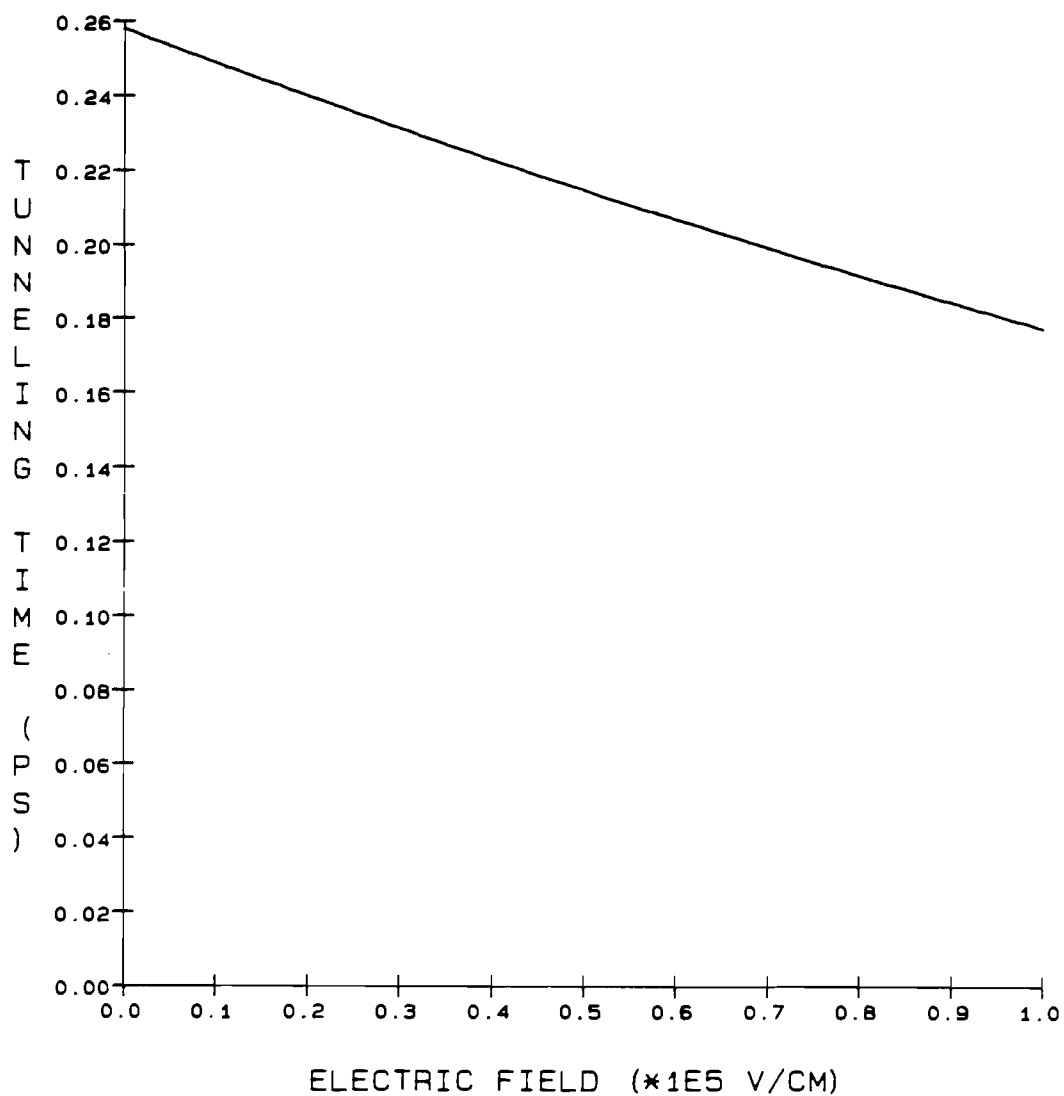
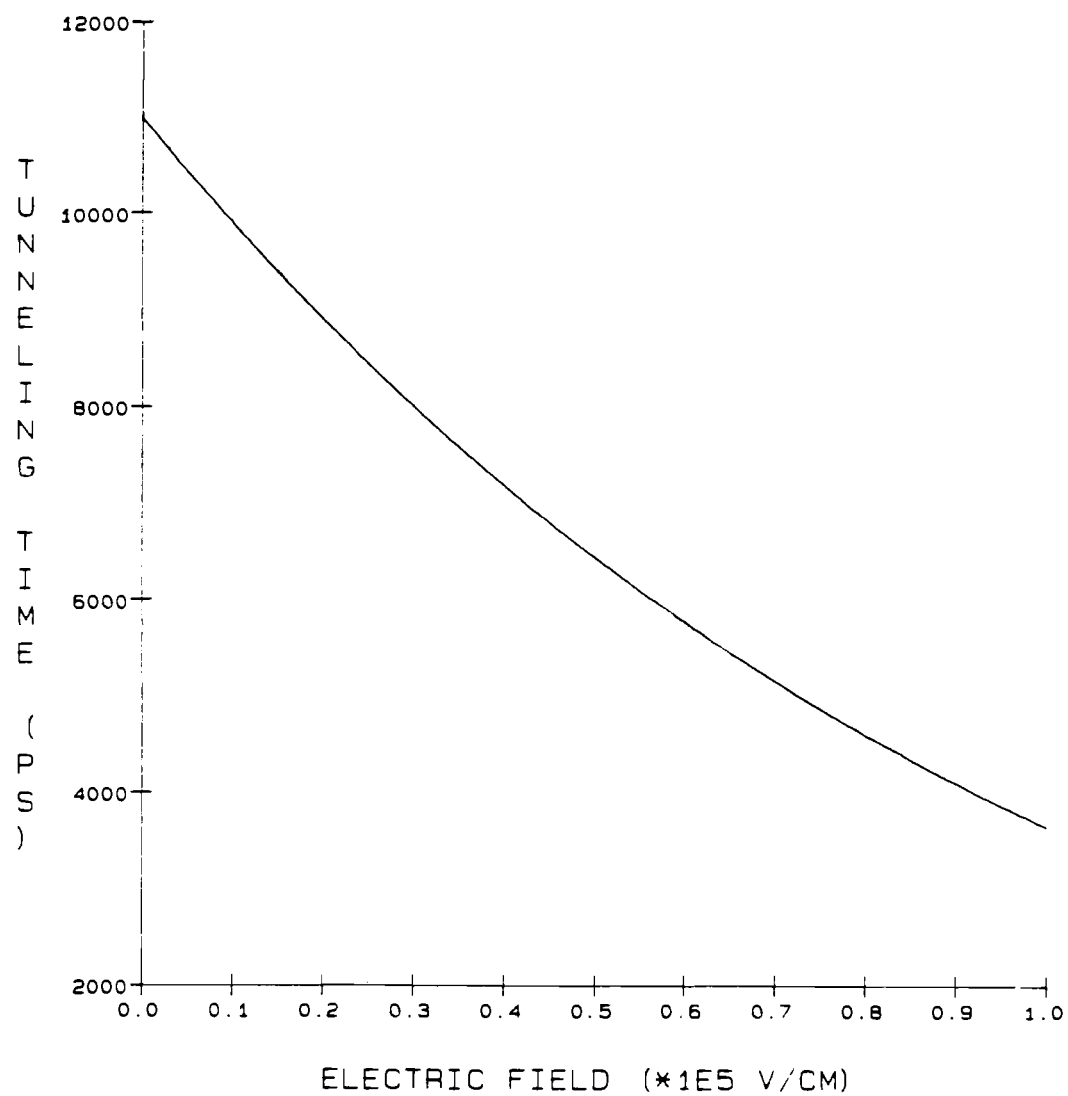Figure 4.22.   Calculated electron QW2⇒QW1 tunneling times for sample A using the tunneling-out theory of section III.C.3.

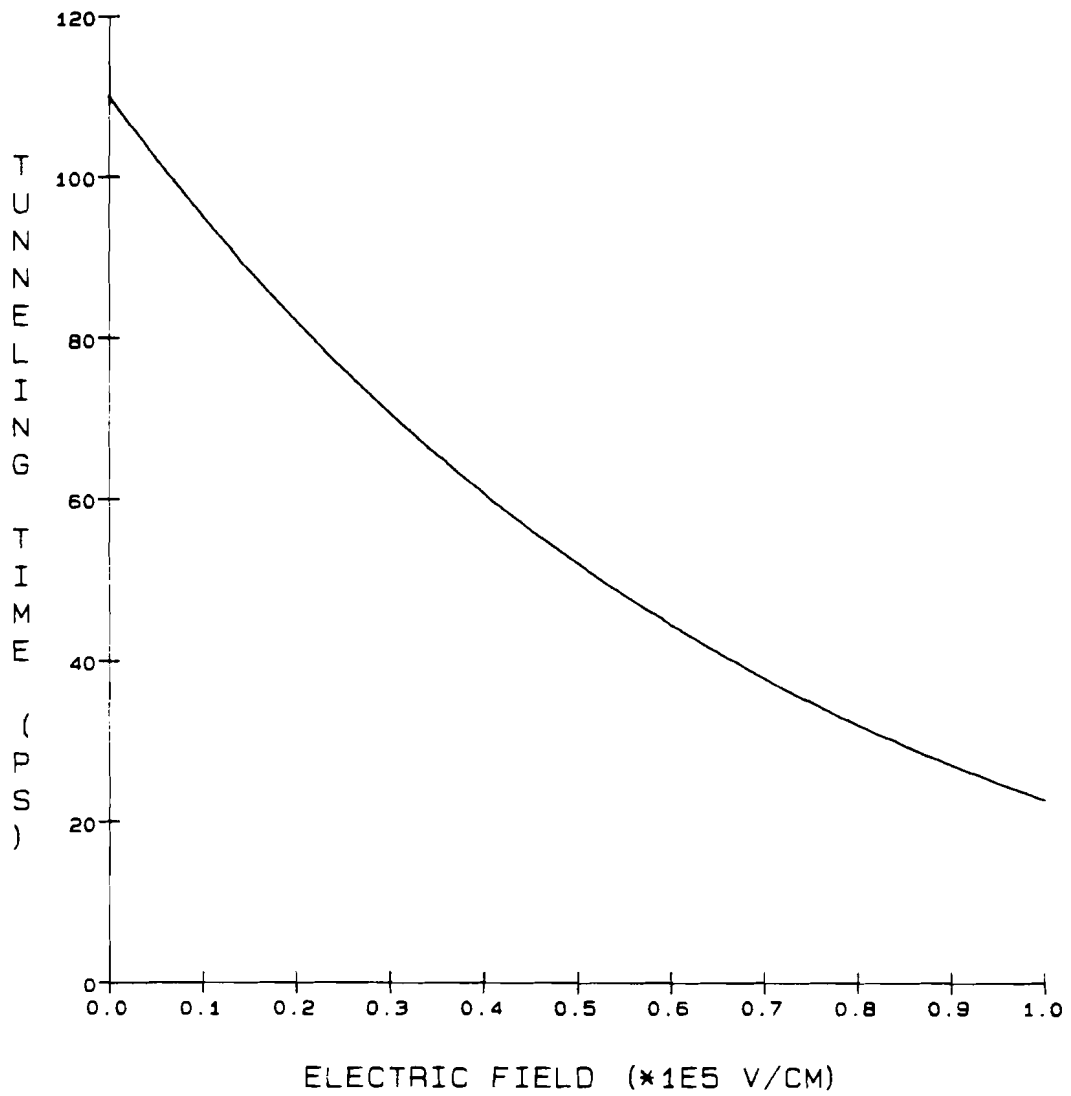Figure 4.23. Calculated heavy hole QW1⇒QW2 tunneling times for sample A using the tunneling-out theory.

Figure 4.24. Calculated electron QW2⇒QW1 tunneling times for sample B using the tunneling-out theory.

substantial charge separation would occur (due to the fact that the holes injected by the laser into QW2 remain there, but most of the electrons would tunnel to QW1 before recombination in QW2 could occur). Hence the ω_2 PL intensity would decrease substantially, and a large Stark-shifted component at ω_{CT} would appear. This is contrary to experimental observations (see Fig. 4.13).

From the above argument it is tempting to conclude that the electron tunneling-out theory does not apply. Before one jumps to this conclusion, however, it is worth repeating the caution that the calculated tunneling rate is an extremely steep function of the assumed barrier height and width. For example, if the barrier is 100 Å thick, the electron tunneling time would be 1 ns at zero field, and would become equal to the PL decay rate only at a field of 6 x 10⁴ V/cm. This field was not attained experimentally (due to the screening of the field by the separated charges. Thus the extreme sensitivity of the theory to the growth parameters (and assumed band offset ratio) makes it difficult to conclude to what extent the tunneling-out theory may apply.

It should also be noted that since the laser injects population into both wells, the bands become filled, and the tunneling rate decreases since the density of available final states decreases by Pauli exclusion. The tunneling-out theory completely ignores this effect.

The results for the hole tunneling for the 86 Å barrier are not displayed. In this case the hole tunneling time is never faster

than a few hundred μs even at high bias; hence the hole tunneling may be ignored.

Returning to the problem of interpreting the time-resolved PL spectra of sample A, it should be noted that the electrons are injected into the QW's with a small excess kinetic energy. They will therefore be warmer than the lattice. It follows that as long as the electron levels in the two QW's are within a few kT_e of each other, where T_e is the electron temperature, then the observed decay of the ω_2 line (in fact, the evolution of the $\omega_2 + \omega_{CT}$ combined lineshape) will depend on both the tunneling rate and the electron cooling rate in the coupled QW system. Polland $et.al.$[30] have shown that for single QW's under experimental conditions otherwise very similar to ours, the electron temperature immediately after injection is a few hundred degrees K ($i.e.$, kT_e is a few tens of meV). After about 150 ps, kT_e is about 3.5 meV, and the electron gas cools with a time constant of several hundred ps. When one also includes the effect of the band-filling due to charge buildup in the QW's, it becomes clear that electrons in QW1 can be thermally excited into QW2 over a bias range of several volts, consistent with experimental observation. The fact that the energy resolution of the time-resolved PL system is about 3 meV further complicates the interpretation of the time-dependent $\omega_2 + \omega_{CT}$ combined lineshape.

A further difficulty with the above interpretation of the ω_1 and ω_2 PL decay rates as hole and electron tunneling, respectively,

is that it cannot account for the low intensity of the ω_1 line unless the hole tunneling has a component that is faster than the streak camera response time of 20 ps. If there were no such fast component, then in fact the ω_1 line would dominate the time-resolved spectra, since the population of QW2 would be depleted by electron tunneling, but all the holes would remain in QW1 (at low bias); hence the instantaneous intensity of ω_1 would be much greater than the ω_{CT} line, which is not what we observe. It is straightforward to show by a simple rate equation analysis that a hole tunneling time of about 36 ps is required to explain the relative intensities of the PL lines in the cw and time-resolved data (with the assumption that the hole tunneling rate is independent of the hole momentum in the plane of the QW). This tunneling rate is several orders of magnitude greater than the simple theoretical estimate given by the tunneling-out theory.

Of course, another interpretation of the relative intensities is that since the QW1 recombination is in $Al_{.15}Ga_{.85}As$, which is lower quality material than GaAs, there may be a nonradiative contribution to the decay which dominates. Possibly there are many hole traps, so there are few holes in QW1 with which the electrons may recombine. Another possibility is that the nonradiative recombination rate is so fast in QW1 that the electrons and holes recombine faster than the transfer time of electrons from QW2. The principal difficulty with this interpretation is that for sample B, which was grown in the MBE

run immediately successive to sample A under identical conditions, the ω_1 and ω_2 lines have roughly equal intensities. It is unfortunately not possible to determine whether the low ω_1 intensity for sample A is due to fast hole tunneling or nonradiative decay on the basis of PL experiments; the only unambiguous way to settle the issue would be to have a third sample with barrier width between that for sample A and for sample B, so that a trend in relative PL intensities could be clearly observed.

What is clear, however, is that at high fields the decay of both ω_1 and ω_2 PL components is streak-camera limited, and therefore we can conclude that at least at high fields the tunneling is fast (less than 20 ps) *for both electrons and holes.* The tunneling-out theory cannot account for the fast observed hole tunneling rate.

IV.C. Subpicosecond Absorption Experiments

IV.C.1. Introduction

As I mentioned in the previous section, the time resolution of the PL system is limited to about 20 ps, and therefore any fast component to the tunneling would be unobservable. Furthermore, in order to see luminescence from both wells and thereby monitor their time-dependent populations, it is necessary to pump both wells with the excitation pulse. Therefore the initial state of the double well system is delocalized over both wells, and it is not possible to observe coherent tunneling. Furthermore, the tunneling rate of carriers from one well to another will be modified by the presence of carriers already present in the second well, which reduce the number of available states for tunneling by the Pauli exclusion principle. Hence the tunneling rate from an initially localized state is still interesting, even if scattering makes the observation of coherent tunneling impossible. With absorption spectroscopy it is possible to monitor the population of each well without requiring that electrons and holes both be present in each well. We have therefore performed experiments using the subpicosecond absorption spectroscopy methods described in chapter 2 in an attempt to observe the fast tunneling from one quantum well to another.

The experimental parameter used to monitor the populations of each QW is the differential absorption spectrum. The transmission T_p of the sample with pump beam incident is first acquired, and the transmission without the pump T_{np} is acquired and subtracted. This difference signal is then normalized to the transmission T_{np}. Thus the result of the experiment is the change in the absorption spectrum due to the pump beam, normalized to remove the effects of a nonuniform probe spectrum.

The differential absorption spectrum is also susceptible to a straightforward interpretation if the injected carrier density is not too high. As I mentioned in chapter I section I.B.3, the two contributions to the absorption spectrum are the exciton lines and the band-to-band (continuum) absorption. The density dependence of the exciton contribution to the absorption coefficient has been shown by Chemla and Miller[31] to be

$$\alpha = \alpha_{ex} - \sigma_{eh}N \tag{1}$$

where α_{ex} is the exciton absorption coefficient with no carriers present, σ_{eh} is the nonlinear absorption cross section, and N is the carrier density. This expression is valid if the density is not so high that the exciton absorption is completely saturated. The continuum absorption coefficient in the presence of carriers is[32]

$$\alpha = \alpha_0 (1 - f_e - f_h)$$ (2)

where f_e (f_h) is the electron (hole) distribution function. As discussed in section I.B.3, the bandgap renormalization must be taken into account, which shifts the edge of the continuum absorption coefficient α_0. Thus if the density is not too high, the differential absorption spectrum is

$$\frac{\Delta T}{T} = \frac{T_p - T_{np}}{T_{np}}$$ (3)

$$= \sigma_{ehh} LN + \sigma_{elh} LN + \alpha_{0p} L(1 - f_e - f_h) - \alpha_0 L$$ (4)

for each quantum well. The nonlinear cross sections for the heavy and light hole excitons are σ_{ehh} and σ_{elh} respectively. The continuum absorption coefficients with and without pump are described separately as α_{0p} and α_p so that the band edge shift may be included. The important thing to notice about equation (4) is that the differential absorption signal in the vicinity of the exciton lines gives the carrier density in the well, particularly at low enough density where the continuum contribution may be ignored. (This is possible since it has been shown[31] that the exciton lines begin to saturate at a density approximately 100x

lower than the threshold for continuum saturation at room temperature).

There is one further complication that must be considered when the pump beam resonantly generates excitons. Knox *et. al.*[33] have shown that the nonlinear cross section for saturation of the exciton absorption due to the presence of other excitons is twice the cross section for the absorption saturation due to free carriers. Furthermore, at room temperature, the resonantly generated excitons ionize in about 300 fs due to scattering by the lattice phonons. These effects must all be considered in the interpretation of the double-well spectra.

In this section I will describe the results of subpicosecond differential absorption experiments on asymmetric coupled QW's, and discuss to what extent the experiments indicate tunneling between the wells. First I will discuss the preparation of samples suitable for optical absorption experiments. Then I will discuss experiments performed on the samples A and B described in section B of this chapter. In these experiments, the experimental conditions were similar to those of the time-resolved PL experiments described in section B. The sample was held at low temperature, and both wells were excited by the pump beam. The goal was of course to look for a fast component to the tunneling which could not be observed with the PL system. I will then describe experiments performed at room temperature, where the pump laser excited only one well, in an attempt to

observe tunneling from an initially localized state in a coupled QW structure as described above. I will conclude with suggestions for further experiments that could clarify and improve on the results presented here.

IV.C.2. Sample Preparation

Because GaAs is opaque to the QW interband transitions, the GaAs substrate was removed by selective etching. For samples A and B, a large portion of the substrate was first removed by grinding and polishing with a series of successively finer-grained abrasive papers, with water used as a lubricant. The final sample thickness after grinding was about 100 μm. The samples were placed epitaxial-side down on a microscope slide and cemented with uv cement. In order to minimize the strain on the etched thin film, the substrate was coated with photoresist (Shipley 1350J) except for a small (1 mm) hole. The resist after baking served to block the chemical etch solution quite effectively. A solution of hydrogen peroxide / ammonium hydroxide was prepared with a volume ratio of 25:1 to yield a pH of 8.4. A stream of the etch solution was directed onto the exposed portion of the GaAs substrate. The etch rate was approximately 5 μm/minute. The AlAs/GaAs (20Å/20Å) superlattice (SL) buffer served as an etch stop. The etch stop was not entirely effective,

and the solution did etch away portions of the sample into the QW region. However, the etch stop did function satisfactorily over 100-200 μm regions on the edge of the exposed sample. (Unfortunately, an approximately 2000-Å thick GaAs region remained between the etch stop layer and the QW region, due to an error in the MBE growth of the samples. This layer absorbed some of the pump light, but did not seem to adversely affect the data presented here.) Ideally, at this point the sample would have been coated on both sides by an anti-reflection coating, but this was not done due to time constraints. As I mentioned above, there were no contacts on the sample for application of an external field.

A third sample, which I will refer to as sample C, was designed as a p-i-n structure, in an attempt to study the tunneling via optical absorption versus an applied electric field. Furthermore, the QW's in this sample are much wider (QW1 = 200Å, QW2 = 60Å), and the absorption edges of the two wells are separated by about 47 meV. This is important because the bandwidth of the 150-fs pump pulse is about 30 meV, and it is essential to avoid accidental direct excitation of QW1 when looking for tunneling from a state initially localized in QW2. For samples A and B, the absorption edges are separated by only about 22 meV, making it more difficult to avoid direct excitation of QW1.

The layer structure of sample C is shown in Fig. 4.25. The processed p-i-n diode structure suitable for optical absorption

p$^+$	Al$_4$Ga$_6$As	5000 Å
i	Al$_5$Ga$_5$As	100 Å
i	GaAs	60 Å
i	Al$_5$Ga$_5$As	60 Å
i	Al$_1$Ga$_9$As	200 Å
i	Al$_5$Ga$_5$As	100 Å
n$^+$	Al$_4$Ga$_6$As / GaAs SL (290/10)	1 μm
n$^+$	GaAs	1 μm
n$^+$	GaAs	substrate

25 x {

Figure 4.25. Growth sequence of double-quantum-well sample C. The Al$_{.4}$Ga$_{.6}$As (290Å) / GaAs (10Å) superlattice serves as an etch stop for the selective etching of the substrate.

experiments is shown in Fig. 4.26. The sample was grown and fabricated at Cornell University by Xiao Song. The mesa diameter is 600 μm, with a 200-μm hole for optical access. The $Al_{.4}Ga_{.6}As/GaAs$ superlattice (SL) served as the etch stop. The back side has an n-type ohmic contact, which was used as the ground plane. The top side has a p-type ohmic contact, which was connected to a thin bias wire with silver paint. The reverse bias breakdown voltage at room temperature is -10V.

IV.C.3. Initial Excitation in Both Wells

The PL experiments described in section IV.B. indicated the possibility of a fast tunneling component for sample A even at low applied electric field. At high electric field, the electron and hole tunneling leading to the CT state are faster than the time resolution of the PL experimental system. Unfortunately, samples A and B could not be prepared for optical absorption measurements with an applied electric field, so the investigation described here is limited to the zero-field case. The goal, of course, is to resolve any tunneling component shorter than the PL time resolution.

The samples were held in the cryostat as before at a temperature of 6 K. The etched thin film was aligned over a small hole in the cold finger to allow passage of the laser pump and
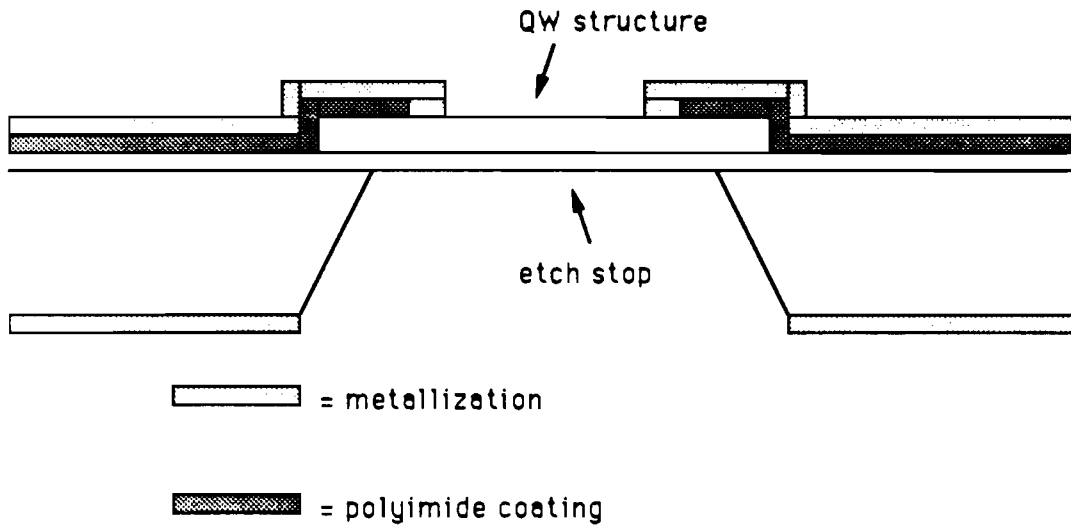
Figure 4.26. Cross section of the p-i-n diode structure used for optical absorption experiments.

probe beams. The time-resolved differential absorption spectra were acquired as described in section II.B. A 10-nm bandpass filter was used to select the pump at 690 nm (1.8 eV) from the white light continuum. At this excitation energy, free electron-hole pairs are created in both wells. I estimate the injected carrier density to be 6×10^{11} cm^{-2}.

The transmissivity spectra for sample B with and without pump are shown in Fig. 4.27. The first peak corresponds to the QW2 heavy-hole (HH) exciton transition, and the central peak to the QW1 HH exciton transition. The third peak contains the QW1 and QW2 light-hole (LH) transitions. (The two peaks are separated by only 4 meV, which is less than the linewidth of the third peak). The pump energy (1.5 nJ) was such that the exciton lines are saturated, but the continuum makes no contribution to the differential spectrum. The transmissivity under strong pumping conditions (pump energy 15 nJ), where the continuum is also saturated, is shown in Fig. 4.28.

Differential absorption spectra for the first 1 ps after the pump pulse are shown in Fig. 4.29 for sample A and Fig. 4.30 for sample B. In both cases all three peaks show a simple rise with the pump pulse to a constant value. A fast tunneling component would appear as a decay in peak 1 or 2, accompanied by a rise on the other. No such behavior is observed for either sample on the 1-ps time scale. The explanation for this is straightforward. A carrier density of 6×10^{11} cm^{-2} results in a band-filling in the
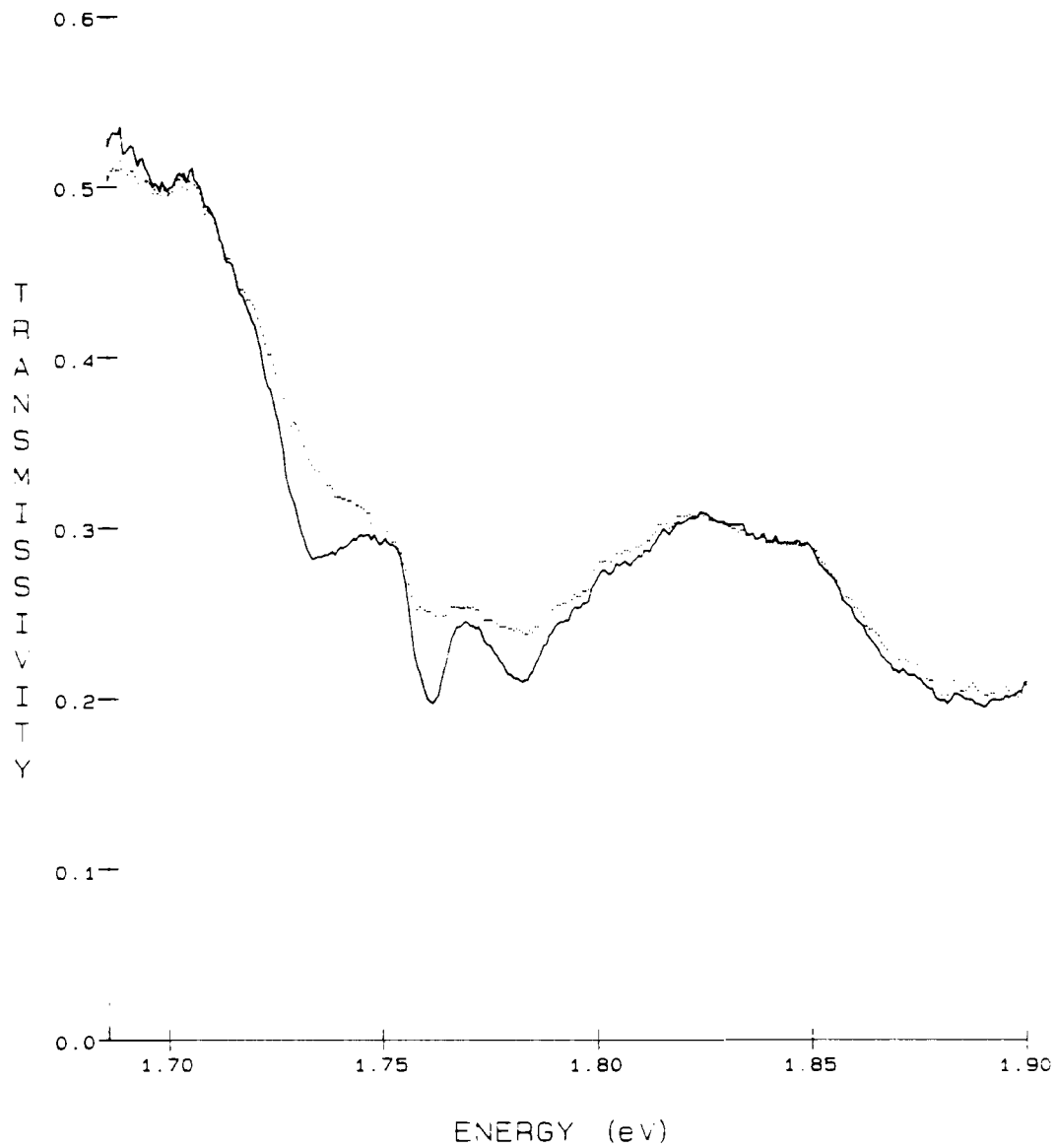
Figure 4.27. Transmissivity spectra for sample B (86 Å barrier).
The solid line shows the transmissivity without pump,
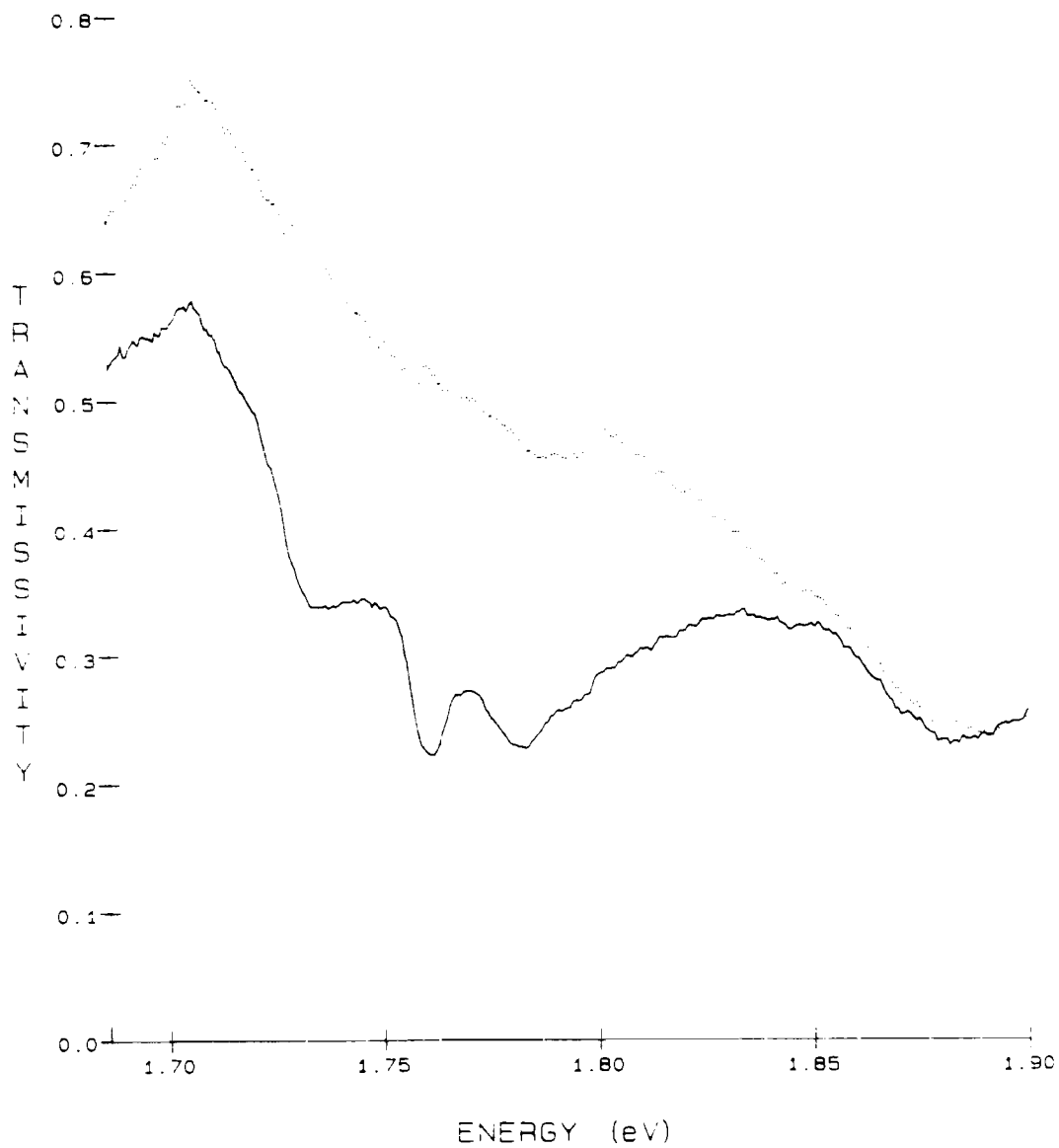the dotted line with 1.5 nJ pump incident on the sample.

Figure 4.28. Transmissivity spectra of sample B with 15 nJ pump (dotted line) compared to unpumped spectrum (solid line).
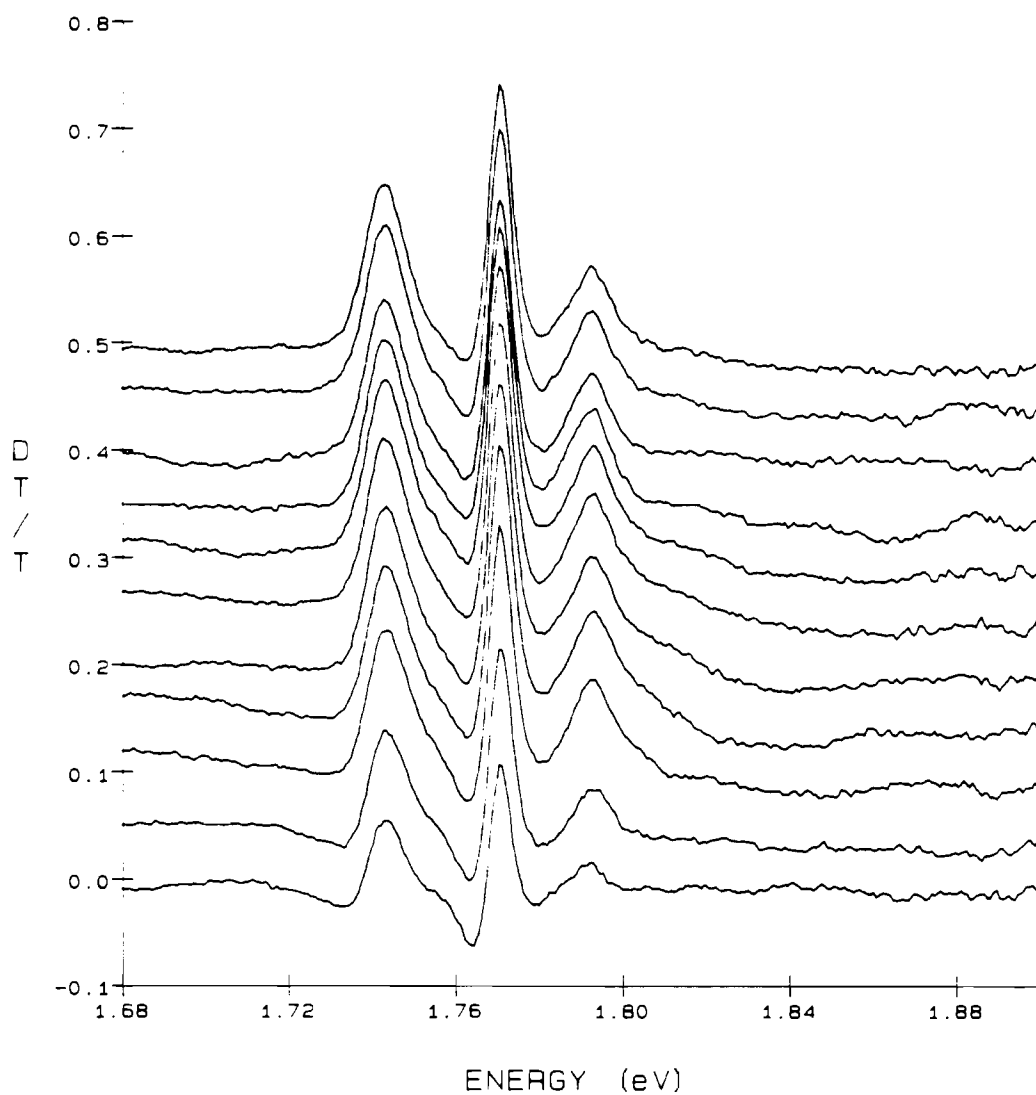
Figure 4.29. Differential absorption spectra for sample A (43 Å barrier) with 1.8 nJ pump at 1.8 eV. The spectra are at time delays from 0 to 1 ps in 100-fs steps (t=0 is the bottom curve). The sample temperature is 6K.
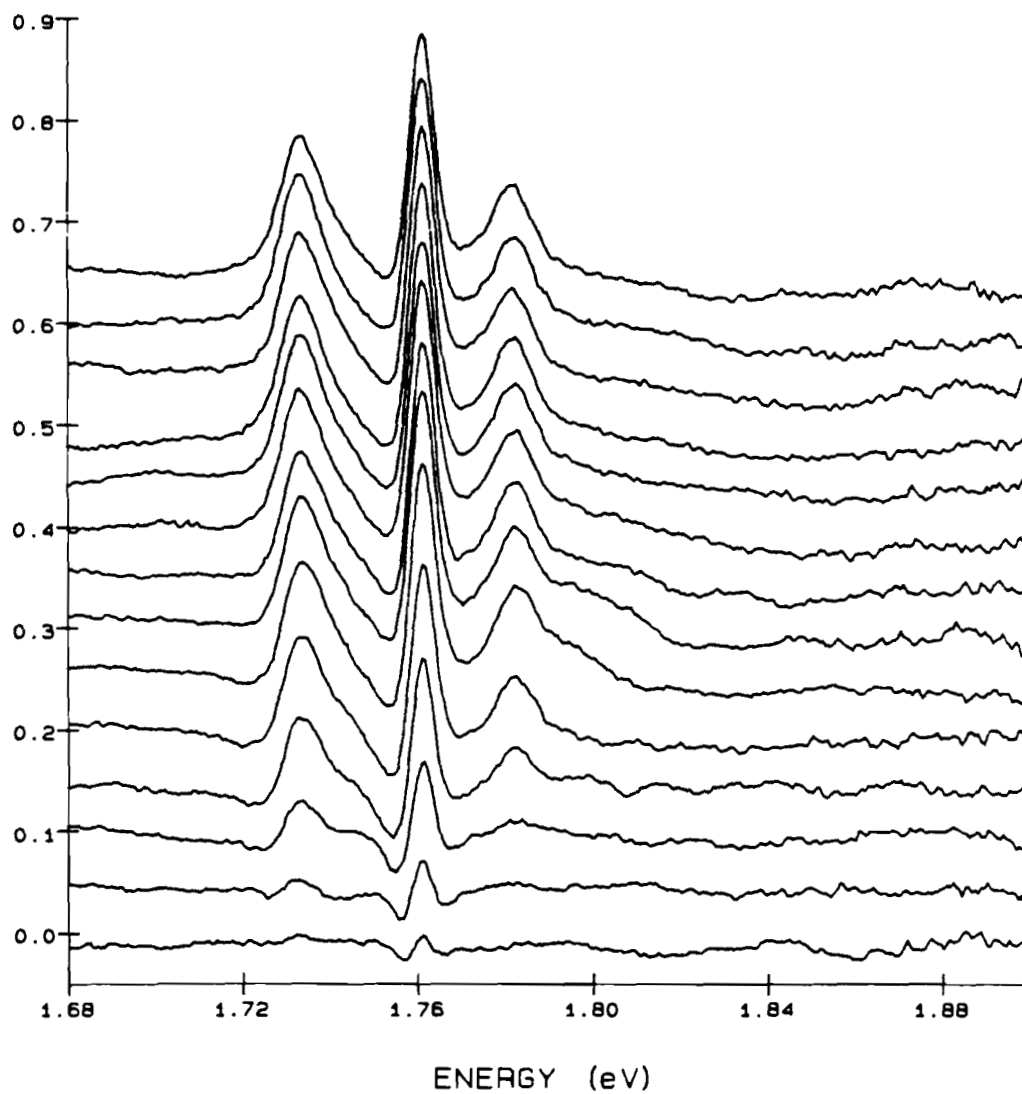
Figure 4.30. Differential absorption spectra for sample B with 1.5 nJ pump at 1.8 eV. The spectra are at time delays from - 300 fs to 1 ps in 100-fs steps (t=-300 fs is the bottom curve). The sample temperature is 6K.

conduction band of 18 meV in QW1 and 21 meV in QW2. However, the electron states of the two wells are separated by only about 5 meV. Hence any tunneling between the two wells is completely blocked by the exclusion principle. The experiment should of course be performed again at a lower density ($\leq 10^{11}$ cm^{-2}), however this will require some improvement in the stability of the white light source so that a good signal-to-noise ratio can be obtained with reasonable integration times. (Each spectrum in the displayed figures required about 2.5 minutes integration time).

Differential absorption spectra are shown for longer probe delay times in Figs. 4.31 (sample A) and 4.32 (sample B). In both cases the area of the central peak (QW1 HH) decreases as the area of the QW2 HH peak increases, the rise and fall time constants being the same (250 ps) for both samples. The rates are most likely determined by the carrier cooling rate rather than the tunneling time.

IV.C.4. Initial Excitation in One Well

In order to localize the initial excitation in QW2, the pump wavelength is tuned to the QW2 heavy-hole (HH) exciton transition. Of course, it is possible to excite the CT exciton (QW2 HH, QW1 electron) as discussed in section IV.A. However, the oscillator strength of this transition is expected to be completely

Figure 4.31. Differential absorption spectra for sample A under same conditions as Fig. 4.29. The probe pulse delays are, from bottom to top, 1, 5, 10, 15, 20, 40, and 80 ps.
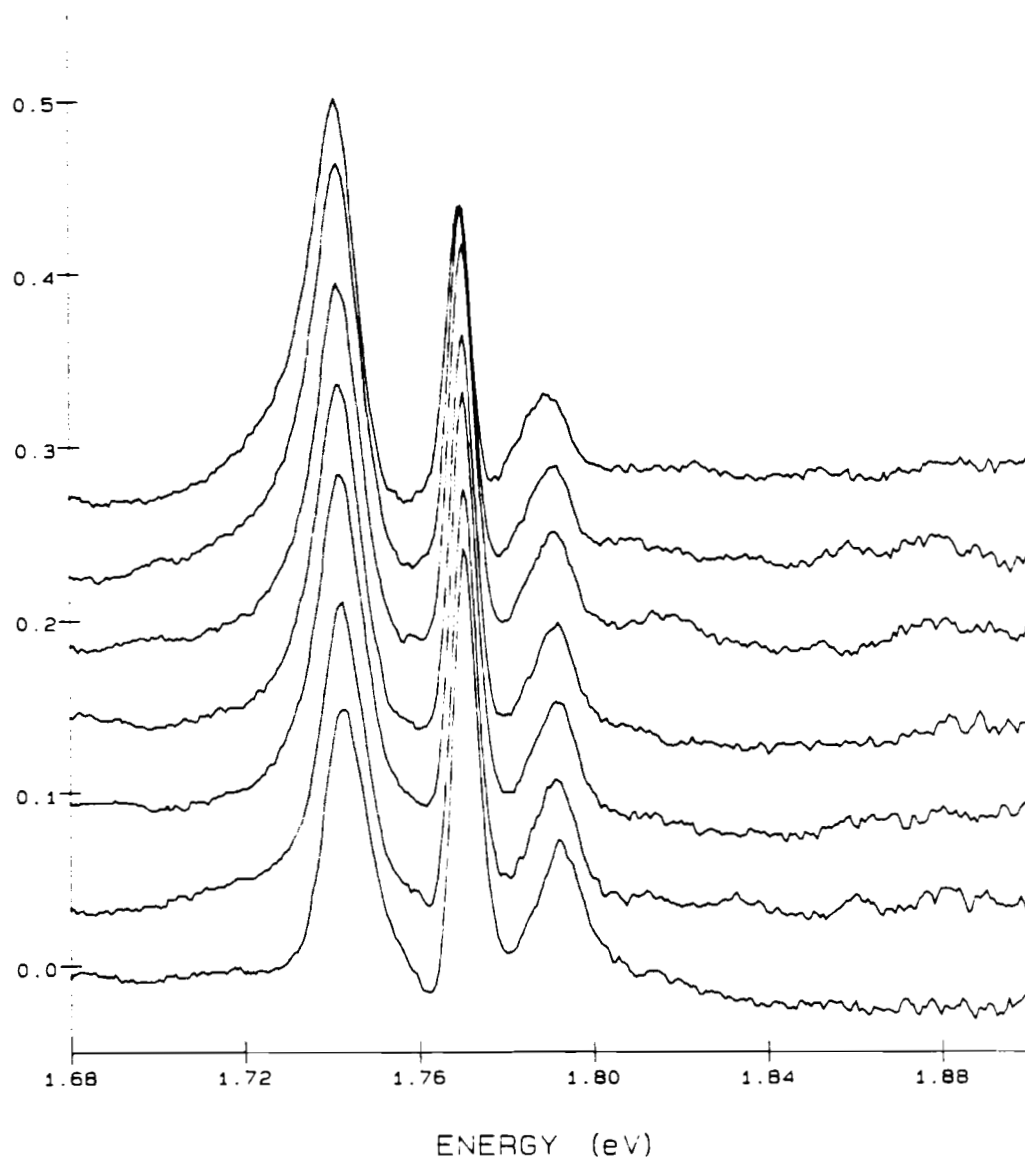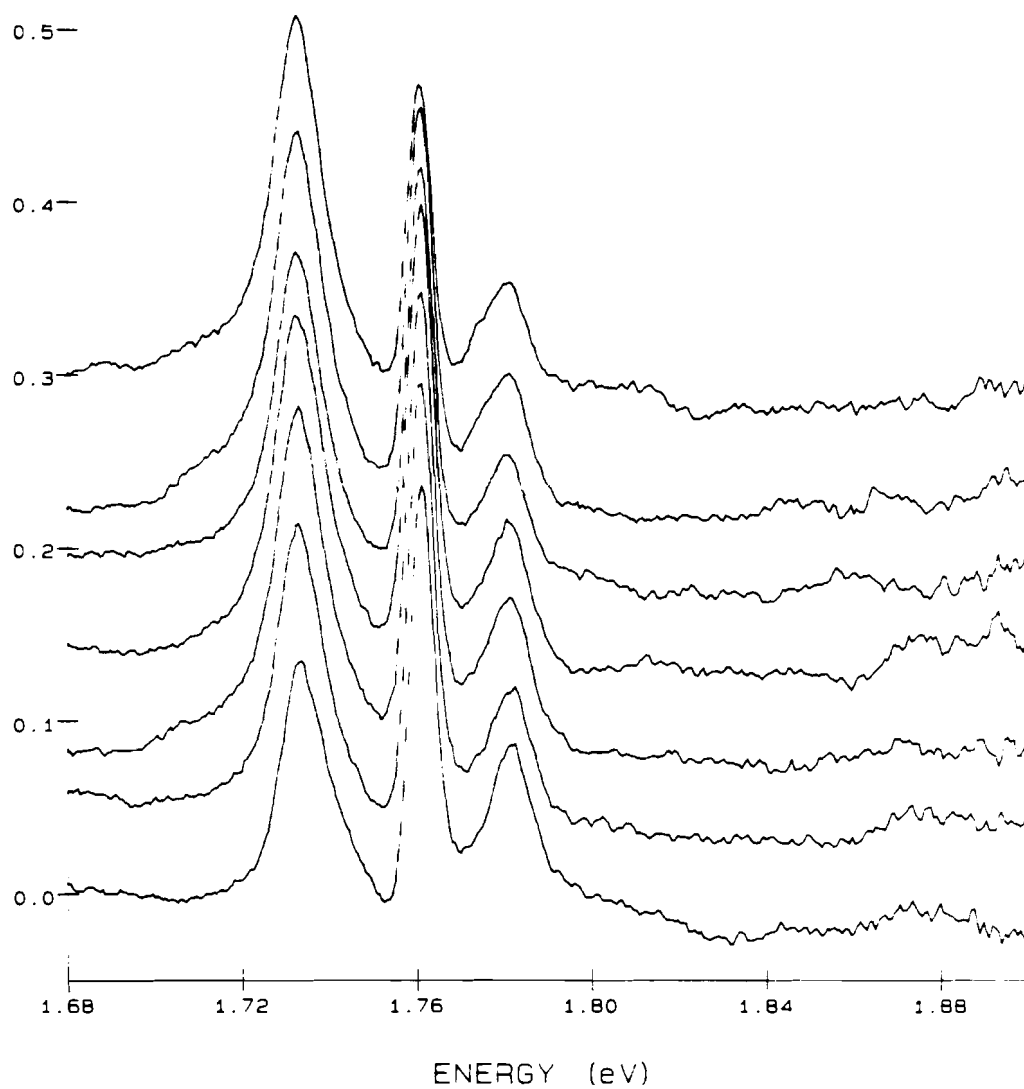
Figure 4.32. Differential absorption spectra for sample B under same conditions as Fig. 4.30. The probe pulse delays are, from bottom to top, 1, 5, 10, 15, 20, 40, and 80 ps.

negligible compared to the strength of the QW2 exciton. This serves to localize the initial excitation, assuming that the pump spectrum is not so large that it overlaps the QW1 HH exciton transition.

The expected temporal behavior of the different exciton peaks in the differential spectrum is as follows. Heavy hole excitons are resonantly created in QW2, and hence the QW2 HH peak should rise with the integral of the pump pulse as the QW2 HH exciton transition bleaches. Because the excitons are resonantly created, the effective carrier temperature is zero at time zero.[3] The excitons will interact with the lattice, which for the experiments reported in this section is at room temperature. The lattice phonons will ionize the excitons in about 300 fs.[3] Since excitons bleach the excitonic absorption more efficiently than free carriers,[34] the QW2 HH exciton peak in the differential absorption spectrum will decrease with time to a constant value, determined by the screening of the exciton by free carriers. (At T=300K, virtually all the excitons are ionized, and only free electrons and holes exist).[35] The QW2 light hole (LH) exciton peak in the differential absorption spectrum will show a rise as free carriers are generated by the ionization of the heavy-hole exciton.

The two QW's are only weakly coupled, so that the appearance of a signal in the differential absorption spectrum at the QW1 HH exciton peak must be associated with carriers in QW1. Hence the modulation of this peak gives the population of QW1

due to tunneling from QW2 (in the absence of direct excitation of QW1). Of course, if the QW1 HH rise is slower than the 300-fs exciton ionization time, it is possible to unambiguously assign the rise to tunneling from QW2 to QW1. If, however, the tunneling is comparable to or faster than the ionization time, the interpretation of the QW1 rise time becomes difficult. If the tunneling is due to free electron tunneling and is very fast, then the QW1 HH peak will rise with the QW2 HH ionization time. The same is true if the phonon-assisted tunneling is fast at 300K; in this case the limiting factor is the heating of the carriers from exciton ionization via phonon scattering, rather than the interwell scattering. If a QW1 HH rise time is observed that is faster than the QW2 exciton ionization, there are several possible explanations. First, and most optimistically, the electron could be tunneling resonantly. (More precisely, the QW2 HH exciton transfers to the CT exciton). Secondly, some scattering process other than LO-phonon scattering could be responsible for the tunneling. Finally, the possibility of direct excitation must be considered.

Differential absorption spectra are shown in Fig. 4.33 for sample B at t=0 and +500 fs, along with the excitation pulse spectrum. The injected carrier density was about 10^{12} cm^{-2}. The pump wavelength was selected to be resonant with the QW2 HH exciton transition at 1.65 eV. At t=0, the QW2 HH transition dominates the differential absorption spectrum. At t=+500 fs,
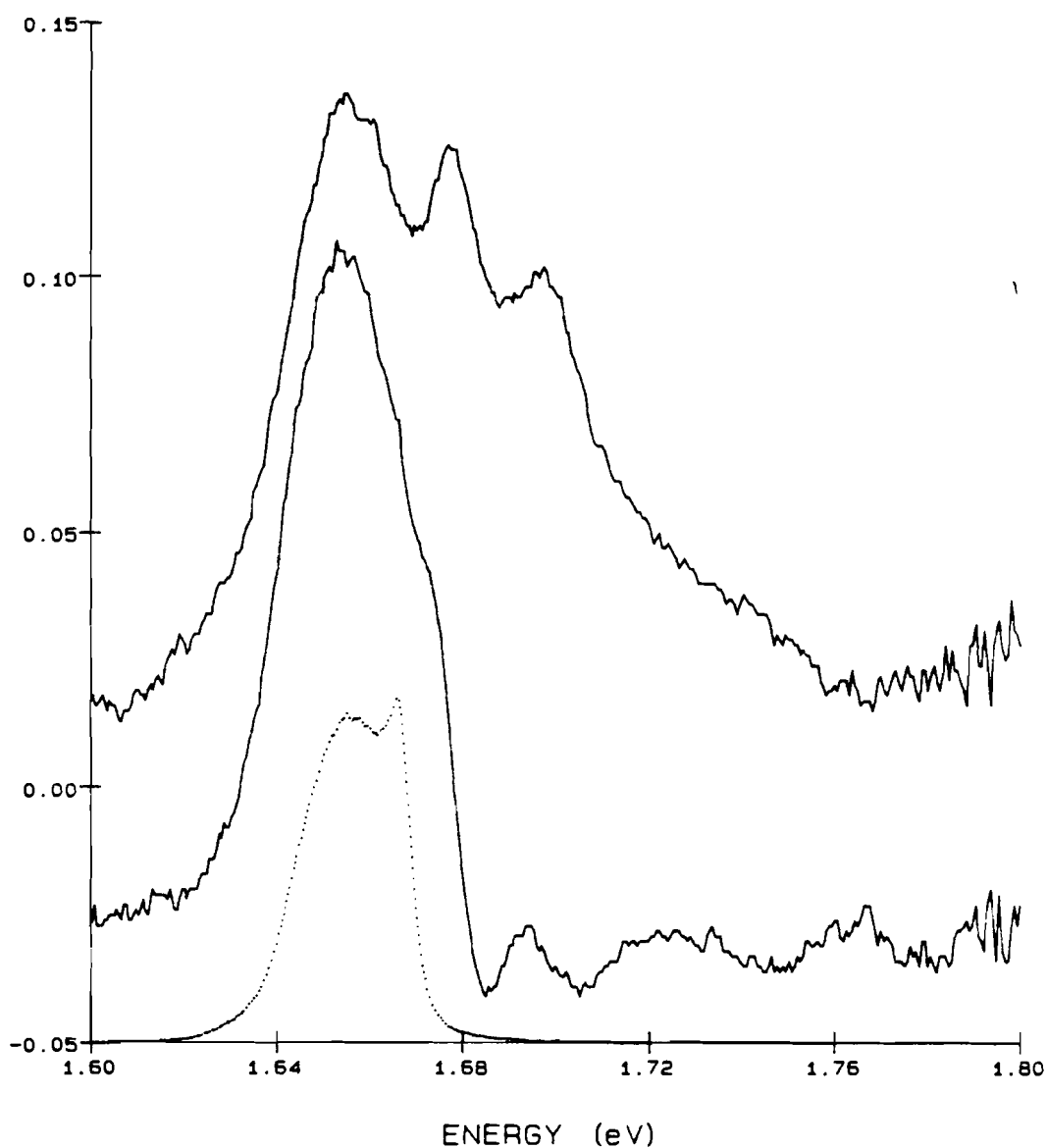
Figure 4.33. The bottom curve is the pump spectrum for the single-well-excitation experiments on samples A and B at room temperature. The middle curve is the differential absorption spectrum of sample B at time zero. The top curve is the differential spectrum at a probe delay of 500 fs. The spectra are offset for ease of viewing.

however, the three peaks observed in the previous experiment of section IV.C.3 are apparent. The peaks are, from red to blue, QW2 HH, QW1 HH, QW2 LH, and QW1 LH (the latter two being within a linewidth and therefore indistinguishable). The lines are not so well separated as in the experiment at 6K described in the previous section, as the lines are broader. There are several possible contributions to the observed broad width. The exciton transition is resonantly pumped by an intense pulse. Hence the linewidth may be larger due to saturation broadening, and there may be a contribution to the differential absorption from band-filling. The thermal broadening is expected to be about 4 meV.[35]

The time-resolved differential absorption spectra are shown for sample B (86 Å barrier) for the temporal range -300 fs to +1 ps in Fig. 4.34. In order to deduce the temporal behavior of each spectral peak, it is necessary to determine the area under each peak. I have used 3 Gaussians to fit the spectra. (The fit was performed visually. This was deemed sufficient since the fluctuations of the spectral intensities were limited by the stability of the white light source, so the accuracy of a least-squares optimized fit would be superfluous, even misleading). Other workers have generally found Gaussian lineshapes for the exciton lines at room temperature, although the physical reason for this is not yet fully understood.[35] Using 3 Gaussians to fit the differential absorption data amounts to an assumption that the signal is entirely due to modulation of the exciton absorption lines,
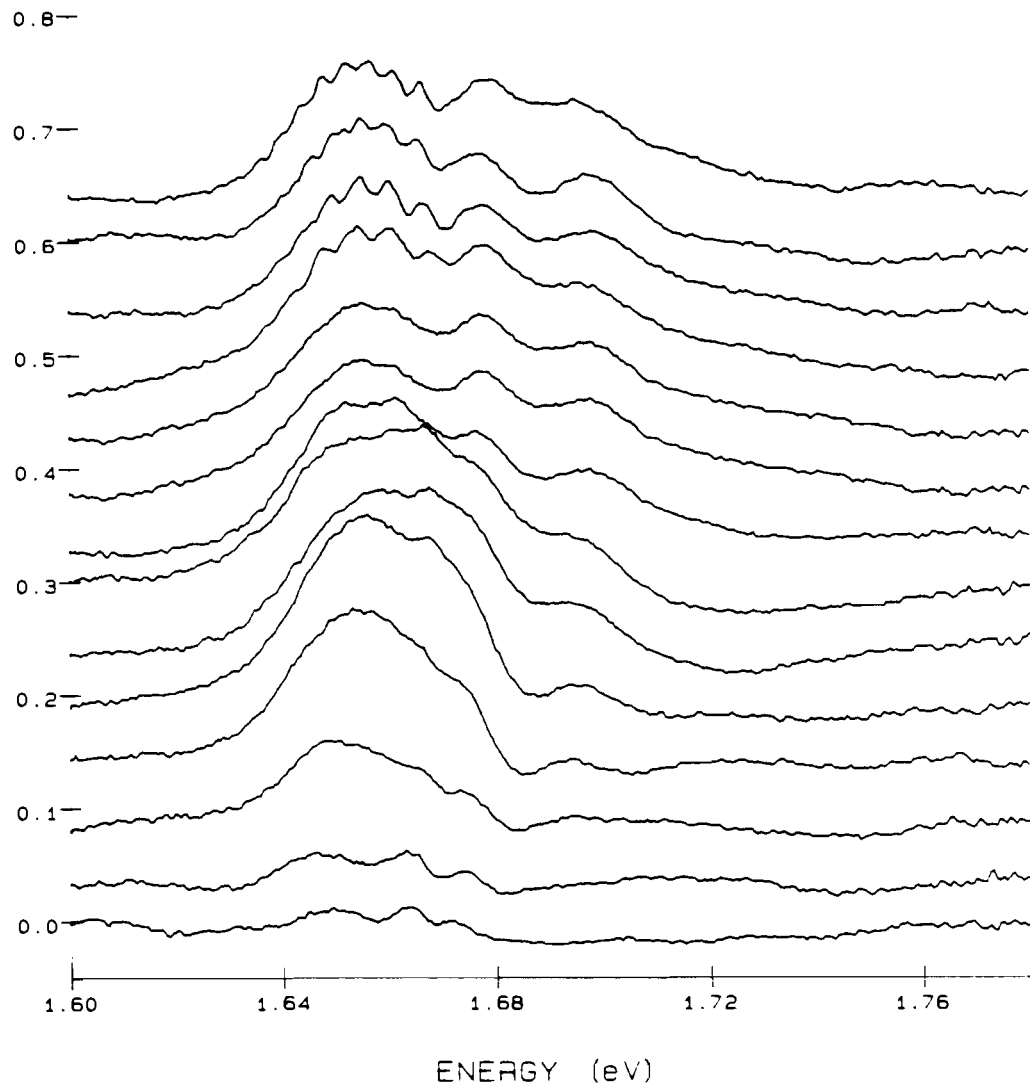
Figure 4.34. Differential absorption spectra for sample B pumped at 1.65 eV for the temporal range -300 fs to 1 ps (from bottom to top) in 100-fs steps.

and that there is no contribution from the interband continuum transitions. A fit including the continuum transitions of both wells can indeed be performed, however doing so introduces eight new free parameters into the fit: the bandgap renormalization, quasi-chemical potential, effective carrier temperature, and the broadening of the continuum edge for each well. I have therefore assumed that to first approximation, the areas using a 3-Gaussian fit will give the well populations.

The results of the fitted peak areas are shown in Fig. 4.35. (The results are scaled to their maximum values). The QW2 HH transition rises approximately with the integral of the laser pulse, and decays to a constant value by 400 fs. The peculiar flat-topped shape I attribute to fluctuations in the white light source spectrum and intensity. Clearly the data is too noisy to draw any quantitative conclusions from it, such as the exciton ionization time, though qualitatively the data behaves as expected. The QW2 LH transition rises more slowly, and is consistent with an ionization time of about 400 fs.

The behavior of the QW1 HH transition is quite surprising. The rise of this peak is approximately as fast as the QW2 HH transition. As I discussed above, this indicates either direct excitation or fast tunneling. For direct excitation, one would expect the QW1 HH peak to behave in qualitatively the same fashion as QW2 HH, namely an overshoot at early times due to resonant generation followed by ionization of the QW1 HH
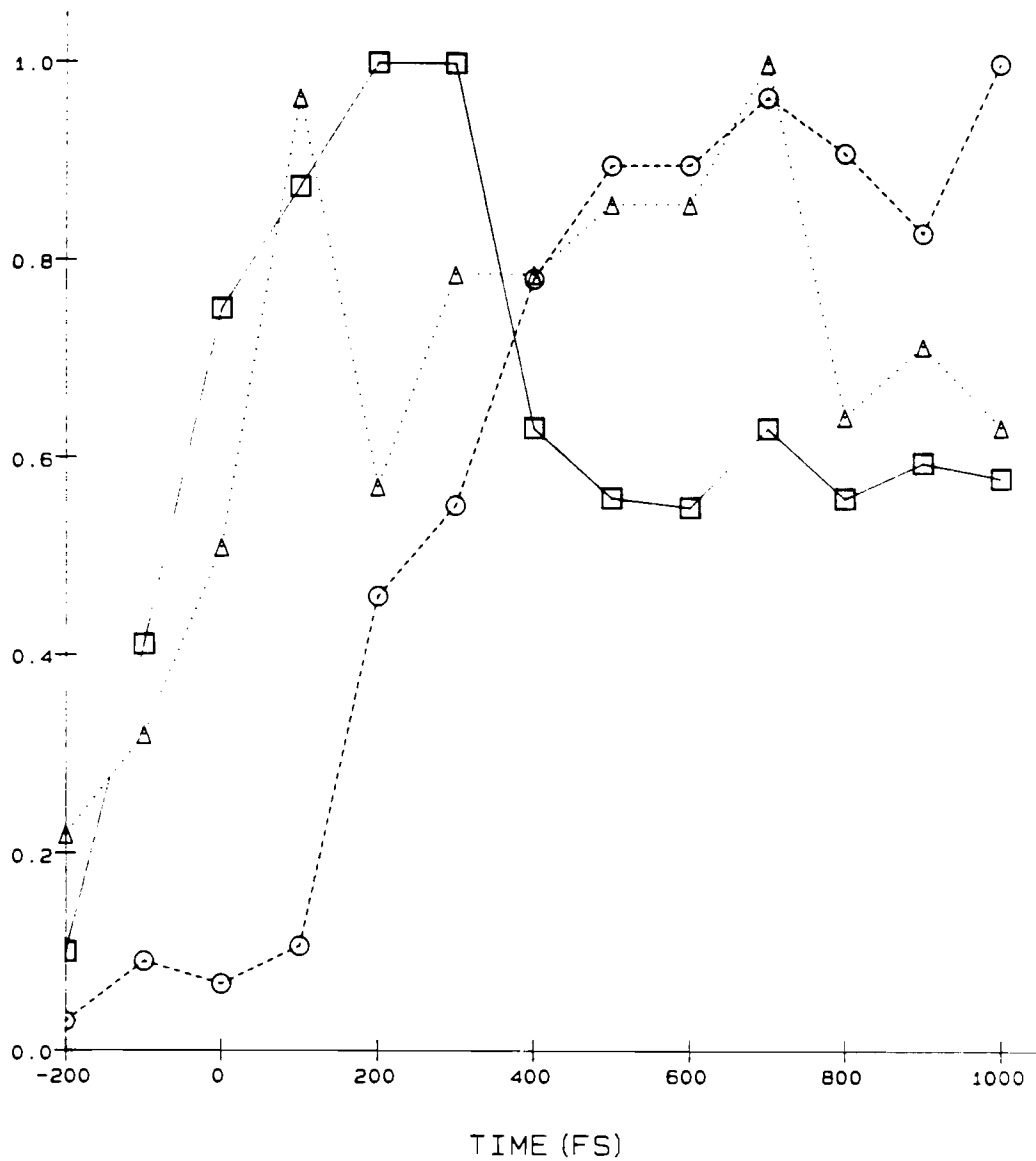
Figure 4.35. Time dependence of the peak areas for sample B
pumped at 1.65 eV. The results are scaled to the
maximum area for each peak in the time window -300 fs
to 1 ps. The solid line is the QW2 heavy-hole (HH)
exciton transition. The dashed line is the QW2 light-hole
(LH) exciton transition. The dotted line is the QW1 HH
transition.

excitons. The QW1 HH peak seems to display a simple rise, however, with no decay obvious above the noise. Hence the fast rise may be due to a fast (incoherent) tunneling process, or is an artifact of the simple fitting procedure. To determine conclusively the origin of the short risetime will require a more complete set of experiments, in which the pump is tuned somewhat further to the red to rule out the possibility of direct excitation. For samples A and B, the transition origins of QW1 and QW2 are too close (22 meV) to allow the pump spectrum to be centered on the QW2 HH transition without some direct excitation of QW1. Furthermore, the experiments must be done at lower excitation density to rule out the continuum contribution to the differential absorption spectrum. If the experiments were performed at a series of densities, along with an improvement in the signal-to-noise ratio by a factor of three or four, it would be possible to perform a more sophisticated fit to the spectra which would include the continuum contributions and yield reliable values for the well populations. From the present experiments done at a single excitation density (and with the present level of white light fluctuations) it is not possible to perform a meaningful fit of the spectra including the continuum of both wells. It is only possible to say that the data indicate the possibility of a very fast (<100 fs) tunneling of electrons from QW2 to QW1 for sample A.

The differential absorption spectra at longer (up to 20 ps) show no significant changes above the noise.

Differential absorption spectra for sample A (43 Å barrier) are shown in Fig. 4.36 for t=-300 fs to +1 ps. Qualitatively, one sees that the second peak (corresponding to the QW1 HH transition) displays a qualitatively different behavior near t=0 from that of sample B. This is borne out by the results of the 3-Gaussian fit shown in Fig. 4.37. The QW2 HH transition behaves as expected, showing a rise that looks more like the integral of the pump pulse than the data for sample B exhibit. The decay of the QW2 HH line occurs in about 300 to 400 fs. The QW2 LH transition displays a rise of about 400 fs, consistent with the interpretation provided by experiments on single QW's that the rise is due to ionization of the QW2 HH exciton. The QW1 HH transition behaves precisely as expected for direct excitation of QW1. The exciton peaks for sample A are all shifted about 10 meV to the red of the corresponding transitions of sample B (probably due to a slight change of the MBE growth parameters between runs). This shift is apparently enough to result in direct excitation of QW1. Thus it is impossible to make any statements regarding the tunneling in this sample; the experiments must be performed again with the pump tuned further to the red.

For sample C, the transition energies of the two QW's are well separated (47 meV), so it is possible to resonantly pump the QW2 HH exciton transition with no danger of directly exciting the QW1 HH transition. I estimate the injected carrier density to be 5 x 10^{11} cm^{-2}. A typical differential absorption spectrum is shown
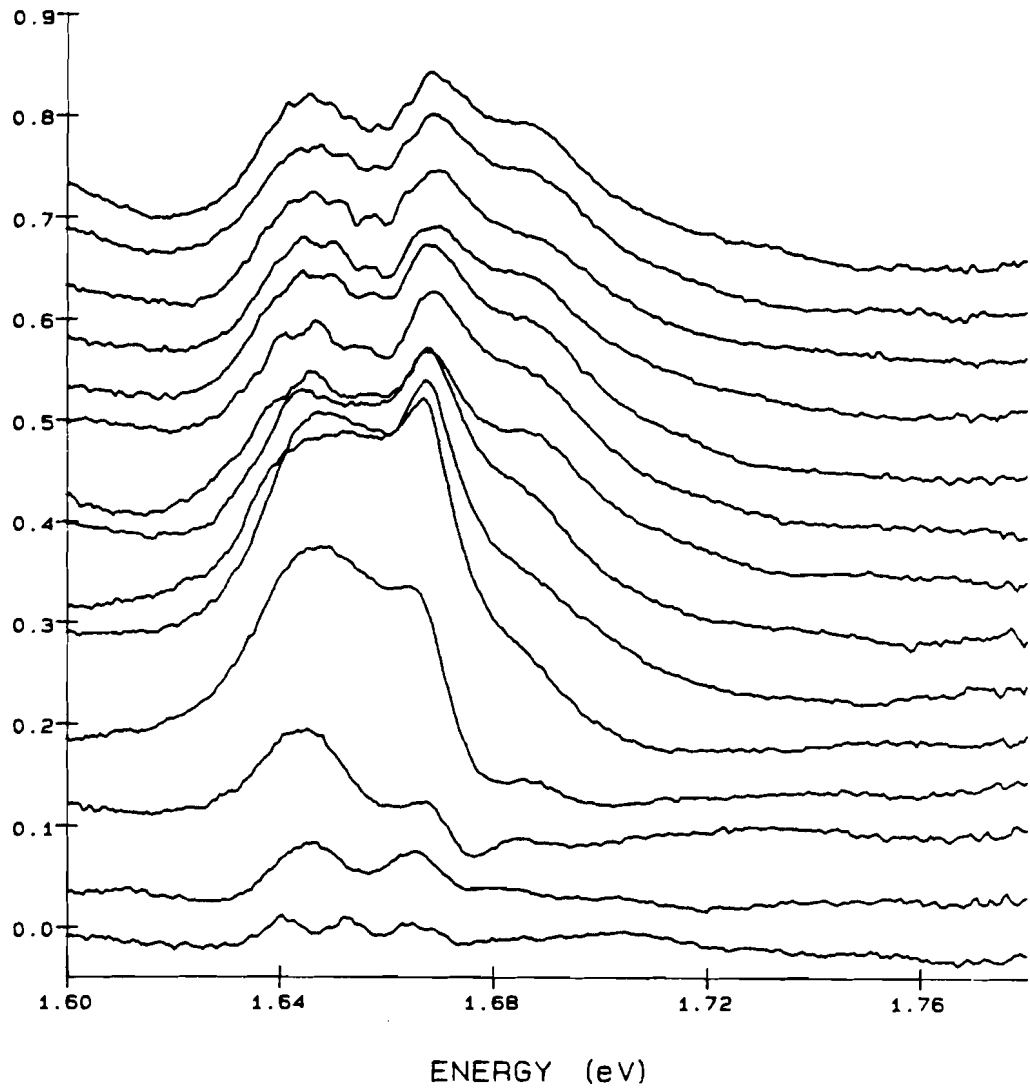
Figure 4.36.   Differential absorption spectra for sample A pumped at 1.65 eV for the temporal range -300 fs to 1 ps (from bottom to top) in 100-fs steps.
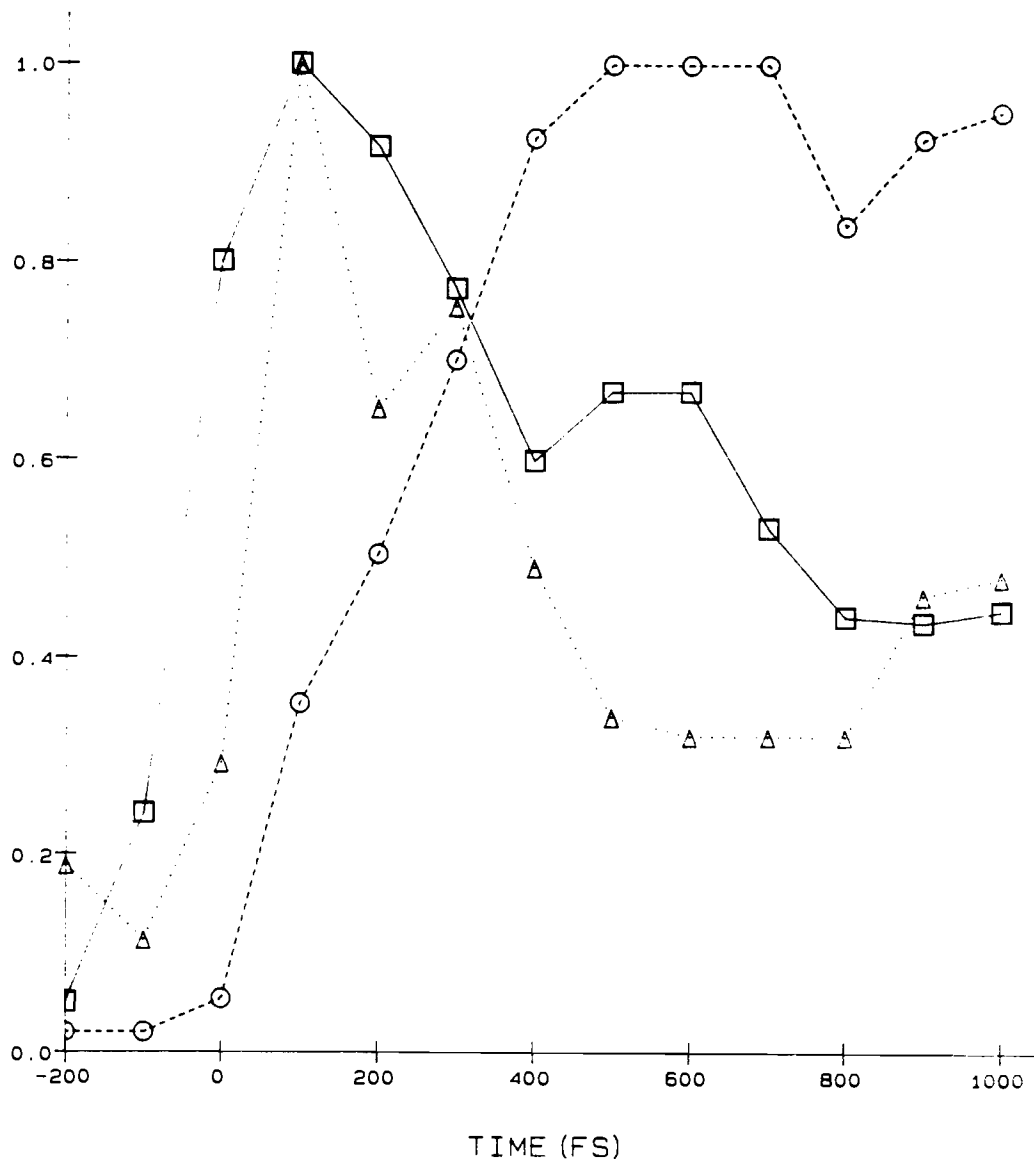
Figure 4.37. Time dependence of the peak areas for sample A
pumped at 1.65 eV. The results are scaled to the
maximum area for each peak in the time window -300 fs
to 1 ps. The solid line is the QW2 heavy-hole (HH)
exciton transition. The dashed line is the QW2 light-hole
(LH) exciton transition. The dotted line is the QW1 HH
transition.

in Fig. 4.38 for t=+500 fs. From red to blue, the peaks are QW2 HH exciton, QW2 LH exciton, and QW1 HH and LH exciton (these are within a linewidth of each other).

The single-particle n=1 electron state of QW2 is below that of QW1 by 18 meV at zero bias. Of course, as I discussed in section IV.A, the Coulomb interaction of the electrons and holes must be considered because the heavy holes are strongly confined to QW2, and thus for an electron to tunnel from QW2 to QW1, it must overcome the difference in binding energy between the QW2 HH exciton and the CT exciton. This difference in binding energy is about 6 meV. Hence the relevant energy splitting between the two QW energies is 24 meV. At this large splitting, the mixing of the two isolated QW states will be very small, and thus the amplitude of the resonant tunneling will be negligible. Hence at low bias any signal that appears at the QW1 transition most likely results from phonon-assisted tunneling. As the bias voltage is increased, the states should become closer to resonance, and the resonant tunneling component should increase. At room temperature, the phonon-assisted tunneling rate will probably also increase,[20] as will any elastic-scattering-assisted tunneling, so the total tunneling rate will increase as the levels approach resonance.

Differential absorption spectra for sample C at 0 V applied bias (and room temperature) are shown in Fig. 39 for t=-300 fs to +500 fs and at +1 ps. The QW2 HH peak shows an overshoot near
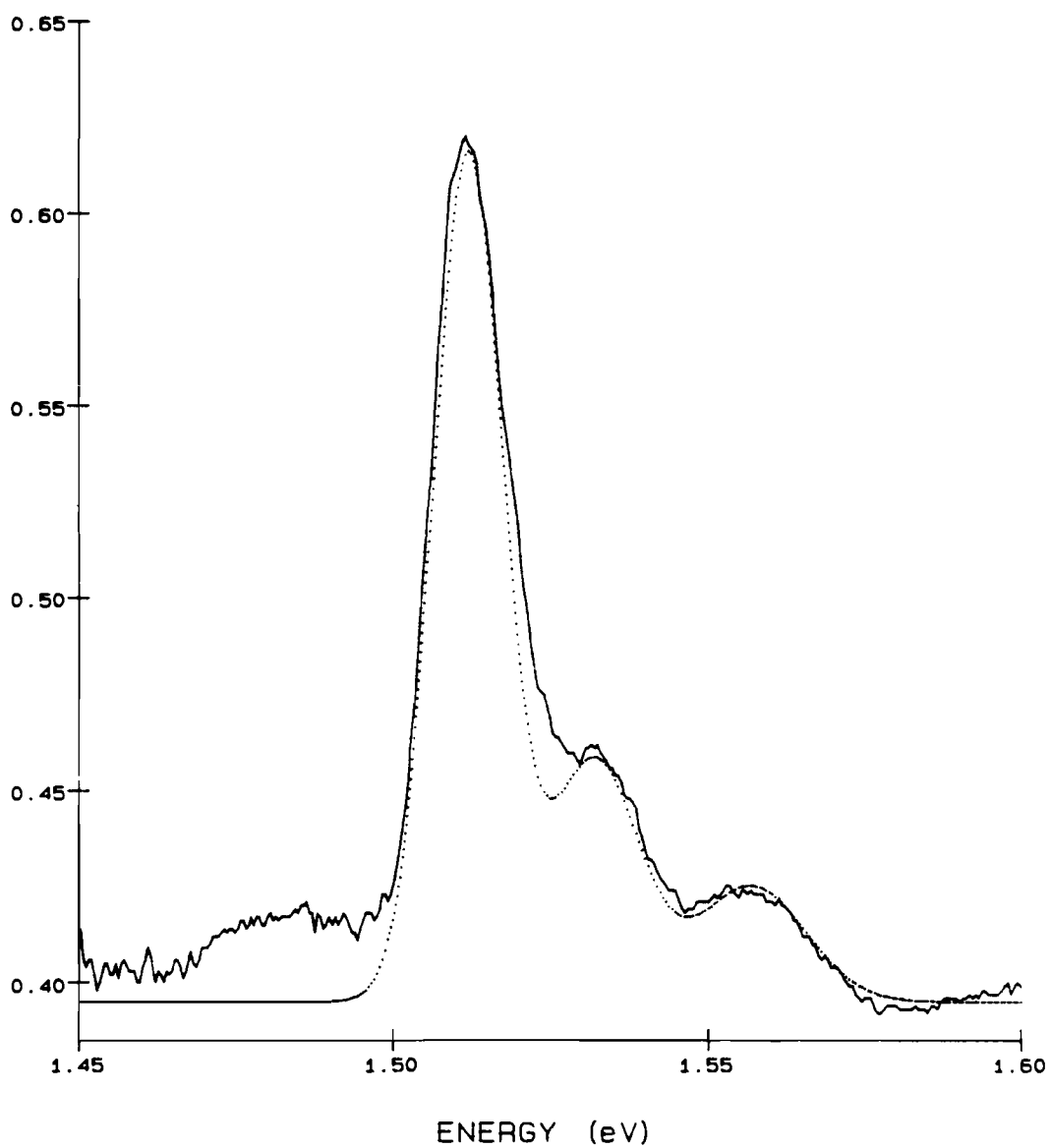
Figure 4.38. Differential absorption spectrum of sample C (solid line). The delay time is t=500 fs. Three Gaussians are used to fit the spectrum (dashed line).
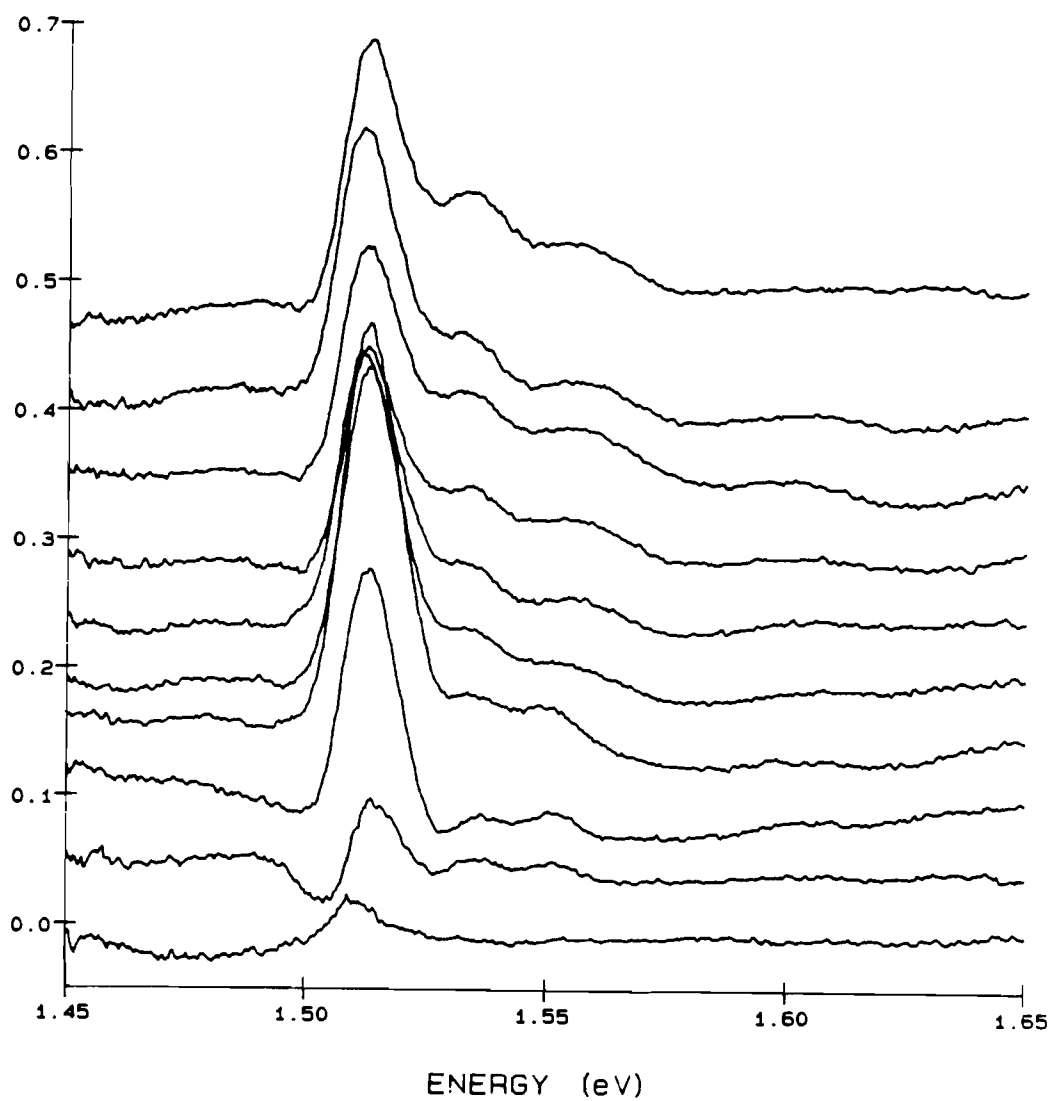
Figure 4.39.   Differential absorption spectra for sample C with 0 V
applied bias.   The delay times are -300 fs to +500 fs; the
top curve is at t= 1 ps.

t=0, whereas the QW2 LH and QW1 peaks show a simple rise. A fit of the spectra using 3 Gaussians to determine the areas under the three peaks yields the results of Fig. 4.40. The QW2 HH peak shows the characteristic fast rise with 300-fs decay for the resonant generation and ionization of the heavy-hole exciton. The behavior of the QW2 LH peak is consistent with a fast scattering-assisted tunneling process, since the rise of this transition is obviously limited by the QW2 HH exciton ionization.

An example of the 3-Gaussian fit is shown in Fig. 4.38. The fit is reasonable, except for the blue side of the QW2 HH line and the spectral region to the red of the QW2 HH line. The poor fit to the red side is due to fluctuations of the white light source (i.e. the broad bump around 1.48 eV is an artifact which varies randomly from spectrum to spectrum). The poor fit on the blue side of the QW2 HH peak is due to a tail on the high energy side of the spectrum which makes the line asymmetric. This could be due to a contribution to the spectrum from the QW2 continuum. 1 have fitted the spectrum including this contribution, and this yields a reasonable fit to the QW2 HH line. However, doing so introduces four additional free parameters (the continuum amplitude, quasi-chemical potential, effective electron temperature, and broadening of the continuum edge), and with so many free parameters the results of such a fit cannot be taken too seriously. Nevertheless 1 believe the fitted areas of the QW1 peak shown in Fig. 4.40 properly display the temporal behavior of the QW1 population.
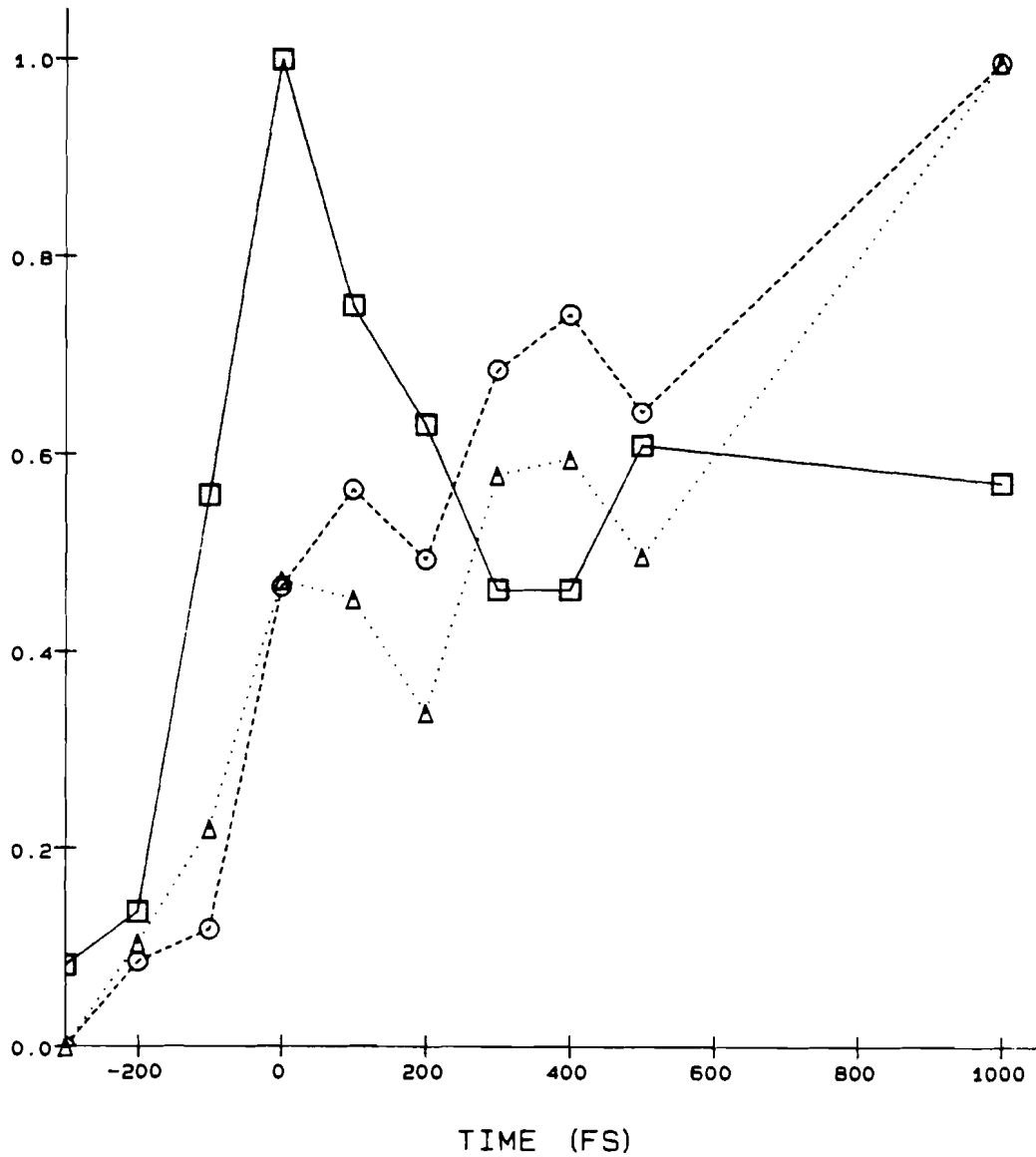
Figure 4.40. Time dependence of the peak areas for sample C pumped at 1.51 eV, and 0 V applied bias. The results are scaled to the maximum area for each peak in the time window -300 fs to 1 ps. The solid line is the QW2 heavy-hole (HH) exciton transition. The dashed line is the QW2 light-hole (LH) exciton transition. The dotted line is the QW1 HH transition.

Differential absorption spectra for sample C with a -9V applied bias are shown in Fig. 4.41. The behavior is not substantially different from the 0V results. The QW2 HH line is noticeably more asymmetric, with a longer tail to the blue. This could be due to nonuniform electric fields over the multiple-QW structure. Another possibility is that is some flaw in the sample construction so that there is a component of the electric field parallel to the QW layers. This would cause very rapid field ionization of the resonantly generated excitons.[36] The fitted peak areas are shown in Fig. 4.42. Both the QW2 LH and QW1 transitions display a faster rise than in the 0V case. This would be consistent with a rapid ionization of the exciton.

The most surprising result is that the exciton lines shift by only a very small amount (about 2 meV) even at a very high applied bias. From previous studies of single QW's in an electric field, one would expect the lines to shift by about 10 meV.[36] This indicates that in fact very little of the expected electric field actually appears across the QW region. I performed a study of the field dependence of the differential spectra in an attempt to see if there was any resonance behavior, in which the tunneling would be efficient in only a limited range of the applied field. Spectra were acquired in 0.2V steps from 0 to -2.2V, and in 0.5V steps from 0 to -8V bias. No resonance behavior was observed; the spectra are quite independent of the applied bias. Three different
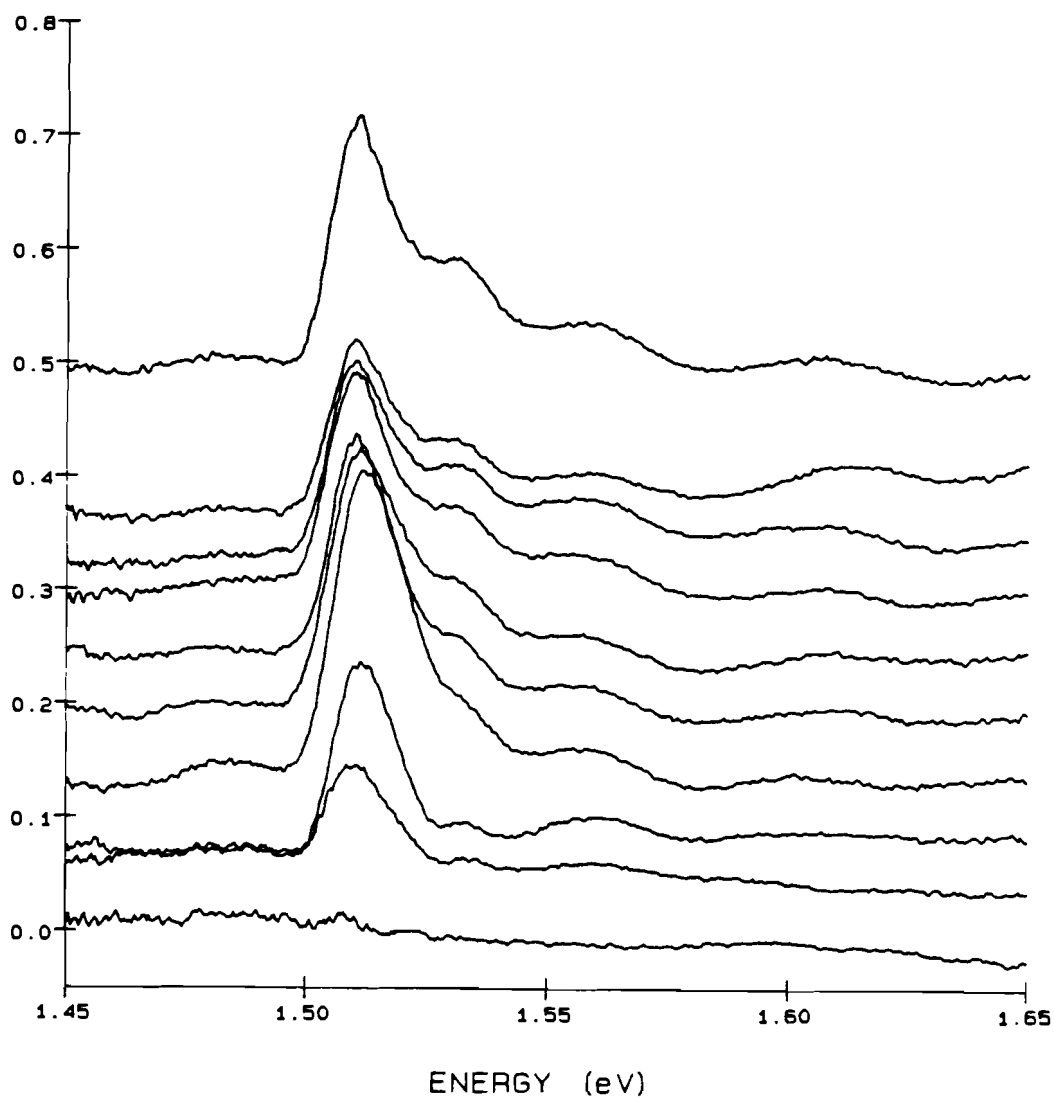
Figure 4.41.   Differential absorption spectra for sample C with -9
V applied bias.   The delay times are -300 fs to +500 fs;
the top curve is at t= 1 ps.
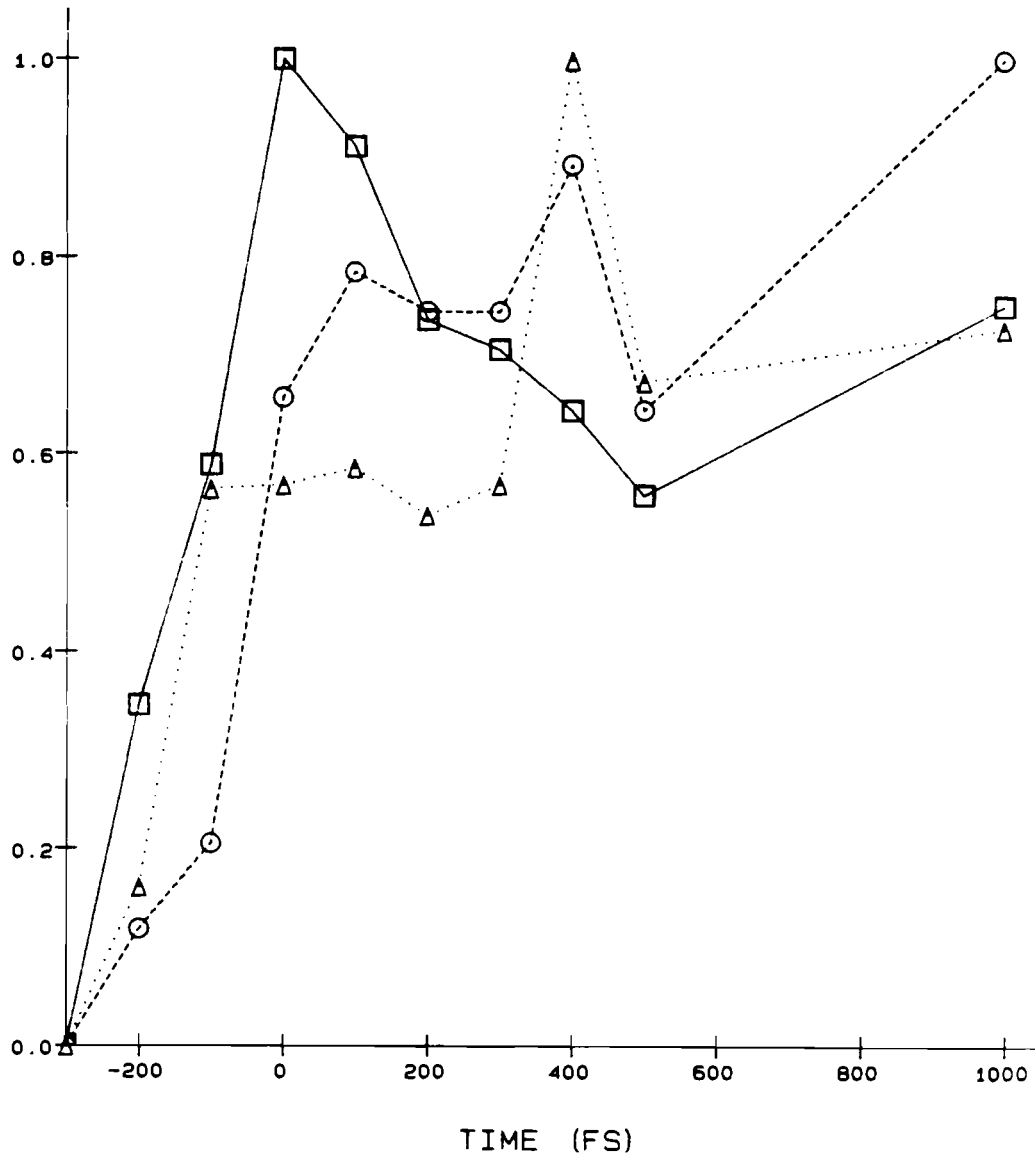
Figure 4.42.   Time dependence of the peak areas for sample C
pumped at 1.51 eV, and -9 V applied bias. The results
are scaled to the maximum area for each peak in the
time window -300 fs to 1 ps. The solid line is the QW2
heavy-hole (HH) exciton transition. The dashed line is
the QW2 light-hole (LH) exciton transition. The dotted
line is the QW1 HH transition.

p-i-n diodes on the sample wafer were studied, but none displayed any field dependence.

Differential spectra were acquired at delay times up to 100 ps with and without bias to determine if there is a slow tunneling component, however no long time dependence was observed.

In conclusion, the experiments on sample C indicate the possibility of a rapid tunneling component. However, no strong conclusions can be made regarding the nature of this tunneling on the basis of the experiments presented here, which were performed at a single excitation density and temperature. Because of the large separation between the $n=1$ electron energies of the two QW's under flat band conditions, the tunneling should be energetically impossible at low temperatures. A conclusive experiment to prove or disprove the tunneling origin of the QW1 peak would be to do the experiment at low temperatures. The experiment should also be performed at different excitation densities to test the validity of the fitting procedure, or ultimately to make a more sophisticated fitting procedure including the continuum contributions possible.

IV.D.   References

1.   R. Dingle, A.C. Gossard, and W. Wiegmann, "Direct Observation of Superlattice Formation in a Semiconductor Heterostructure," Phys. Rev. Lett. **34**, 1327 (1975).

2.   H. Kawai, J. Kaneko, and N. Watanabe, "Doublet State of Resonantly Coupled AlGaAs/GaAs Quantum Wells Grown by Metalorganic Chemical Vapor Deposition," J. Appl. Phys. **58**, 1263 (1985).

3.   H. Shen, S.H. Pan, F.H. Pollak, M. Dutta, and T.R. AuCoin, "Conclusive Evidence for Miniband Dispersion in the Photoreflectance of a GaAs/ $Ga_{0.74}Al_{0.26}As$ Coupled Multiple-Quantum-Well Structure," Phys. Rev. B **36**, 9384 (1987).

4.   M.N. Islam, R.L. Hillman, D.A.B. Miller, D.S. Chemla, A.C. Gossard, and J.H. English, "Electroabsorption in GaAs/AlGaAs Coupled Quantum Well Waveguides," Appl. Phys. Lett. **50**, 1098 (1987).

5.   H.Q. Le, J.J. Zayhowski, and W.D. Goodhue, "Stark Effect in $Al_xGa_{1-x}As$ Coupled Quantum Wells," Appl. Phys. Lett. **50**, 1518 (1987).

6.   Y.J. Chen, E.S. Koteles, B.S. Elman, and C.A. Armiento, "Effect of Electric Fields on Excitons in a Coupled Double-Quantum-Well Structure," Phys. Rev. B **36**, 4562 (1987).

7.   S.R. Andrews, C.M. Murray, R.A. Davies, and T.M. Kerr, "Stark Effect in Strongly Coupled Quantum Wells," Phys. Rev. B **37**, 8198 (1988).

8. J. Khurgin, "Second-Order Susceptibility of Asymmetric Coupled Quantum Well Structures," Appl. Phys. Lett. **51**, 2100 (1987).

9. B. Vinter, private communication, 1988.

10. R.S. Knox and W. Sha, unpublished (1988).

11. R.S. Knox, "Localized and Delocalized Tunneling States," in Tunneling in Biological Systems (B. Chance *et. al.* eds., Academic Press, N.Y. 1979), p. 91.

12. V.M. Kenkre and R.S. Knox, "Generalized-Master-Equation Theory of Excitation Transfer," Phys. Rev. B **9**, 5279 (1974).

13. C.B. Duke, "Concepts in Quantum Mechanical Tunneling in Systems of Biological and Chemical Interest," in Tunneling in Biological Systems (B. Chance *et. al.* eds., Academic Press, N.Y. 1979), p. 31, and references therein.

14. T.B. Norris, "Quantum Beat Experiments on Calcium," Honors Thesis, Oberlin College, 1982 (unpublished).

15. P.K. Schenck, R.C. Hilborn, and H. Metcalf, "Time-Resolved Fluorescence From Ba and Ca Excited by a Pulsed Tunable Dye Laser," Phys. Rev. Lett. **31**, 189 (1973).

16. W.C. Carithers, T. Madis, D.R. Nygren, T.P. Pun, E.L. Schwartz, H. Sticker, and J.H.Christensen, "Measurement of the Phase of the CP-Nonconservation Parameter η_{+-} and the K_s Total Decay Rate," Phys. Rev. Lett. **34**, 1244 (1975).

17. C. Weisbuch, "Fundamental Properties of III-V Semiconductor Two-Dimensional Quantized Structures: The Basis for Optical

and Electronic Device Applications," in <u>Applications of Multiquantum Wells, Selective Doping, and Superlattices,</u> Semiconductors and Semimetals vol 24, ed. by R. Dingle, (Academic, San Diego, 1987), pp. 78-91.

18. H.L. Störmer, A.C. Gossard, W. Wiegmann, and K. Baldwin, "Dependence of Electron Mobility in Modulation-Doped GaAs-(AlGaAs) Heterojunction Interfaces on Electron Density and Al Concentration," Appl. Phys. Lett. **39**, 912 (1981).

19. F. Capasso, K. Mohammed, and A.Y. Cho, "Resonant Tunneling Through Double Barriers, Perpendicular Quantum Transport Phenomena in Superlattices, and Their Device Applications," IEEE J. Quant. Electron. **QE-22**, 1853 (1986).

20. T. Weil and B. Vinter, "Calculation of Phonon-Assisted Tunneling Between Two Quantum Wells," J. Appl. Phys. **60**, 3227 (1986).

21. B. Vinter, private communication, 1988.

22. T. Weil and B. Vinter, *op. cit.* Figure 5.

23. N. Sawaki, M. Suzuki, E. Okuno, H. Goto, I. Akasaki, H. Kano, Y. Tanaka, and M. Hashimoto, "Real Space Transfer of Two Dimensional Electrons in Double Quantum Well Structures," Solid-State Electronics **31**, 351 (1988).

24. T. Ando, A.B. Fowler, and F. Stern, "Electronic Properties of Two-Dimensional Systems," Rev. Modern Phys. **54**, 437 (1982).

25. G. Wicks, private communication, 1986.

26. B. Vinter, private communication, 1988.

27. E.J. Austin and M. Jaros, " Electric Field Induced Shifts and Lifetimes in GaAs-GaAlAs Quantum Wells," Appl. Phys. Lett. **47**,274 (1985).

28. S.M. Sze, Physics of Semiconductor Devices, 2nd ed., (J. Wiley, New York, 1981), p.291.

29. N. Vodjdani, private communication, 1988.

30. H.-J. Polland. W.W. Ruhle, J. Kuhl, K. Ploog, K. Fujiwara, and T. Nakayama, " Nonequilibrium Cooling of Thermalized Electrons and Holes in GaAs/AlGaAs Quantum Wells," Phys. Rev. B **35**, 8273 (1987).

31. D.S. Chemla and D.A.B. Miller, "Room-Temperature Excitonic Nonlinear-Optical Effects in Semiconductor Quantum Well Structures," J. Opt. Soc. Am. B **2**, 1155 (1985).

32. H. Haug and S. Schmitt-Rink, "Electron Theory of the Optical Properties of Laser-Excited Semiconductors," Prog. Quantum Electron. **9**, 3 (1984).

33. W.H. Knox, R.L. Fork, M.C. Downer, D.A.B. Miller, D.S. Chemla, and C.V. Shank, "Femtosecond Dynamics of Resonantly Excited Excitons in Room Temperature GaAs Quantum Wells," Phys. Rev. Lett. **54**, 1306 (1985).

34. S. Schmitt-Rink, D.S. Chemla, and D.A.B. Miller, "Theory of Transient Excitonic Optical Nonlinearities in Semiconductor Quantum Well Structures," Phys. Rev. B **32**, 6601 (1985).

213

35. D.S. Chemla, D.A.B. Miller, P.W. Smith, A.C. Gossard, and W. Wiegmann, "Room Temperature Excitonic Nonlinear Absorption and Refraction in GaAs/AlGaAs Multiple Quantum Well Structures," IEEE J. Quantum Electron. **QE-20**, 265 (1984).

36. D.A.B. Miller, D.S. Chemla, T.C. Damen, A.C. Gossard, W. Wiegmann, T.H. Wood, and C.A. Burrus, "Electric Field Dependence of Optical Absorption Near the Band Gap of Quantum Well Structures," Phys. Rev. B **32**, 1043 (1985).

CHAPTER V

CONCLUSION

V.A. Summary and Suggestions for Future Work

A major portion of this work was concerned with the development of new experimental techniques for picosecond and femtosecond spectroscopy. At the time this work was begun, generation of a white light continuum had been demonstrated in our laboratory at a 10 Hz repetition rate.[1] The amplified dye laser pulse used to generate the continuum, however, had a pulsewidth of 300 fs with large wings, and the white light continuum was rather unstable. In this thesis I have described the development of a system that provides a very stable continuum at a 1 kHz repetition rate, enabling us to perform spectroscopy with a sensitivity of up to 1 part in 10^3. Furthermore, the amplified pulsewidth is 100 fs, which was achieved by the development of a synchronously pumped, colliding-pulse mode-locked dye laser, and through careful control of amplifier dispersion and saturation. Development of a new Nd:YAG regenerative amplifier based on a Quantronix 117 laser head has made it possible to amplify 100-fs dye laser pulses to the 15 μJ level without pulse broadening.

The femtosecond white light spectroscopy system is now a useful tool of research, but of course many improvements are

214

possible. Particularly fruitful would be improvements in the long-term stability of the dye oscillator and a higher amplifier repetition rate. These would enable a higher sensitivity to be obtainable for reasonable integration times. This is particularly important because most time-resolved absorption experiments on semiconductor systems require higher injected carrier densities than one generally would like to have. In the long term, the replacement of dye laser systems with all-solid-state short pulse lasers, and the development of short-pulse lasers (and ultimately a continuum source) in the 1-μm region of the spectrum would be most interesting.

In chapter III I described time-resolved photoluminescence experiments which probed the tunneling-out problem in detail, including the dependence of the tunneling rate on the barrier thickness and height and on an applied electric field. We found reasonable agreement with a straightforward semiclassical theory of tunneling. We also observed a novel blue shift of the luminescence peak with applied electric field. The origin of this shift remains something of a mystery, which could possibly be solved by further experiments probing the injected carrier density dependence and by a high-resolution analysis of the luminescence spectral lineshape.

Chapter IV was devoted to an investigation of the double-well tunneling problem. Using time-resolved photoluminescence, we directly observed the buildup of a "charge-transfer" state via

electron and hole tunneling in opposite directions. This state was manifested by a large (up to 25 meV) Stark shift and long (of order 10 ns) decay time. At the highest fields obtained in this experiment (a modest 2.5×10^4 V/cm), the charge separation occurred in a time faster than the time resolution of the experimental system (20 ps), which implies a hole tunneling rate that is much faster than one would estimate from the simple tunneling-out theory.

The time-resolved photoluminescence experiments on coupled QW's required that the laser pump both wells in order to monitor the well populations. Thus in order to study tunneling from an initially localized state it was necessary to perform absorption spectroscopy, and to design a novel asymmetric double-QW structure that allowed the electron levels to be close in energy, while keeping the absorption edges of the two wells sufficiently well separated that a short laser pulse would localize the initial excitation. Our experiments represent the first attempt to study carrier dynamics and tunneling in coupled QW structures with subpicosecond time resolution.

For samples A and B (described in section IV.B.1), the excitonic states of the two wells were so close that when the short pump laser pulse was tuned to the narrow-well resonance, the laser spectrum overlapped to some extent the wide well resonance, thus generating an undesired population in the wide well. This was particularly apparent for sample A, making it

impossible to draw any conclusions about tunneling for that sample. It is not clear that there was any significant resonant excitation of the wide well for sample B (since no overshoot in the differential absorption due to exciton ionization was observed). Thus the results indicate the *possibility* of very fast (<100 fs) tunneling from the state initially localized in the narrow well. For sample C (described in section IV.C.2), there was no danger of accidental resonant pumping of the wide well. In this case we found that the wide well population rose with the exciton ionization time, indicating the possibility of fast tunneling (possibly phonon-assisted) into the wide well.

There are a number of obvious extensions of the work presented here on tunneling in coupled QW's that would be of considerable interest. First, samples A and B were designed so that the anticrossing of the electron levels could be observed. However, the actual sample dimensions were not as desired due to MBE difficulties in the growth, preventing the observation of the resonance. New samples should be grown and another attempt made at observing the anticrossing. Higher time resolution (such as can be obtained using the frequency up-conversion techniques described by Deveaud and Shah[2,3]) would also be quite useful. For the absorption experiments, it would be particularly useful to perform the experiments again at low temperatures. The temperature dependence would confirm or deny the possibility of phonon-assisted tunneling in these structures. This would be of

great interest, since to my knowledge there have been no time-resolved observations of phonon-assisted tunneling. Finally, the elusive goal of observing coherent, reversible tunneling between coupled wells remains.

V.B.   References

1. T. Sizer II, J.D. Kafka, I.N. Duling III, C.W. Gabel, and G.A. Mourou, "Synchronous Amplification of Subpicosecond Pulses," IEEE J. Quant. Electron. **QE-19**, 506 (1983).

2. J. Shah, T.C. Damen, B. Deveaud, and D. Block, "Subpicosecond Luminescence Spectroscopy Using Sum Frequency Generation," Appl. Phys. Lett. **50**, 1307 (1987).

3. J. Shah, "Ultrafast Luminescence Spectroscopy Using Sum Frequency Generation," IEEE J. Quant. Electron. **QE-24**, 276 (1988).